NASA TECHNICAL NOTE

NASA TN D-8488

NASA TN D-8488

LOW-SPEED WIND-TUNNEL INVESTIGATION OF A SWEPT-WING MODEL HAVING DISTRIBUTED UPPER-SURFACE BLOWING NEAR THE WING LEADING EDGE OR AT THE FLAP KNEE

William C. Sleeman, Jr., and David R. Forsyth

Langley Research Center
Hampton, Va. 23665

NATIONAL AERONAUTICS AND SPACE ADMINISTRATION • WASHINGTON, D. C. • NOVEMBER 1977

1. Report No.	2. Government Accession No.	3. Recipient's Catalog No.
NASA TN D-8488		

4. Title and Subtitle	5. Report Date
LOW-SPEED WIND-TUNNEL INVESTIGATION OF A SWEPT WING MODEL HAVING DISTRIBUTED UPPER-SURFACE BLOWING NEAR THE WING LEADING EDGE OR AT THE FLAP KNEE	November 1977
	6. Performing Organization Code

7. Author(s)	8. Performing Organization Report No.
William C. Sleeman, Jr., and David R. Forsyth	L-11272
	10. Work Unit No. 505-11-16-03

9. Performing Organization Name and Address	11. Contract or Grant No.
NASA Langley Research Center Hampton, VA 23665	
	13. Type of Report and Period Covered
12. Sponsoring Agency Name and Address	Technical Note
National Aeronautics and Space Administration Washington, DC 20546	14. Sponsoring Agency Code

15. Supplementary Notes

William C. Sleeman, Jr.: Langley Research Center.
David R. Forsyth: The George Washington University, Joint Institute for Advancement of Flight Sciences.

16. Abstract

A low-speed investigation was conducted in the Langley V/STOL tunnel to determine the power-on static turning characteristics and powered-lift aerodynamic performance of an upper-surface blown transport configuration. Most of the tests used distributed blowing from a full-span slot nozzle near the wing leading edge. Limited studies were made of blowing at the flap knee only, since the wing of the model already had provisions for blowing from a full-span slot just ahead of the flap knee. A few tests were also made with blowing at the leading edge and the flap knee together. The wing had a leading-edge sweep of 34.5° and an aspect ratio of 6.84. The high-lift system consisted of a double-hinged plain trailing-edge flap that extended across the wing span outboard of the circular fuselage.

17. Key Words (Suggested by Author(s))	18. Distribution Statement
Jet-blown flap Powered-lift aerodynamics Upper-surface blowing	Unclassified - Unlimited Subject Category 02

19. Security Classif. (of this report)	20. Security Classif. (of this page)	21. No. of Pages	22. Price*
Unclassified	Unclassified	77	$5.00

* For sale by the National Technical Information Service, Springfield, Virginia 22161

LOW-SPEED WIND-TUNNEL INVESTIGATION OF A SWEPT-WING MODEL HAVING DISTRIBUTED UPPER-SURFACE BLOWING NEAR THE WING LEADING EDGE OR AT THE FLAP KNEE

William C. Sleeman, Jr., and David R. Forsyth*
Langley Research Center

SUMMARY

A low-speed investigation was conducted in the Langley V/STOL tunnel to determine the power-on static turning characteristics and powered-lift aerodynamic performance of an upper-surface blown transport configuration. Most of the tests used distributed blowing from a full-span slot nozzle near the wing leading edge. Limited studies were made of blowing at the flap knee only, since the wing of the model already had provisions for blowing from a full-span slot just ahead of the flap knee. A few tests were also made with blowing at the leading edge and the flap knee together. The wing had a leading-edge sweep of 34.5° and an aspect ratio of 6.84. The high-lift system consisted of a double-hinged plain trailing-edge flap that extended across the wing span outboard of the circular fuselage.

The test results obtained with leading-edge blowing showed good static turning characteristics, with a maximum static turning angle of about 84° achieved for 100° total flap deflection. Power-on lift coefficients at 0° angle of attack obtained with various combinations of deflection of the forward and rear flap elements showed that, in most cases, 45° deflection of the forward element provided the highest lift for a given deflection of the rear element. Static turning angles obtained with flap blowing generally were 10° to 15° higher than with leading-edge blowing at the same flap deflection; however, the power-on lift coefficients at 0° angle of attack were about the same for the two blowing modes. Lift characteristics obtained over the angle-of-attack range with flaps deflected generally showed a gradual stall and a small loss in lift for leading-edge blowing. With flap blowing alone, or with no blowing, an abrupt stall and large loss of lift occurred at moderate angles of attack because the wing did not have a leading-edge device to protect it from early stall. The model with combined blowing at the leading edge and flap provided the highest powered-lift coefficients and had favorable stall characteristics similar to those with leading-edge blowing alone.

INTRODUCTION

The use of attached upper-surface blowing for developing propulsive lift for low-speed flight at high lift has been studied in numerous investigations

---

*The George Washington University, Joint Institute for Advancement of Flight Sciences.

by the National Aeronautics and Space Administration (NASA). (See refs. 1 to 5.) The configurations used in these investigations directed the efflux from simulated turbofan engines over the wing upper surface and high-lift system to provide large increases in the lift-producing potential of the wing by means of Coanda turning of the propulsive jets. The results from these investigations indicated that the propulsive lift capabilities of a given configuration were greatly dependent upon details of the exhaust nozzle geometry and its relation to the geometry of the wing and flaps. Generally, thin, well-spread jets had good Coanda turning when directed over a trailing-edge flap with a fairly gentle curvature at the knee of the flap. Thinning and spreading of the jet efflux were achieved by means of high-aspect-ratio, spread exhaust nozzles with an appreciable internal angle on the upper lip, or by means of external flow deflectors attached to the top of each exhaust nozzle.

The present investigation was undertaken in the Langley V/STOL tunnel to define the high-lift performance of a swept-wing, upper-surface blown configuration that discharged all the propulsive exhaust through a thin, full-span slot located near the wing leading edge. The wing of the model also had provisions for blowing over the flap knee and was previously tested as an internally blown jet-flap configuration without leading-edge blowing. The present investigation, therefore, included limited studies with blowing at the flap knee only and with combined leading-edge blowing and blowing at the flap knee.

SYMBOLS

The static longitudinal aerodynamic characteristics are presented about the stability-axis system and the positive directions of forces, moments, and angles are indicated in figure 1. The model moment-reference point was located at 45.2-percent mean aerodynamic chord on the fuselage reference line.

The measurements and calculations of this investigation were made in the U.S. Customary Units. Results are presented in the International System of Units (SI), except for the thrust values, which are given in both systems with U.S. Customary Units as the primary system. (A waiver has been granted for this exception.) Factors relating the two systems are presented in reference 6.

C_D drag coefficient, $\frac{\text{Drag}}{qS}$

C_L lift coefficient, $\frac{\text{Lift}}{qS}$

$C_{L,o}$ lift coefficient for zero thrust at $\alpha = 0^o$

C_m pitching-moment coefficient, $\frac{\text{Pitching moment}}{qS\bar{c}}$

C_μ total-thrust coefficient, $\frac{\text{Total thrust}}{qS}$

$C_{\mu,f}$ thrust coefficient for blowing at flap, $\frac{\text{Thrust at flap}}{qS}$

c local wing chord, m

$\bar{c}$ mean aerodynamic chord of wing, m

c' aerodynamic chord of wing before addition of extension for blowing, m

F_A axial force, N

F_N normal force, N

F_Y side force, N

L.E. leading edge

q free-stream dynamic pressure, Pa

S wing area, 0.5386 m^2

T total static-thrust force, N

T_f static-thrust force for blowing at flap, N

α angle of attack of fuselage reference line, deg

δ_f flap deflection angle measured streamwise, deg (Dual notation, such as 45-15, indicates deflection of forward element with respect to basic airfoil chordline, followed by deflection of rear element with respect to chord line of forward element. See fig. 2(b).)

$\delta_{f,t}$ total flap deflection, deg (sum of deflections of forward and rear flap elements)

δ_j static turning angle, $\tan^{-1}\frac{F_N}{F_A}$, deg

$\delta_{j,o}$ static turning angle for 0° flap deflection, deg

η static-thrust-recovery efficiency, $\frac{\sqrt{F_N^2 + F_A^2 + F_Y^2}}{T}$

MODEL DESCRIPTION

The model used in this investigation was the same general research model that was tested as an internally blown jet-flap model. The present model differed from the jet-flap model only near the wing leading edge, which was extended to provide for blowing from a full-span slot nozzle over the modified airfoil. A drawing of the general arrangement of the model is given in figure 2(a). Details of the trailing-edge flap and of the provisions for blowing near the leading edge and at the flap knee are given in figure 2(b). Photographs of the model in the Langley V/STOL tunnel are shown in figure 3.

Wing

The wing of the model was swept 34.45° at the leading edge and had an aspect ratio of 6.84 and a taper ratio of 0.258, based on a linear extension of the leading and trailing edges to the plane of symmetry. Blowing near the leading edge was accomplished by fitting an extension to the leading edge of the wing with the same contour as the basic 17-percent-thick supercritical airfoil section. The extension was fabricated with a hollow portion which was a plenum for the high-pressure air that exhausted through a full-span slot nozzle over the upper surface of the wing. (See fig. 2(b).) The slot nozzle location and height at three spanwise stations on the wing are also given in figure 2(b). The high-lift system on the wing consisted of a full-span double-hinged plain flap which extended from the wing-fuselage juncture to the wing tip. (See fig. 2(b).) There were no gaps between the flap elements or between the forward element and the wing inasmuch as fixed deflection plates which spanned the underside of the flap elements were used to set the deflections. Forward-element deflection angles of 0°, 15°, 30°, 45°, 60°, and 70°, measured in the streamwise direction, were used with rear-element deflection angles of -20°, 0°, 15°, and 30°. (See fig. 2(b).) No wing leading-edge high-lift devices were used on the model.

The wing had a slot nozzle composed of many closely spaced holes that discharged over the knee of the flap. The size of these holes decreased from root to tip because of the taper in height of the $0.00745c'$ ledge as the chord decreased. (See fig. 2(b).) This reduction in the hole diameter was useful in attaining nearly constant wing-section momentum coefficients across the wing span. Separate plenums located in the fuselage provided the blowing air for the leading-edge slot and for the flap slot. The flow of high-pressure air into each slot could thereby be separately controlled by valves to provide leading-edge blowing only, flap blowing only, or combinations of leading-edge and flap blowing.

Fuselage

The fuselage of the model had circular cross sections except at the afterbody, where the circular shape was modified on the underside to accommodate the support sting. Overall dimensions of the fuselage are given in figure 2(a). A fiberglass-resin shell, 0.32 cm thick, formed the outer shape of the fuselage and was attached to a metal strongback which housed the model air plenums and

the six-component electrical strain-gage balance. An electronic angle-of-attack sensor was mounted to the internal strongback to provide the measured geometric angle of attack of the model during the tests.

TESTS AND CORRECTIONS

The investigation was conducted in the Langley V/STOL tunnel. Aerodynamic tests were conducted at a dynamic pressure of 766 Pa and the corresponding test Reynolds number was 7.6×10^5 based on the wing mean aerodynamic chord of 0.3146 m.

Thrust Calibrations

Static-thrust calibrations were made prior to testing in order to determine the static thrust for each of the leading-edge and flap blowing elements as a function of a reference pressure within each slot plenum. All static calibrations were made with the wing flaps removed and with the model at 0° angle of attack. Mathematical curve fits were determined for each calibration. Static-thrust calibrations were also made with the left and right leading-edge elements blowing together, as were the calibrations for the flap blowing elements. These calibrations were made after the thrusts of the individual elements were balanced, based on their individual calibrations and balancing out the yawing moment of the model with the left and right elements thrusting together. The static thrust from the calibrations was computed as the resultant of the normal, axial, and side forces. Individual reference pressures were recorded at each wind-on test point, and the thrust for each element was computed from its mathematical curve fit. The thrust coefficients for the aerodynamic tests were verified from summations of the individual thrust of each element computed by use of the mathematical curve fit.

Static Tests

Static tests of the model were made for all flap configurations investigated. A relatively large number (10 to 14) of equally spaced thrust values were set in the static tests in order to obtain good definition of the variation of static and aerodynamic characteristics with thrust. Static turning angles and thrust-recovery efficiency for the jet flow were computed from the measurements of normal, axial, and side forces. The thrust used in computing the thrust-recovery efficiency was computed for each data point from the mathematical curve fit for each thrusting element to obtain the total thrust. Values of thrust-recovery efficiency presented herein for very low thrust levels show erratic variations because of the inaccuracies inherent in measuring low forces and in dividing by small numbers which are subject to experimental variations and to mathematical curve-fit inaccuracies of the calibrations. Since the basis for the efficiency parameter η is the static thrust without flaps, η represents the effects of flaps and the associated jet turning on thrust recovery. Also, thrust-recovery efficiency does not account for internal losses and, therefore, does not represent the thrust efficiency normally associated with jet-engine installations.

Aerodynamic Tests

Aerodynamic tests of the model at 0° angle of attack were made for all the model configurations and thrust settings in the static tests. Longitudinal aerodynamic characteristics were obtained from tests over an angle-of-attack range from approximately -4° to 24° which were conducted with power off and at several values of thrust which were held constant as the angle of attack was varied. Nominal values of C_μ were 0, 0.5, 1.5, and 2.0 for most of the tests. The investigation of aerodynamic characteristics with combined blowing at the leading edge and flap used leading-edge blowing as the primary thrust source with relatively small amounts of blowing at the flap (5, 13, and 28 percent of the total thrust).

The primary objective of the present investigation was the determination of the aerodynamic performance potential of a swept-wing model with upper-surface blowing near the leading edge. All the results were therefore obtained for the wing, fuselage, vertical-tail configuration. No tests were made with a horizontal tail.

Corrections

Jet-boundary corrections for the influence of the closed tunnel boundaries were determined from reference 7 and applied to the measured aerodynamic data.

PRESENTATION OF RESULTS

The data obtained in this investigation are presented in the following figures:

DISCUSSION

Static Characteristics

Basic data obtained over the range of static thrust, which show effects of flap deflection on the static turning angles and thrust-recovery efficiencies of the model, are given in figures 4 to 6. These basic data are summarized in figure 18 for a constant thrust equivalent to that used for $C_\mu = 1.0$ in the aerodynamic tests (T = 405.7 N (91.2 lb)).

Static turning and static-thrust-recovery efficiency with leading-edge blowing.- The basic data for leading-edge blowing (fig. 4) generally showed increasing values of static turning angle as the thrust and flap deflection increased. Thrust-recovery efficiency generally decreased as the flap deflection increased and, in some cases, showed erratic variations with thrust at the lowest thrust values. These erratic variations in efficiency at thrust values below about 50 N (11 lb) are believed to be associated with inaccuracies in measuring low forces and inaccuracies in the curve fit of the calibrations.

The summary of static turning angles given in figure 18 provides a simplified overall assessment of effects of total flap deflection for leading-edge blowing. Static turning angles showed fairly consistent increases with increasing total flap deflection, and a maximum turning angle of about 84° was obtained with total flap deflection of 100°. Static turning angles for a given value of total flap deflection were generally slightly lower with positive deflection of the rear element, whereas a negative deflection of the rear element increased the static turning angles. Static-thrust-recovery efficiencies decreased with increasing total flap deflection, with the lowest values of efficiency lying between 0.6 and 0.7 at the highest flap deflections.

Static turning parameter with leading-edge blowing.- The effectiveness of the trailing-edge flap in turning the jet flow is shown in figure 18(b) as a function of total flap deflection for a thrust level corresponding to that used for $C_\mu = 1.0$. The static turning parameter expresses the static turning δ_j obtained in relation to the turning that should have been obtained $\delta_{j,o} + \delta_{f,t}$ if the flow remained attached to the deflected flap in the same manner as with the flap undeflected. Normally, deflection of the flap would be expected to decrease the static turning parameter from the value for the undeflected flap, inasmuch as flow turning conditions over a deflected flap are usually more adverse than over an undeflected flap. The static turning parameters shown in figure 18(b) were therefore unexpected in that several flap combinations turned the jet more effectively in the deflected condition than in the undeflected condition.

The airfoil upper-surface slope over the rear 2.5 percent of the chord varied across the span from about 16° to 17.7°. The static turning obtained with leading-edge blowing at 0° total flap deflection was about 5° (figs. 4(a) and 18), which was significantly less than the basic airfoil slope. Deflection of only the forward element of the flap (rear-element deflection 0°) apparently generated a more favorable pressure gradient over the flap that caused the jet flow to adhere more to the airfoil at low and moderate flap deflections. Static turning parameters obtained with the -20° rear-element deflection showed very high values of turning (fig. 19(b)) for total flap deflections less than 40°. These high values suggest that the final effective jet turning was determined more by the deflection of the forward flap element than by the deflection of the rear element, and possibly that the efflux from the leading-edge slot nozzle was appreciably thickened when it reached the rear element.

Effects of flap blowing on static characteristics.- Static characteristics obtained with blowing at the flap knee generally showed the same overall results as with leading-edge blowing (figs. 5 and 18); however, for a given total flap deflection, static turning angles were at least 10° higher for flap blowing (rear-element deflection 0°) than for leading-edge blowing. The summary of static turning angles with flap blowing presented in figure 18(a) shows a continuous increase in static turning angle with increasing total flap deflection and a maximum turning angle of 85° obtained for a total flap deflection of 70°. Static-thrust-recovery efficiencies (fig. 18) showed much less variation with flap deflection for flap blowing than for leading-edge blowing, with values of efficiency ranging only from 0.80 to 0.87.

Static characteristics obtained with combined leading-edge and flap blowing for three different ratios of combined blowing are presented in figure 6 and are compared with leading-edge blowing alone and flap blowing alone in figure 19. The static turning angles obtained with combined blowing were generally a little higher than with leading-edge blowing and somewhat lower than with flap blowing. Static turning angles for the 60-0 flap deflection (fig. 19) showed small and inconsistent effects of the amount of combined blowing, whereas data for the 45-15 flap deflection at the intermediate blowing rate ($T_f = 0.13T$) showed less static turning at low thrust than for leading-edge blowing alone. These turning-angle results at low thrust for the inter-

mediate (T_f = 0.13T) combined blowing condition do not appear reasonable in light of the results obtained for lower and higher (T_f = 0.05T and 0.28T) combined blowing rates, or the results obtained with the 60-0 flap deflection.

Assessment of Static and Aerodynamic Performance at $\alpha = 0^\circ$

The determination of static-thrust characteristics for powered-lift configurations with and without high-lift systems deflected has generally been an important element in investigations of these types of configurations. Past experience has indicated that externally blown flap (EBF) configurations that exhibited poor static turning characteristics also had poor powered-lift aerodynamic performance. Conversely, EBF configurations with good static turning also showed generally good powered-lift aerodynamic characteristics. An analogous correlation of good static turning characteristics with expected aerodynamic performance, however, has not been as straightforward for upper-surface blown configurations. (See ref. 4.) In general, it has been found that the static turning results can be indicative of wind-on powered-lift performance for very good and for poor conditions; for marginal conditions, the static results can lead to an overly optimistic assessment of wind-on powered-lift potential.

The static turning angles summarized in figure 18(a) show a fairly continuous increase with increasing total flap deflection to $\delta_{f,t} = 100^\circ$. If these static turning characteristics are indicative of the wind-on aerodynamic performance, the lift coefficients should show a corresponding increase with increasing flap deflection. The variation of lift coefficient with total flap deflection (fig. 20(a)) shows that an increase in lift coefficient accompanied increases in total flap deflection only up to about 60° for leading-edge blowing. The maximum lift coefficient attained at 0° angle of attack and $C_\mu = 1.0$ with leading-edge blowing was 5.2 for the 45-15 flap deflection. For all positive deflections of the rear element, 45° deflection of the forward element provided the maximum lift for a given total flap deflection for both leading-edge blowing (fig. 20(a)) and combined leading-edge and flap blowing (fig. 9). For flap blowing alone, the 60-0 and 70-0 flap deflections provided slightly higher lift coefficients than those obtained with the 45-15 flap deflection (fig. 20(a)).

Trends shown in the variation of drag coefficients with total flap deflection (fig. 20(a)) were similar to the trends for the lift coefficients in that the drag became more positive as the flap deflection increased. At the highest flap deflections the drag coefficients approached near-zero values.

Another interesting aspect of the static and aerodynamic characteristics is shown in the comparative static turning and lift coefficients between flap blowing and leading-edge blowing. Static turning angles obtained with flap blowing were 10° to 15° higher than with leading-edge blowing at the same flap deflection (fig. 18(a)), yet the lift coefficients obtained (fig. 20(a)) were about the same up to 45° forward-element deflection (δ_f = 45-0), beyond which lift began to decrease with increasing flap deflection for leading-edge blowing.

The parity of lift coefficients at low flap deflections suggests that the addition of the free-stream flow may have aided flow attachment along the airfoil with leading-edge blowing. The relatively high positive values of drag coefficient obtained at the highest flap deflections for flap blowing (fig. 20(a)) and the fact that the lift did not show the fall-off at high flap deflections that was typical for leading-edge blowing suggest that the jet efflux from flap blowing remained fairly well attached in the presence of the free-stream flow up to the highest flap deflection of the tests.

Additional insight into the power-on aerodynamic characteristics may be gained by considering the effects of powered circulation lift, which are inferred from a combination of static and aerodynamic characteristics. Past practice in analyzing lift increments due to power has generally been to represent the direct thrust effects with free-stream flow by the vertical component of the static resultant force inclined at the static turning angle. This analysis identifies powered circulation lift as the remaining lift increment between the total power-on lift and the power-off lift plus the direct thrust component of lift. Powered circulation-lift effects for the present investigation are presented in figure 20(b) in terms of a ratio of the total power-on lift coefficient to the power-off lift coefficient plus the lift component of the thrust at each flap deflection.

The derived powered circulation-lift ratios presented in figure 20(b) show that leading-edge blowing provided up to a threefold increase in lift, and the highest powered circulation-lift ratio occurred with 30° deflection of the forward element and 15° deflection of the rear element (δ_f = 30-15). Blowing at the flap knee provided lift-ratio increases almost as high as leading-edge blowing with 0° rear-element deflection, but was somewhat lower than with the 30-15 and 45-15 flap deflections with leading-edge blowing. The powered circulation-lift ratios presented in figure 20(b), along with the total lift (fig. 20(a)), and the static turning data of figure 18 suggest that the capabilities of flap blowing to provide total lift were more directly related to the static turning capabilities than was leading-edge blowing, and the greater increases in powered circulation lift with leading-edge blowing more than compensated for its lower flow-turning capabilities.

The results of this investigation showed that static turning angles increased with increasing flap deflection, whereas the wind-on lift coefficients at $\alpha = 0°$ increased with flap deflection only up to a point, beyond which the lift decreased with increasing flap deflection. Wind-on lift coefficients at $\alpha = 0°$ with flap blowing were about the same as with leading-edge blowing for a given total flap deflection even though the static turning angles obtained with flap blowing were appreciably higher.

Aerodynamic Performance Over Angle-of-Attack Range

The model used in the present investigation did not have a leading-edge high-lift device and consequently the wing stalled at fairly low angles of attack without power. (See figs. 10 to 12.) The use of increasing amounts of leading-edge blowing generally delayed the stall to higher angles of attack for forward-element deflections up to 45° (figs. 10(a) to 10(d), 11(a) to

11(c), and 12(a) and 12(b). At the highest thrust, little or no leading-edge stall was evident at high angles of attack. These results indicate that leading-edge blowing generally provided the type of stall protection that would be expected from a leading-edge high-lift device.

Longitudinal aerodynamic characteristics over the angle-of-attack range have been summarized in figures 21 to 25 to illustrate effects of flap deflection and the powered-lift blowing mode for a constant nominal thrust level of approximately 2.0.

Effects of flap deflection with leading-edge blowing.- Effects of forward-element deflection are summarized in figure 21 for 0° deflection of the rear element and in figure 22 for 15° deflection of the rear element. Lift characteristics throughout the angle-of-attack range (figs. 21 and 22) reflect the characteristics shown at 0° angle of attack (fig. 20) in regard to the progressive increase in lift coefficient with increasing flap deflection up to 45° for the forward element and also reflect the reduction in lift that accompanied higher deflections of the forward element. Most of the power-on lift curves with low and moderate flap deflections show a considerable decrease in lift-curve slope at high angles of attack. The lift-curve slopes were usually lowest as the flap deflection became higher, and at high angles of attack the 30-15 deflection flap resulted in almost the same lift as the 45-15 deflection flap (fig. 22). Lift curves for the 70° forward-element deflection (figs. 21 and 22) were considerably lower than those for the 45° and 60° forward-element deflections, and data for the 70° deflection did not show the lift-curve slope reduction at high angles of attack typical of the other flap deflections because with the 70° deflection the wing was probably stalled throughout the test angle-of-attack range.

The drag polars presented in figures 21 and 22 are of interest because they appear to define an envelope over a broad range of lift coefficients where the drag data lie on the envelope except at the high angles of attack, where stall effects were evident. Drag polars for the two highest forward-element flap deflections in figure 22 (60-15 and 70-15), which showed relatively low lift coefficients at low angles of attack, are completely separated from the envelope defined by the other drag polars and reflect wing stall and loss in flow turning with the wind on. This loss in flow turning is also shown in figure 21 at $\alpha = 0^\circ$. The drag polars generally provide good indications of the overall flow turning inasmuch as appreciable flow turning would be required to provide positive drag at high thrust and low angles of attack.

The powered-lift performance of the model at 0° angle of attack (fig. 20) indicated that 45° deflection of the forward element was close to optimum in lift-producing capability. Effects of rear-element deflection on the lift and drag characteristics over the angle-of-attack range for 45° forward-element deflection are shown in figure 23. Increasing the rear-element deflection from 0° to 15° increased the lift coefficient at 0° angle of attack from about 5.9 to 6.5. The maximum lift coefficient, however, showed only a relatively small increase from about 7.3 to 7.5 because of the lower lift-curve slope and loss in lift at high angles of attack for the 15° rear-element deflection. An increase in the rear-element deflection to 30° caused a reduction in lift coefficients throughout the test angle-of-attack range. A comparison of lift data

for the 45-30 flap deflection (fig. 23) and the 60-15 flap deflection (fig. 22), both combinations providing 75° total flap deflection, shows that the more gradual turning provided by the 45° forward-element deflection provided significantly higher aerodynamic lift than the 60° deflection.

The overall lift and drag characteristics obtained in the investigation of leading-edge blowing indicated that the most effective flap deflection combination for the present model, from the standpoint of high-lift performance throughout the angle-of-attack range, was 45° deflection of the forward element and 15° deflection of the rear element with respect to the forward element.

Effects of flap deflection with flap blowing.- A comparatively small number of flap-angle combinations were investigated with flap blowing inasmuch as a previous investigation of this model with flap blowing covered a broad range of flap-angle combinations. Test results obtained in the present investigation are summarized in figure 24 for a range of forward-element deflections with the rear element undeflected and for the 45-15 flap setting that showed the best performance with leading-edge blowing.

The most distinguishing characteristic of the lift curves obtained with flap blowing was the large loss of lift at high angles of attack that resulted from early wing stall. The angle of attack for stall decreased as flap deflection increased, and varied from about 18° for undeflected flaps to about 8° for the highest flap deflection. Wing stall at fairly low angles of attack with and without flap blowing occurred because there was no leading-edge high-lift device on the wing to prevent or delay leading-edge flow separation at moderate to high angles of attack. The basic data of figure 14 show very early stall (5° to 10° angle of attack) without power. The application of flap blowing increased both the lift and the stall angle; however, stall was not alleviated by flap blowing at high angles of attack.

Increasing the flap deflection increased the lift up to stall for flap blowing (fig. 24). These trends with increasing flap deflection were also shown at $\alpha = 0^\circ$ for $C_\mu = 1.0$. (See fig. 20(a).) With flap blowing, the maximum lift coefficient obtained with the 45-15 flap deflection was about the same as for the 60-0 deflection. Drag polars for flap blowing (fig. 24) showed essentially the same type of envelope variation at prestall lift coefficients as was shown for leading-edge blowing (fig. 20). The occurrence of positive drag over most of the angle-of-attack range for high-thrust and high-lift conditions with flap blowing indicates that the jet efflux was being effectively turned over the flap in the presence of the free-stream flow.

Effects of combined leading-edge and flap blowing.- The combined blowing of this investigation used a relatively small amount of blowing at the flap knee, in addition to the leading-edge blowing, to promote additional flow turning over the flap. A comparison of lift characteristics with leading-edge blowing alone (fig. 11(c)) with those with smaller amounts of combined blowing (figs. 17(a) and 17(b)) shows that an appreciable loss in lift coefficient occurred over most of the angle-of-attack range when small amounts of blowing at the flap knee were added. Increasing the flap blowing to 28 percent of the total thrust (fig. 17(c)) provided appreciably higher lift over the angle-of-attack range than was obtained with leading-edge blowing alone (fig. 11(c)).

Flow separation problems at moderate and high angles of attack were evident for most test conditions at which combined blowing was used (fig. 17). Leading-edge blowing combined with flap blowing of 5 percent or 13 percent of total thrust was not adequate to eliminate the separation effects (figs. 17(a) and 17(b)); the combination having flap blowing of 28 percent of total thrust did not alleviate stalling except at the highest thrust coefficient (fig. 17(c)).

Comparison of results with leading-edge, flap, and combined blowing.- A comparison of lift and drag characteristics for the 45-15 flap deflection at a thrust coefficient of approximately 2.0 is presented in figure 25 for leading-edge blowing, flap blowing, and combined leading-edge and flap blowing. For the combined blowing, about 28 percent of the thrust was from flap blowing and about 72 percent was from leading-edge blowing. The lift results of figure 25 show a high level of powered lift and good stall protection with leading-edge blowing. Flap blowing provided an improvement in flow turning over the flap and attendant higher lift at low and moderate angles of attack in comparison to leading-edge blowing. The lack of leading-edge flow protection with flap blowing caused an early abrupt stall which was followed by a large loss in lift. The lift characteristics obtained with combined leading-edge and flap blowing provided the highest overall lift obtained in this investigation. With combined blowing, the leading-edge blowing provided the same type of stall protection provided by a good leading-edge high-lift device, and a maximum lift coefficient of 8.1 was achieved. However, the need for some type of leading-edge device with combined blowing is still evident at the highest angle of attack (fig. 25). The present leading-edge blowing arrangement demonstrates the aerodynamic capabilities of this form of upper-surface blowing alone or in combination with flap blowing. A practical airplane design would have to use some form of leading-edge protection, however, to avoid the early and abrupt stall encountered without leading-edge blowing.

SUMMARY OF RESULTS

A low-speed investigation was made of the static turning characteristics and powered-lift aerodynamic performance of an upper-surface blown transport configuration having leading-edge blowing across the wing span. The results obtained may be summarized as follows:

1. Static turning angles increased with increasing total deflection of the flap, and a maximum turning angle of about 84° was obtained with a total deflection of 100°. Static-thrust-recovery efficiencies generally decreased with increasing total flap deflection, with the lowest efficiencies being between 0.6 and 0.7.

2. Static turning angles obtained with blowing at the knee of the flap were consistently higher than with leading-edge blowing; however, wind-on lift coefficients at 0° angle of attack were essentially the same for these two modes of blowing.

3. Power-on lift coefficients obtained at 0° angle of attack showed that various optimal combinations of forward- and rear-element deflections were obtained. Increases in total flap deflection beyond these optimal deflections

caused the lift to decrease. Generally, the 45° deflection of the forward flap element provided the highest lift for a given deflection of the rear flap element.

4. The model wing did not have a leading-edge high-lift device and consequently the wing stalled at fairly low angles of attack with no blowing or with blowing only at the flap knee. Application of increasing amounts of leading-edge blowing generally delayed the stall to higher angles of attack for forward-element deflections up to 45°.

5. Very small amounts of flap blowing along with leading-edge blowing caused appreciable losses in lift with combined blowing compared with leading-edge blowing alone. The highest flap blowing (28 percent of the total blowing) provided the highest lift coefficient obtained in this investigation, slightly over 8.0, for a total thrust coefficient of about 2.0.

Langley Research Center
National Aeronautics and Space Administration
Hampton, VA 23665
September 29, 1977

REFERENCES

1. Smith, Charles C., Jr.; Phelps, Arthur E., III; and Copeland, W. Latham: Wind-Tunnel Investigation of a Large-Scale Semispan Model With an Unswept Wing and an Upper-Surface Blown Jet Flap. NASA TN D-7526, 1974.

2. Phelps, Arthur E., III; and Smith, Charles C., Jr.: Wind-Tunnel Investigation of an Upper Surface Blown Jet-Flap Powered-Lift Configuration. NASA TN D-7399, 1973.

3. Phelps, Arthur E.; Letko, William; and Henderson, Robert L.: Low-Speed Wind-Tunnel Investigation of a Semispan STOL Jet Transport Wing-Body With an Upper-Surface Blown Jet Flap. NASA TN D-7183, 1973.

4. Sleeman, William C., Jr.; and Hohlweg, William C.: Low-Speed Wind-Tunnel Investigation of a Four-Engine Upper Surface Blown Model Having a Swept Wing and Rectangular and D-Shaped Exhaust Nozzles. NASA TN D-8061, 1975.

5. Johnson, William G., Jr.: Aerodynamic Characteristics of a Powered, Externally Blown Flap STOL Transport Model With Two Engine Simulator Sizes. NASA TN D-8057, 1975.

6. Mechtly, E. A.: The International System of Units - Physical Constants and Conversion Factors (Second Revision). NASA SP-7012, 1973.

7. Heyson, Harry H.: Use of Superposition in Digital Computers To Obtain Wind-Tunnel Interference Factors for Arbitrary Configurations, With Particular Reference to V/STOL Models. NASA TR R-302, 1969.

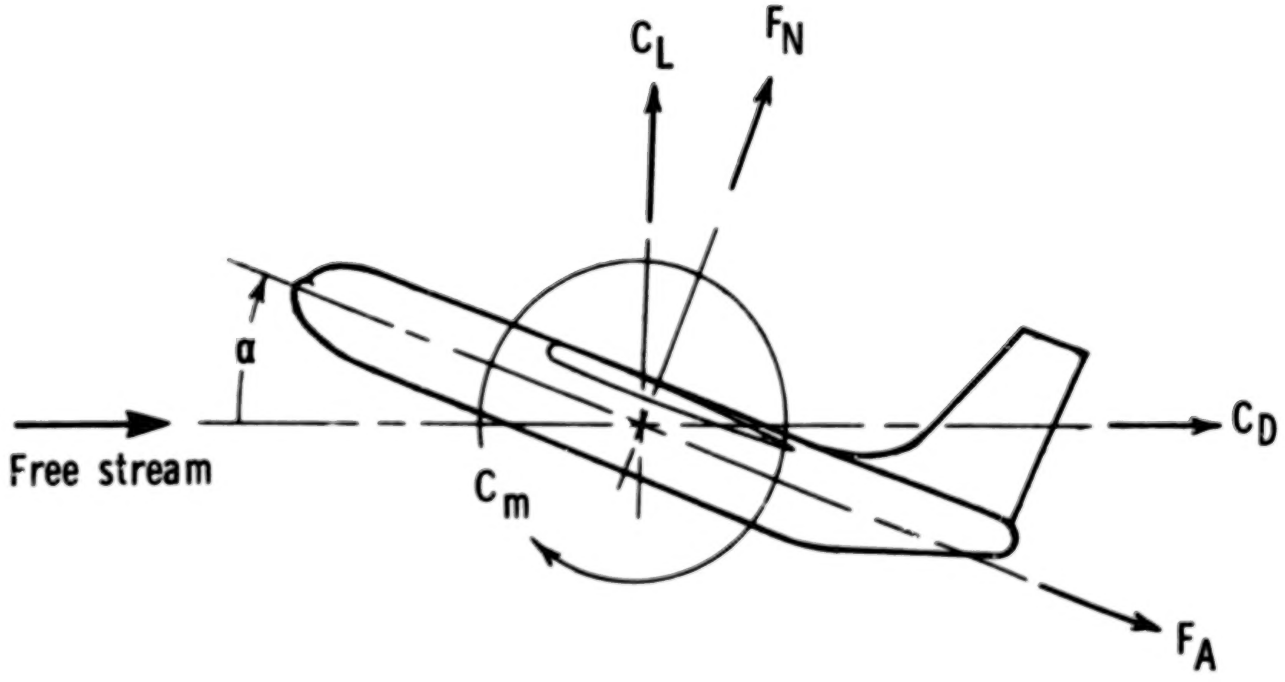

Figure 1.- System of axes. Positive directions of forces, moments, and angle of attack are indicated by arrows.

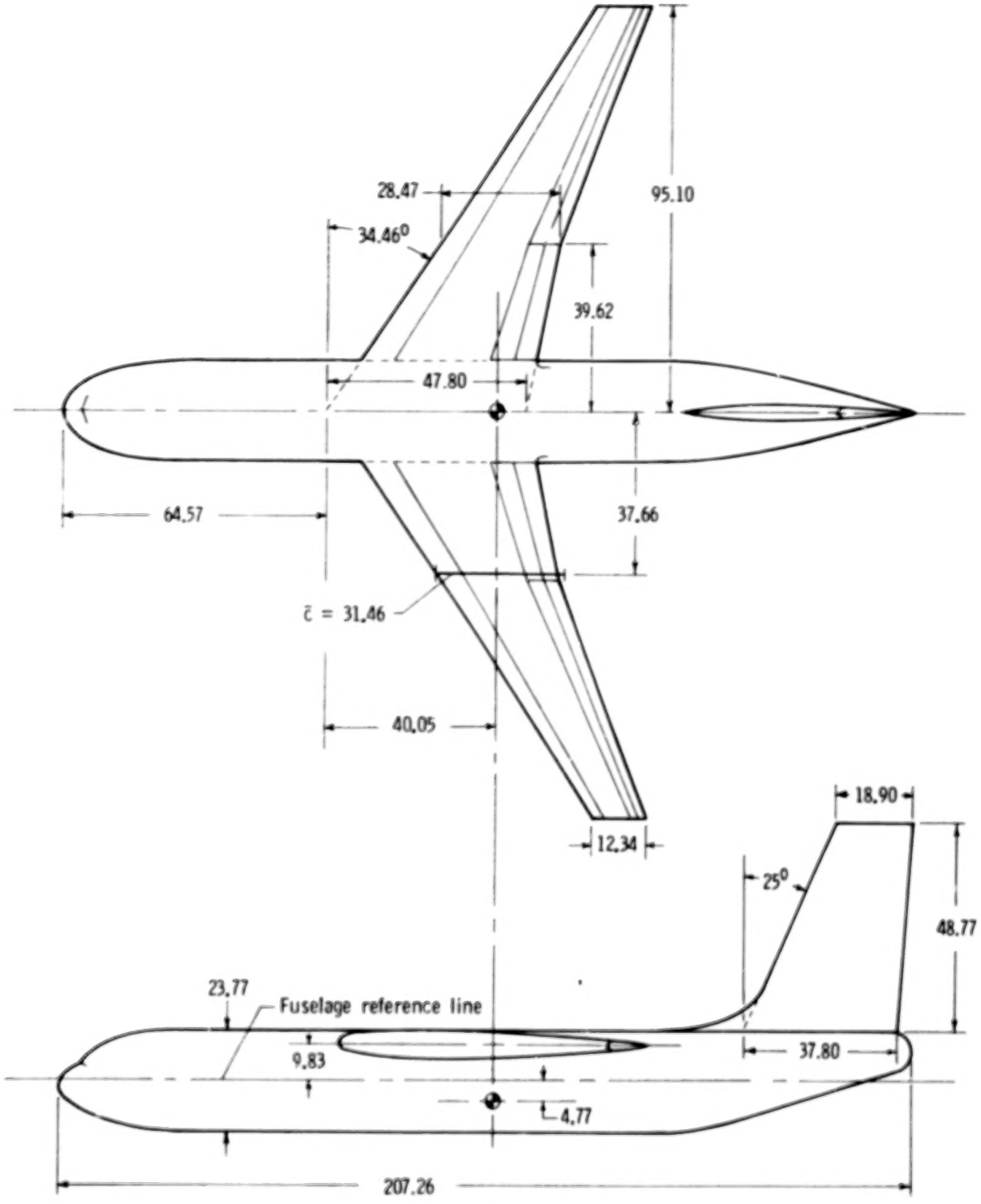

(a) General arrangement and principal dimensions of model.

Figure 2.- Geometric characteristics of model. All dimensions are in centimeters.

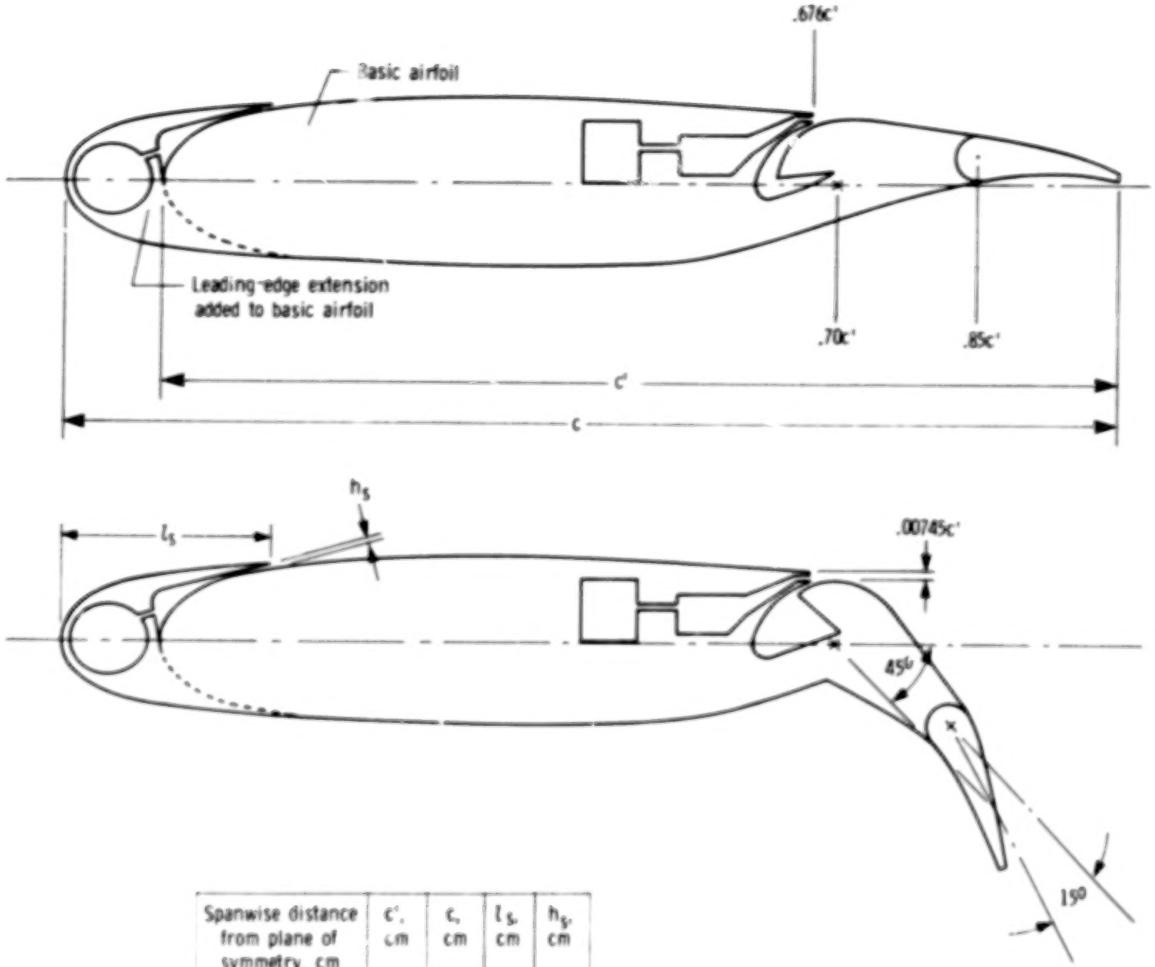

Spanwise distance from plane of symmetry, cm	c', cm	c, cm	l_s, cm	h_s, cm
0 (root)	44.42	47.80	---	----
11.89 (fuselage)	38.88	42.00	6.98	0.102
39.62 (break)	25.93	28.47	5.47	.076
95.10 (tip)	10.97	12.34	2.43	.025

(b) Airfoil section with extended leading edge and with 45-15 flap deflection.

Figure 2.- Concluded.

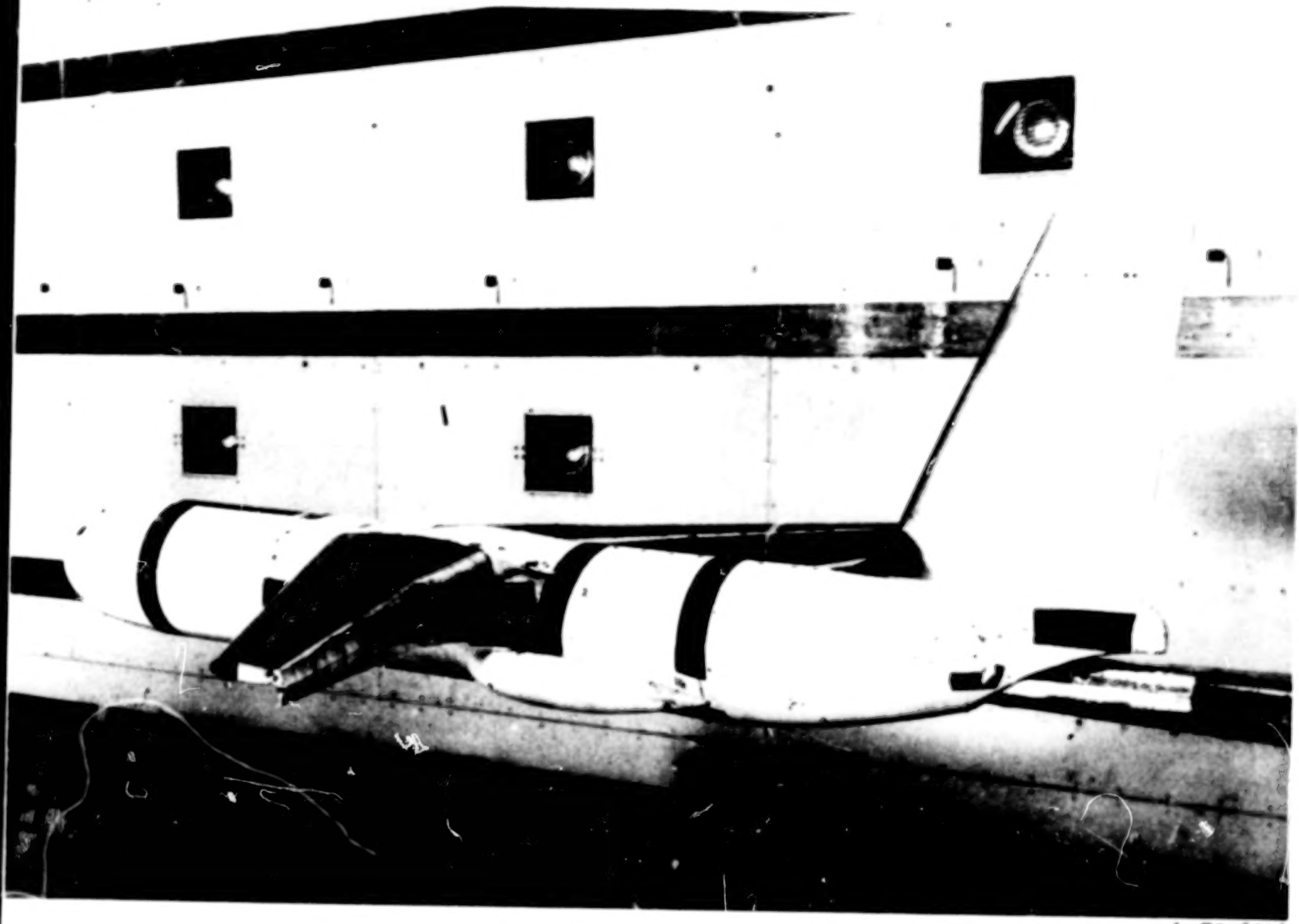

L-73-6326

(a) General view.

Figure 3.- Model in Langley V/STOL tunnel.

L-73-5446

(b) Upper surface of wing showing forward and rear slots.

Figure 3.- Concluded.

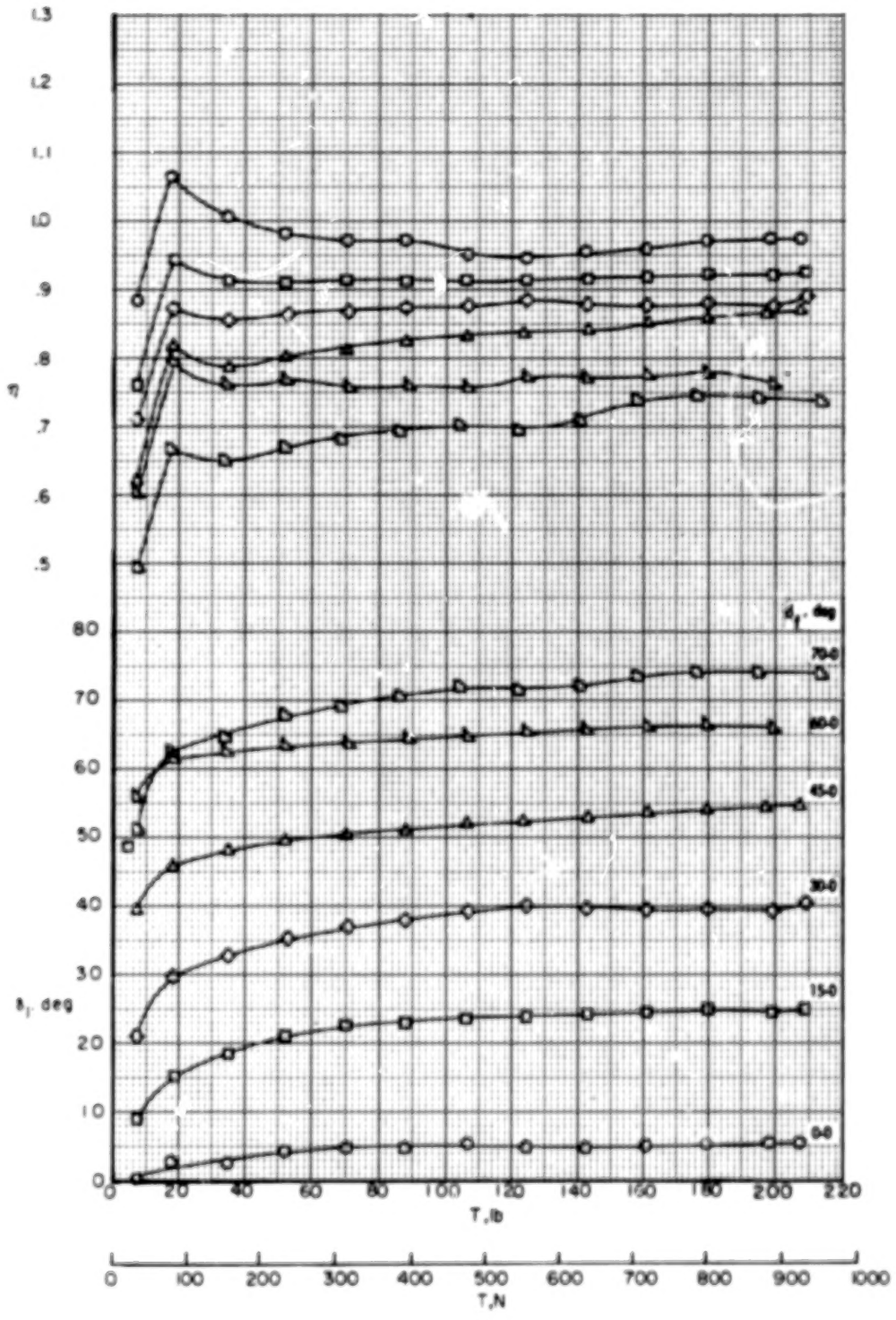

(a) Rear-element deflection, 0°.

Figure 4.- Effects of forward-element deflection on static turning characteristics and static-thrust-recovery efficiency characteristics of model with leading-edge blowing.

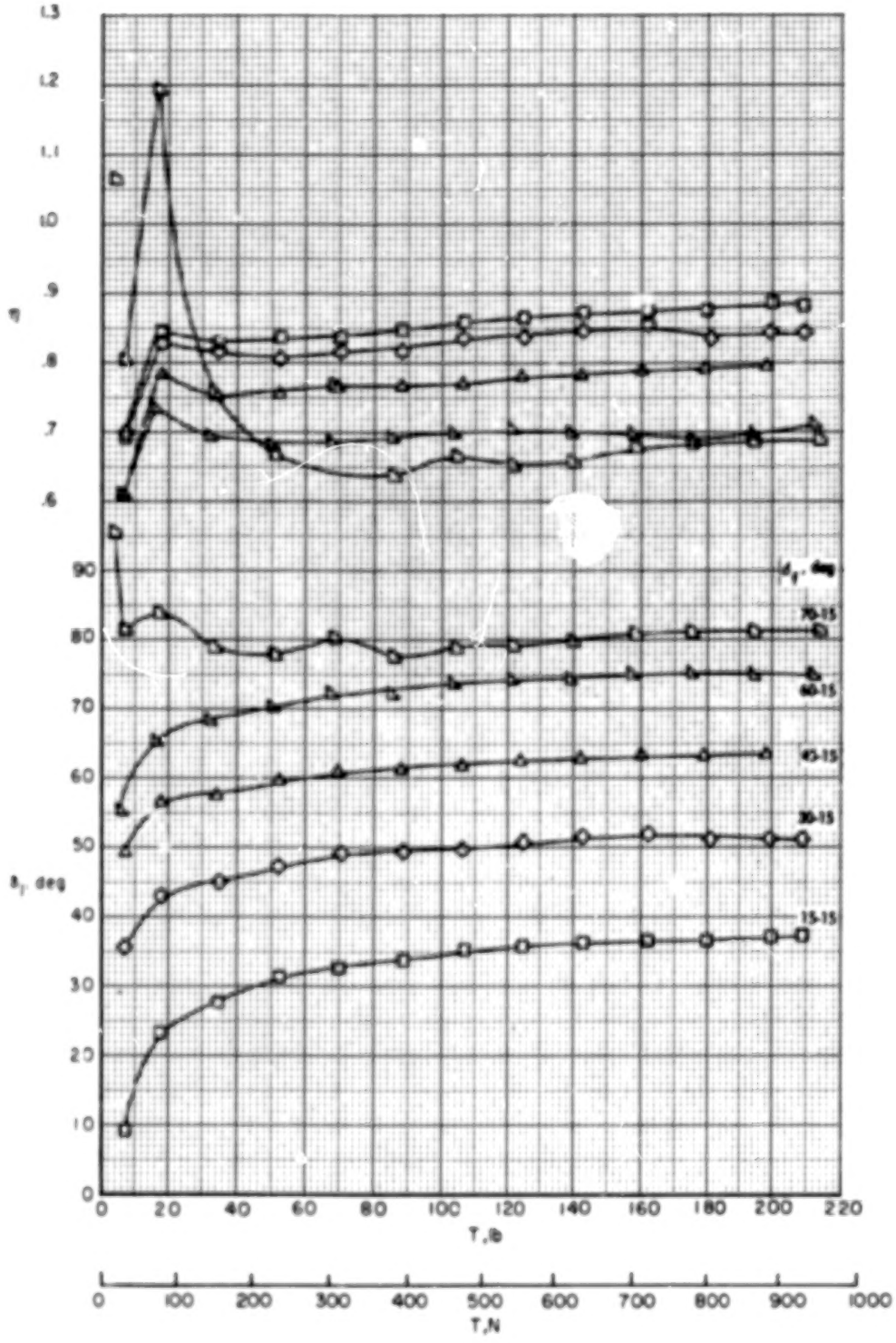

(b) Rear-element deflection, 15°.

Figure 4.- Continued.

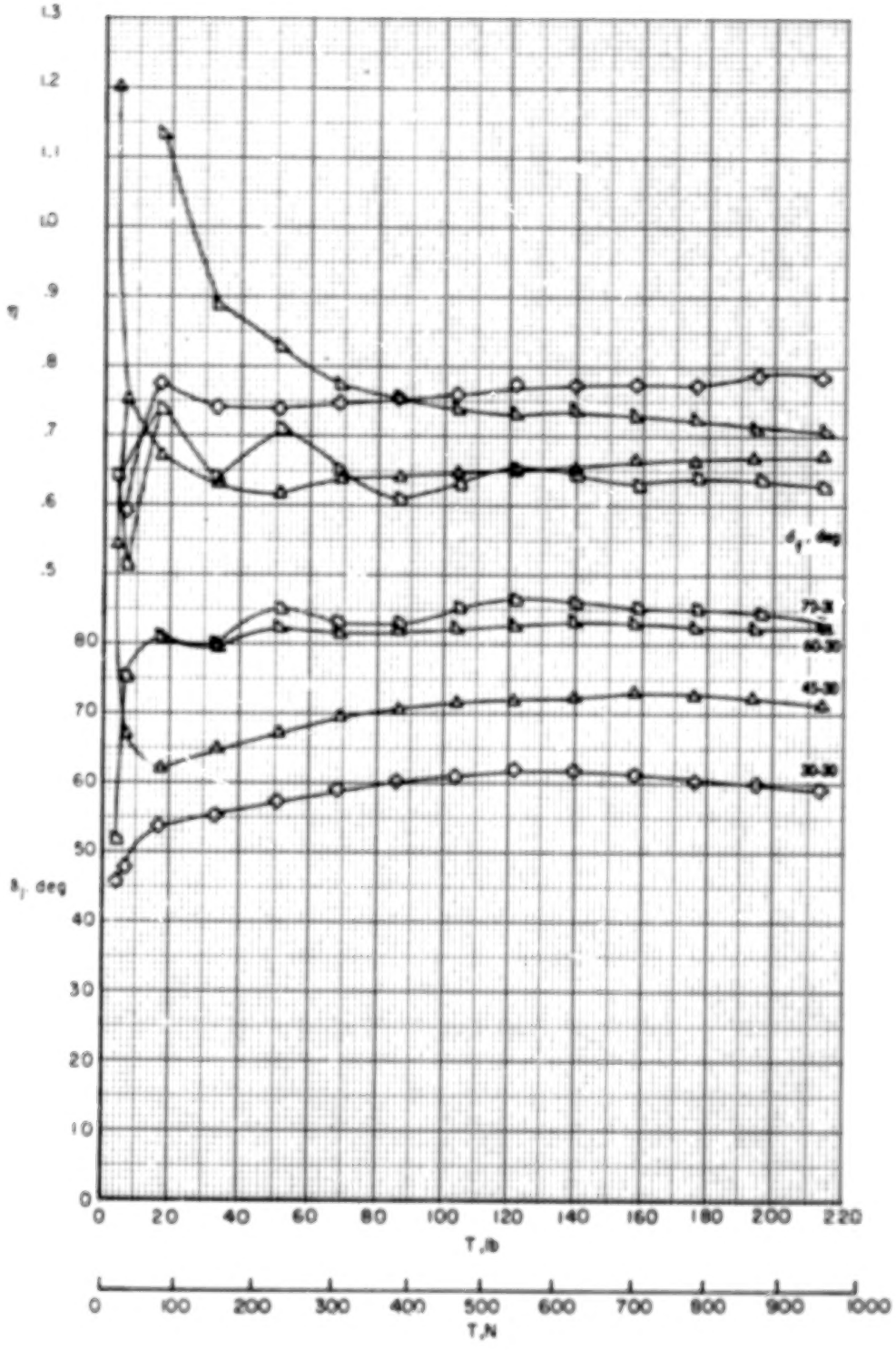

(c) Rear-element deflection, 30°.

Figure 4.- Continued.

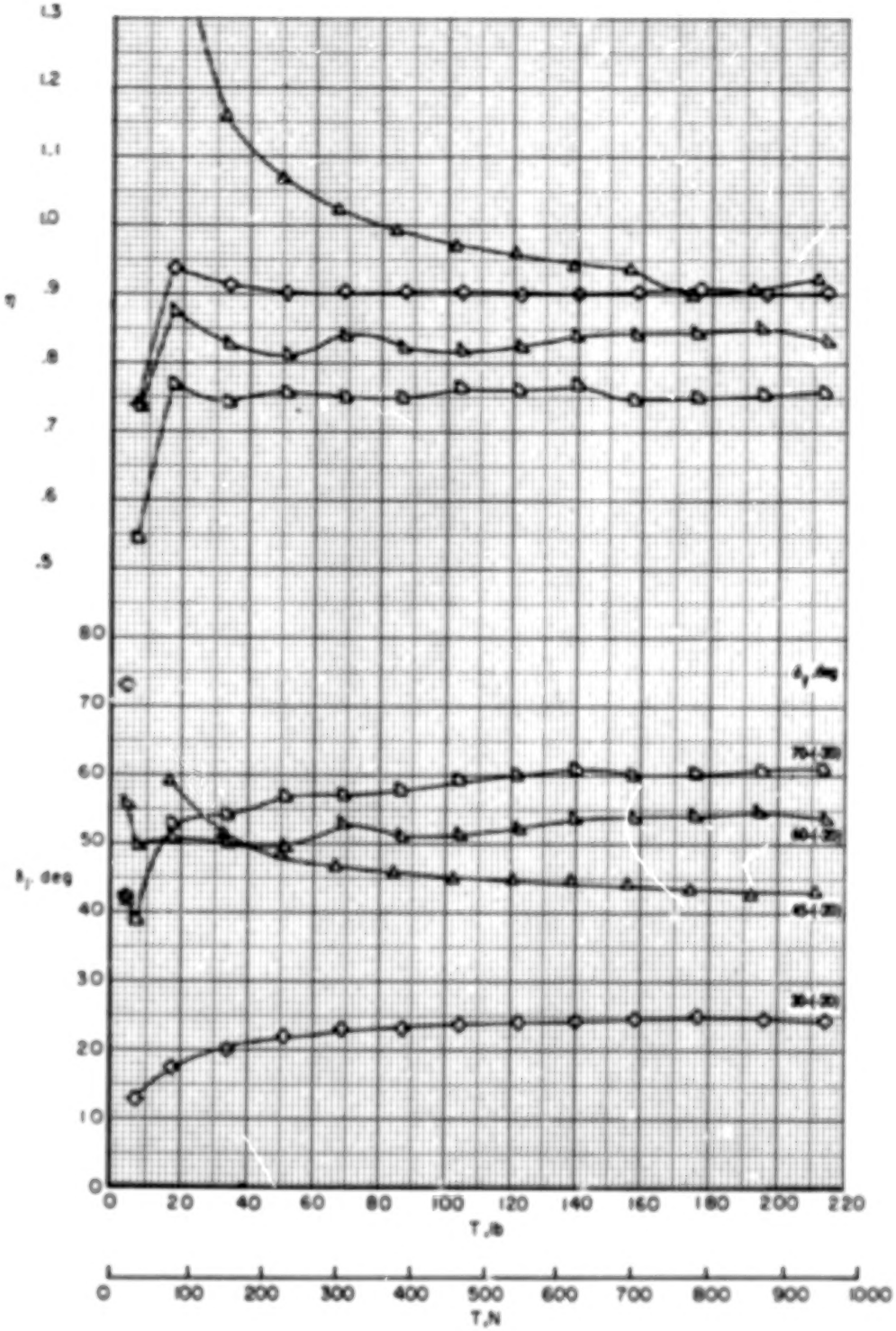

(d) Rear-element deflection, -20°.

Figure 4.- Concluded.

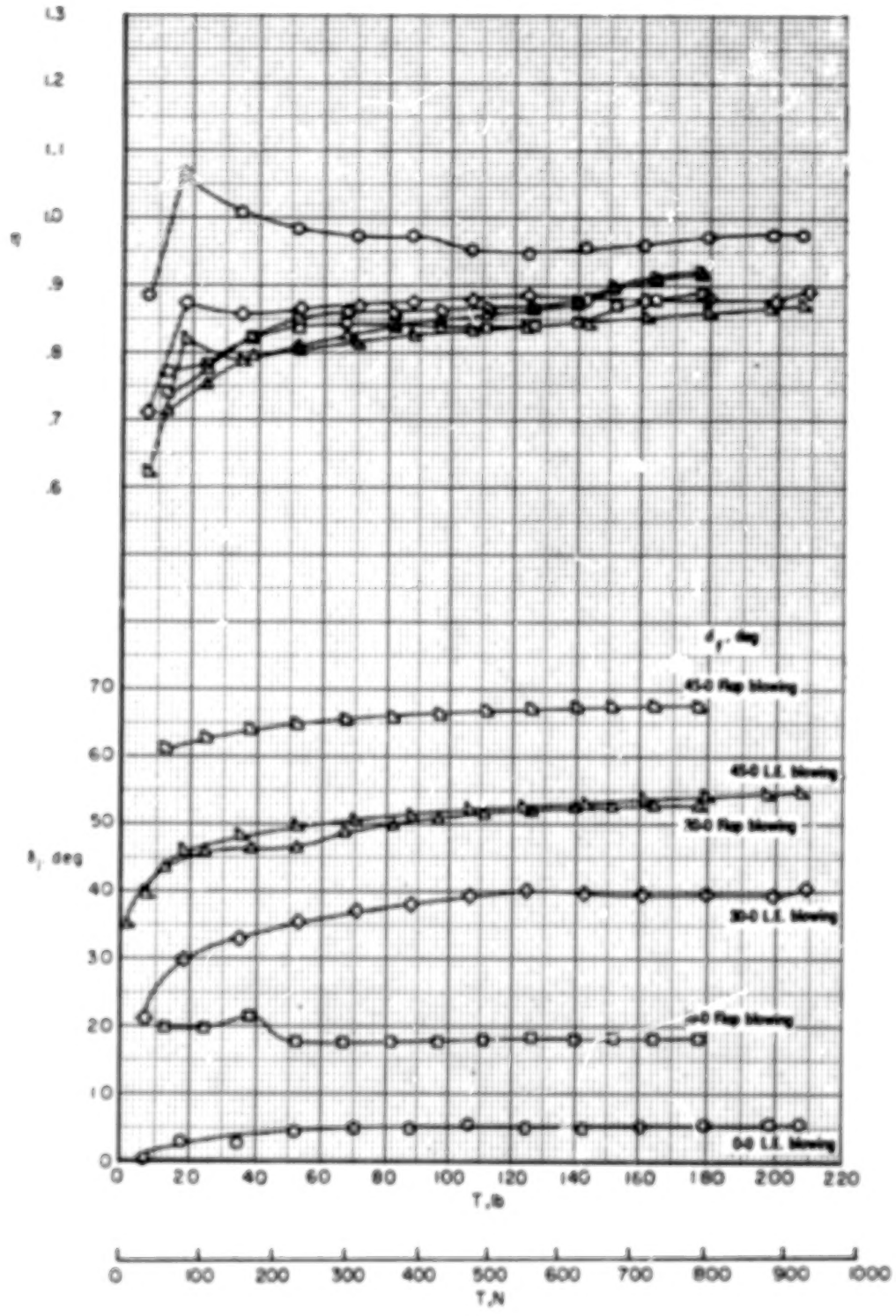

(a) δ_f = 0-0, 30-0, and 45-0.

Figure 5.- Comparison of static turning characteristics and static-thrust-recovery efficiency characteristics obtained with leading-edge blowing alone and flap blowing alone.

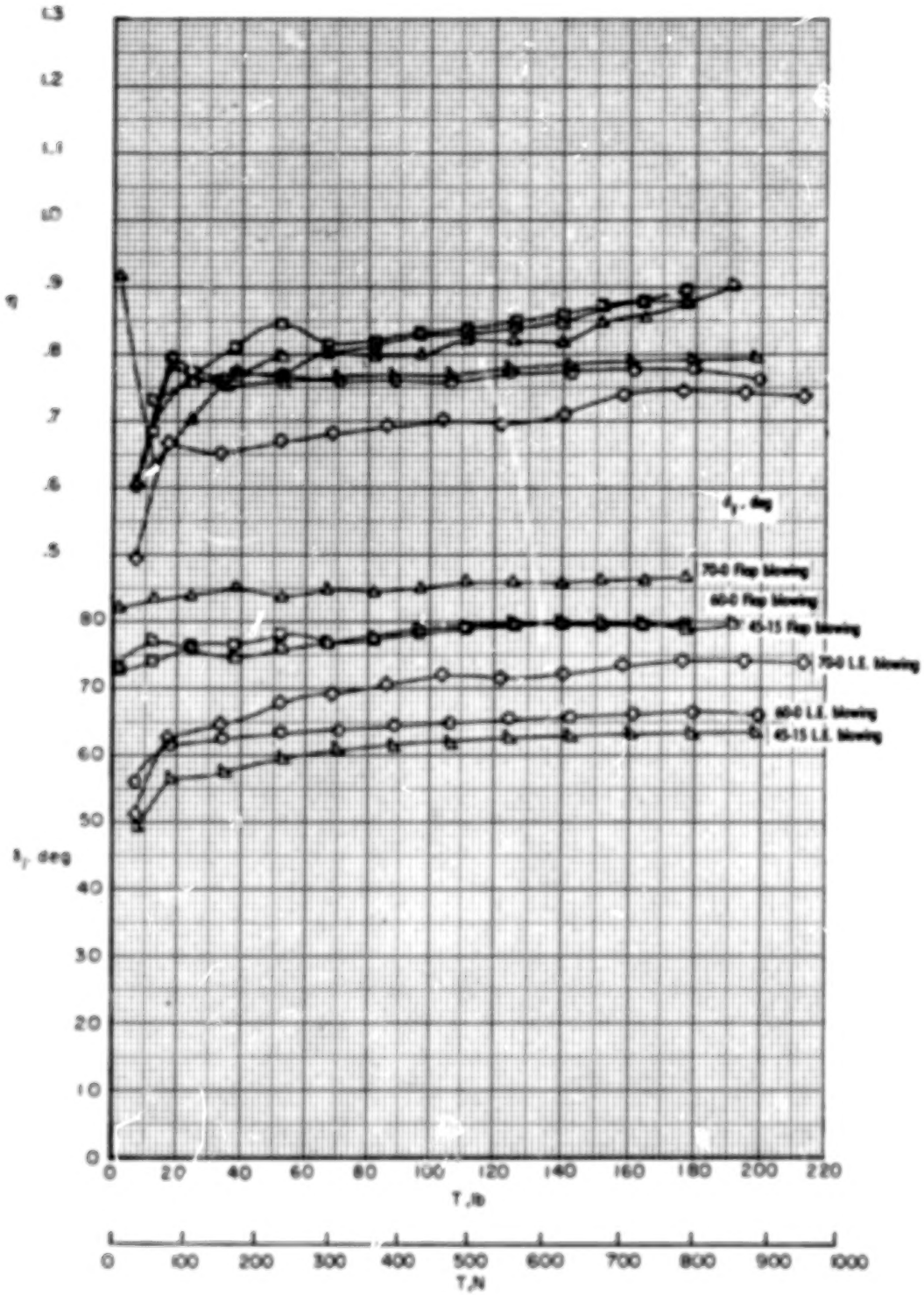

(b) δ_f = 45-15, 60-0, and 70-0.

Figure 5.- Concluded.

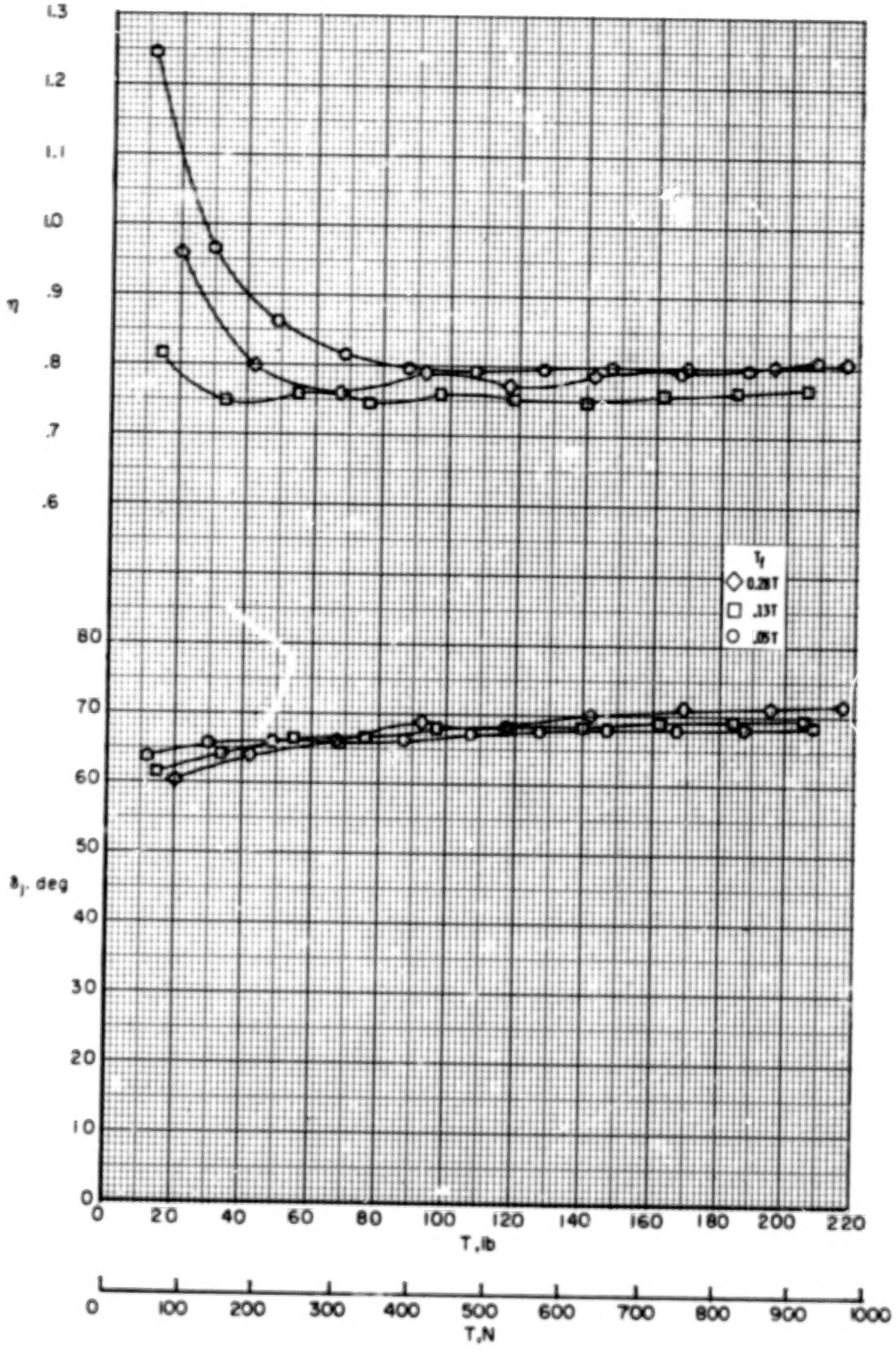

(a) δ_f = 60-0.

Figure 6.- Static turning and static-thrust-recovery efficiency for model with combined leading-edge blowing and flap blowing.

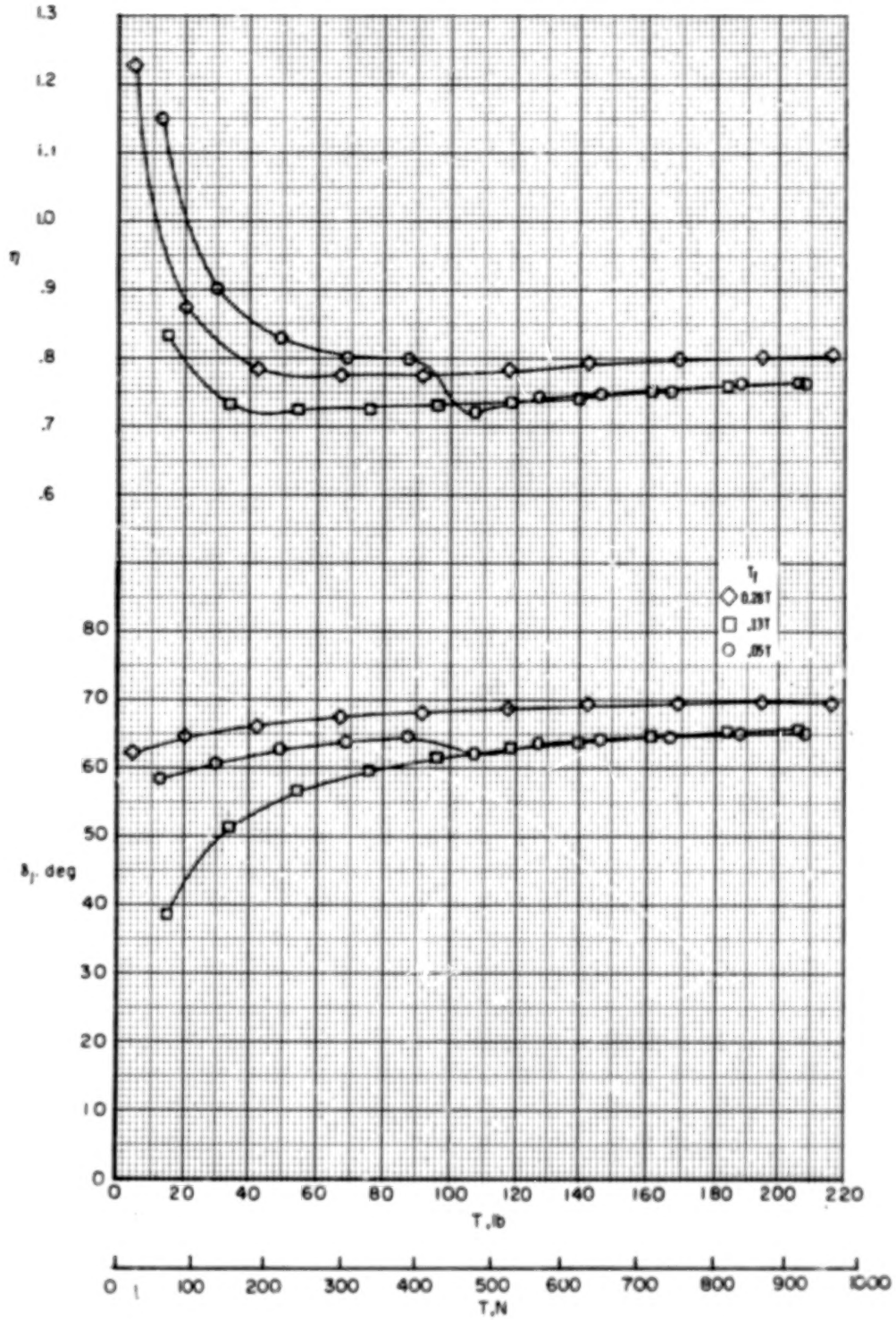

(b) δ_f = 45-15.

Figure 6.- Concluded.

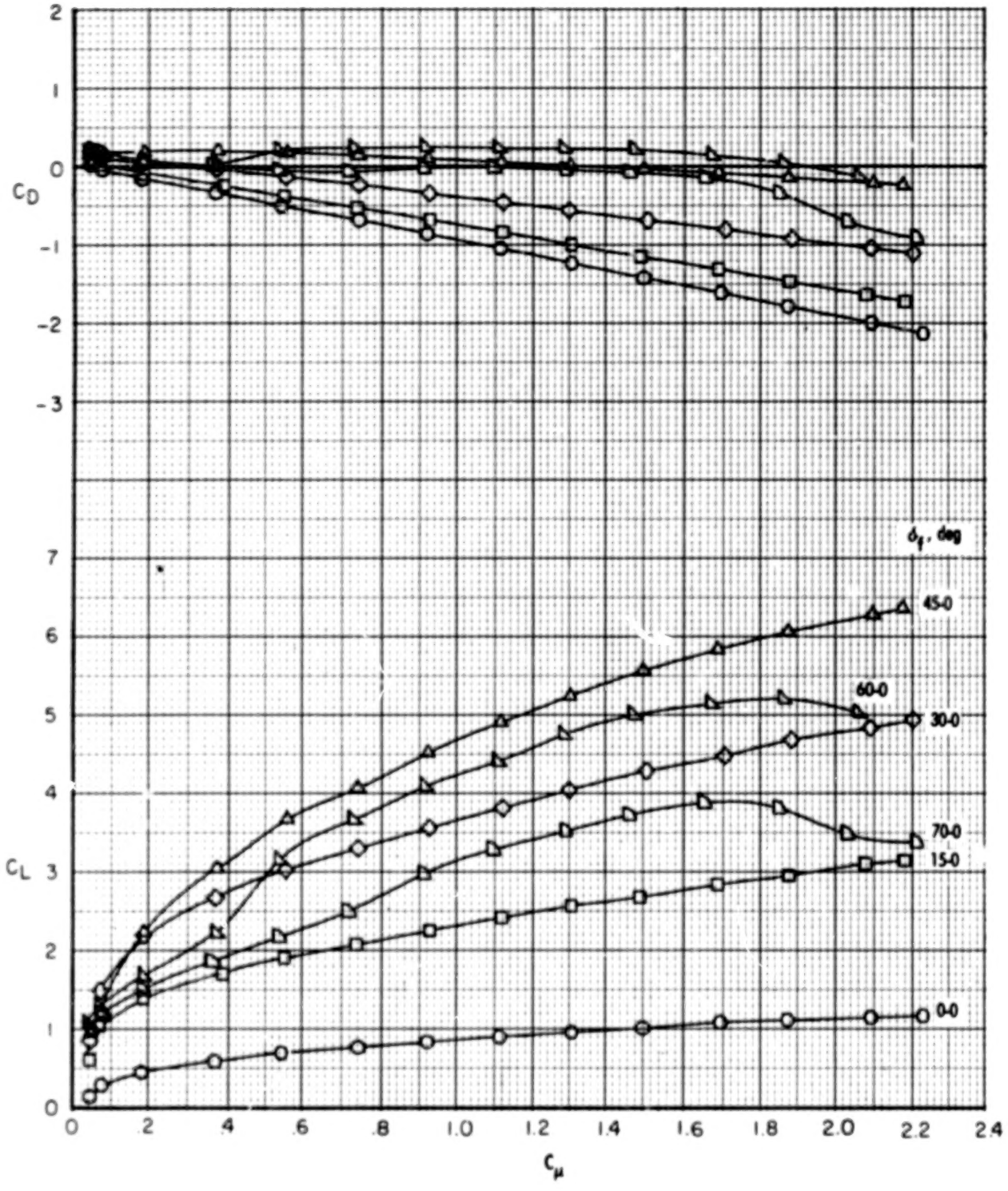

(a) Rear-element deflection, 0°.

Figure 7.- Effects of forward-element deflection on lift and drag coefficients of model at 0° angle of attack with leading-edge blowing.

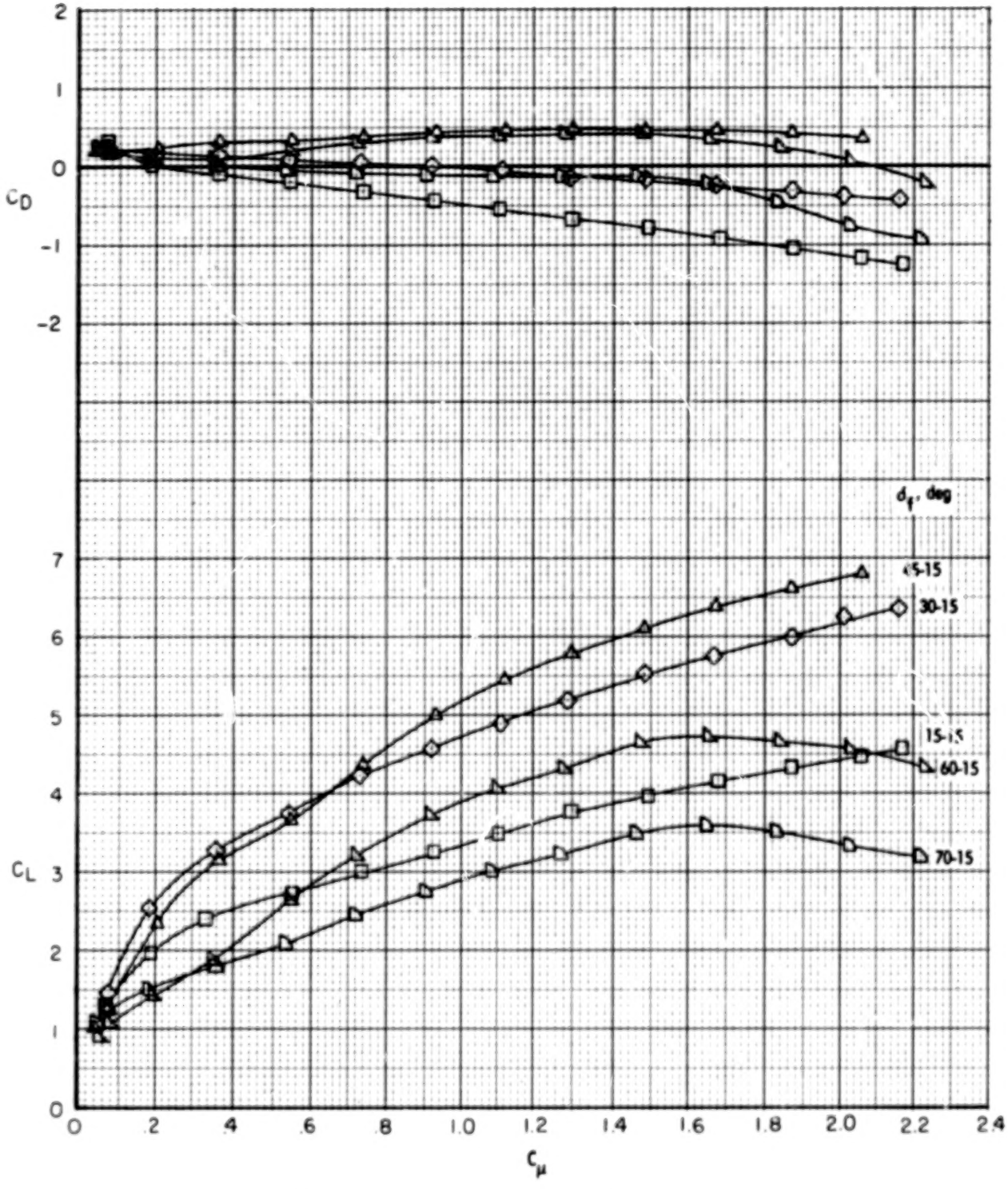

(b) Rear-element deflection, 15°.

Figure 7.- Continued.

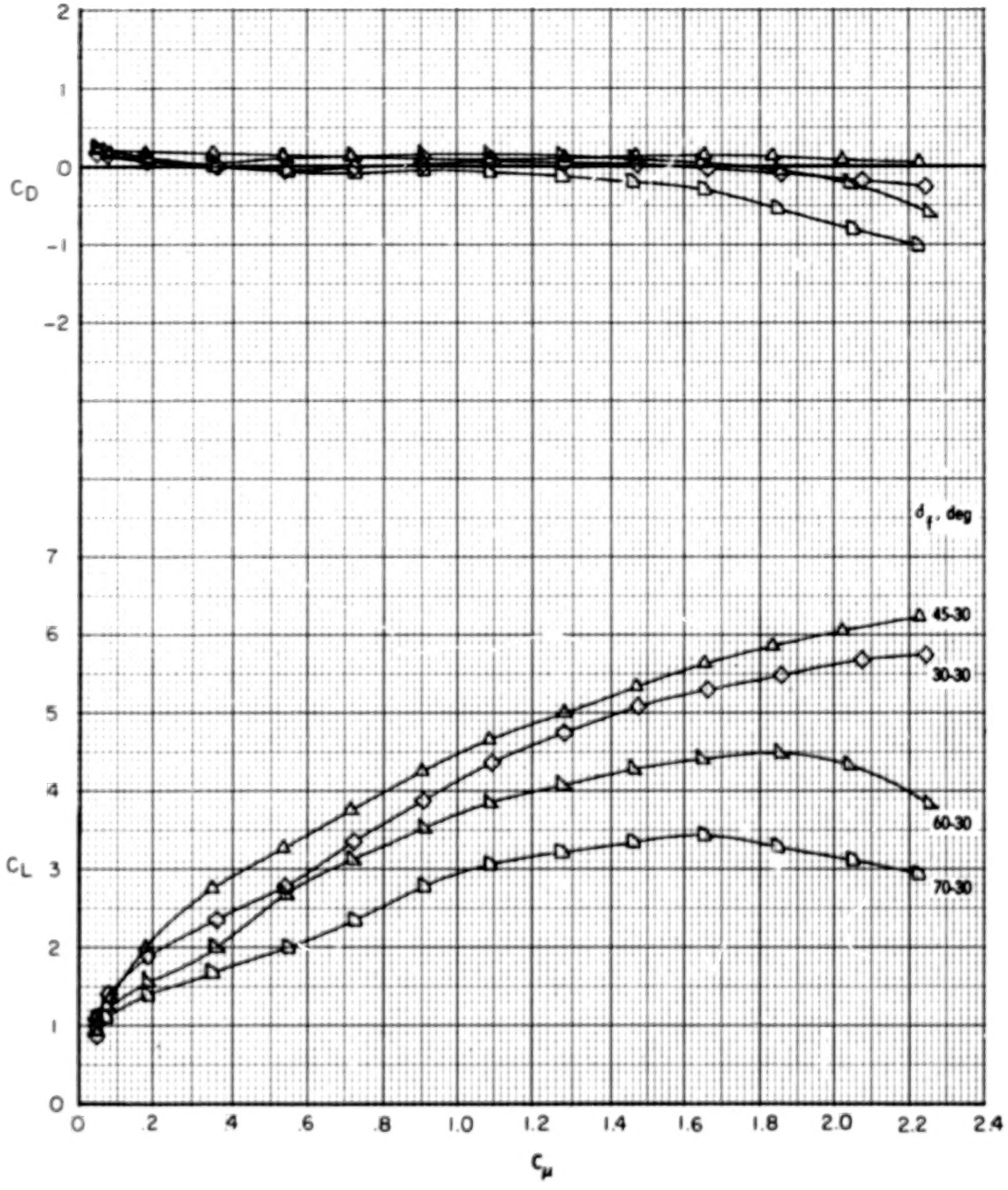

(c) Rear-element deflection, 30°.

Figure 7.- Continued.

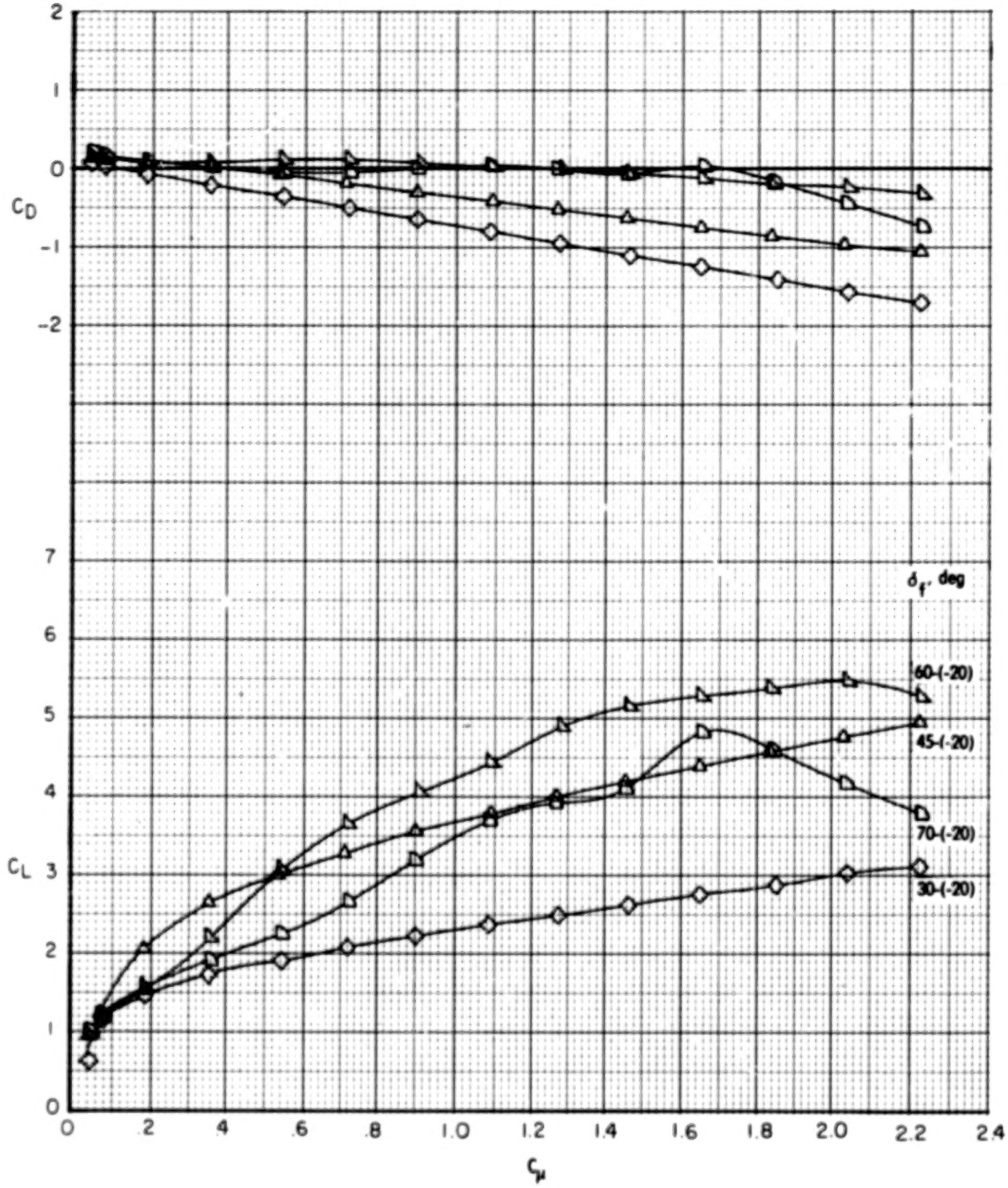

(d) Rear-element deflection, -20°.

Figure 7.- Concluded.

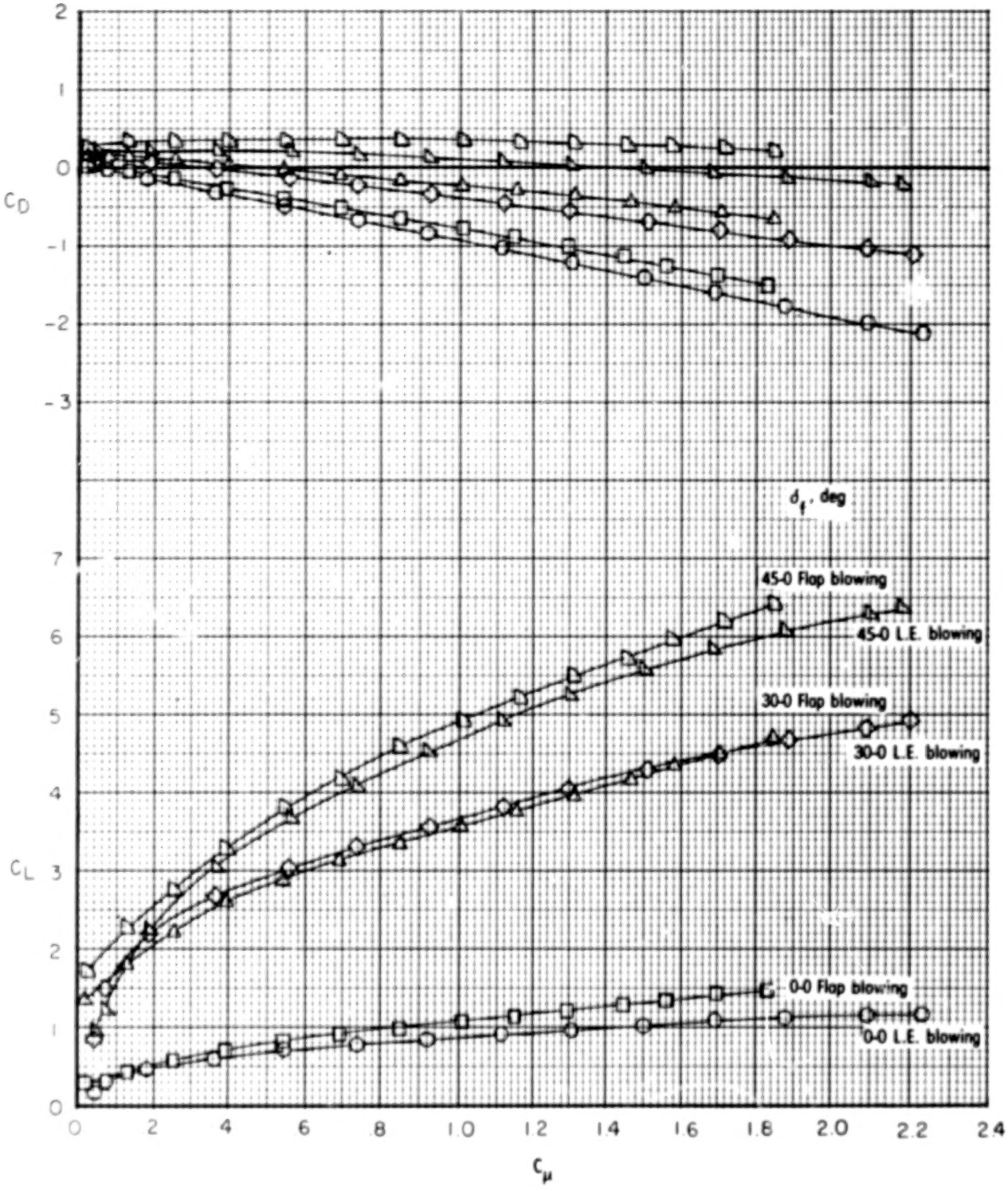

(a) δ_f = 0-0, 30-0, and 45-0.

Figure 8.- Comparison of lift and drag coefficients of model at 0° angle of attack obtained with leading-edge blowing alone and flap blowing alone.

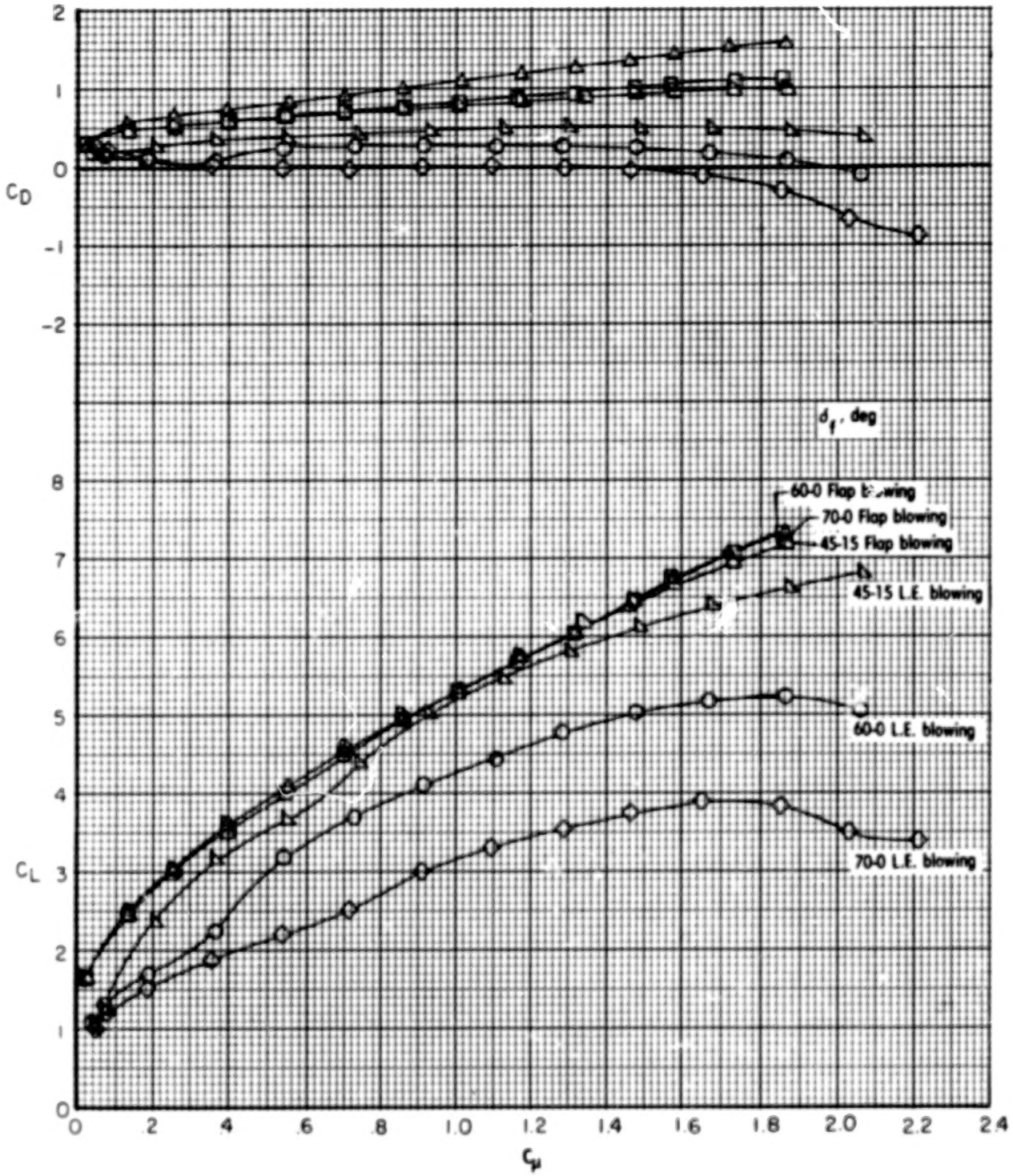

(b) δ_f = 45-15, 60-0, and 70-0.

Figure 8.- Concluded.

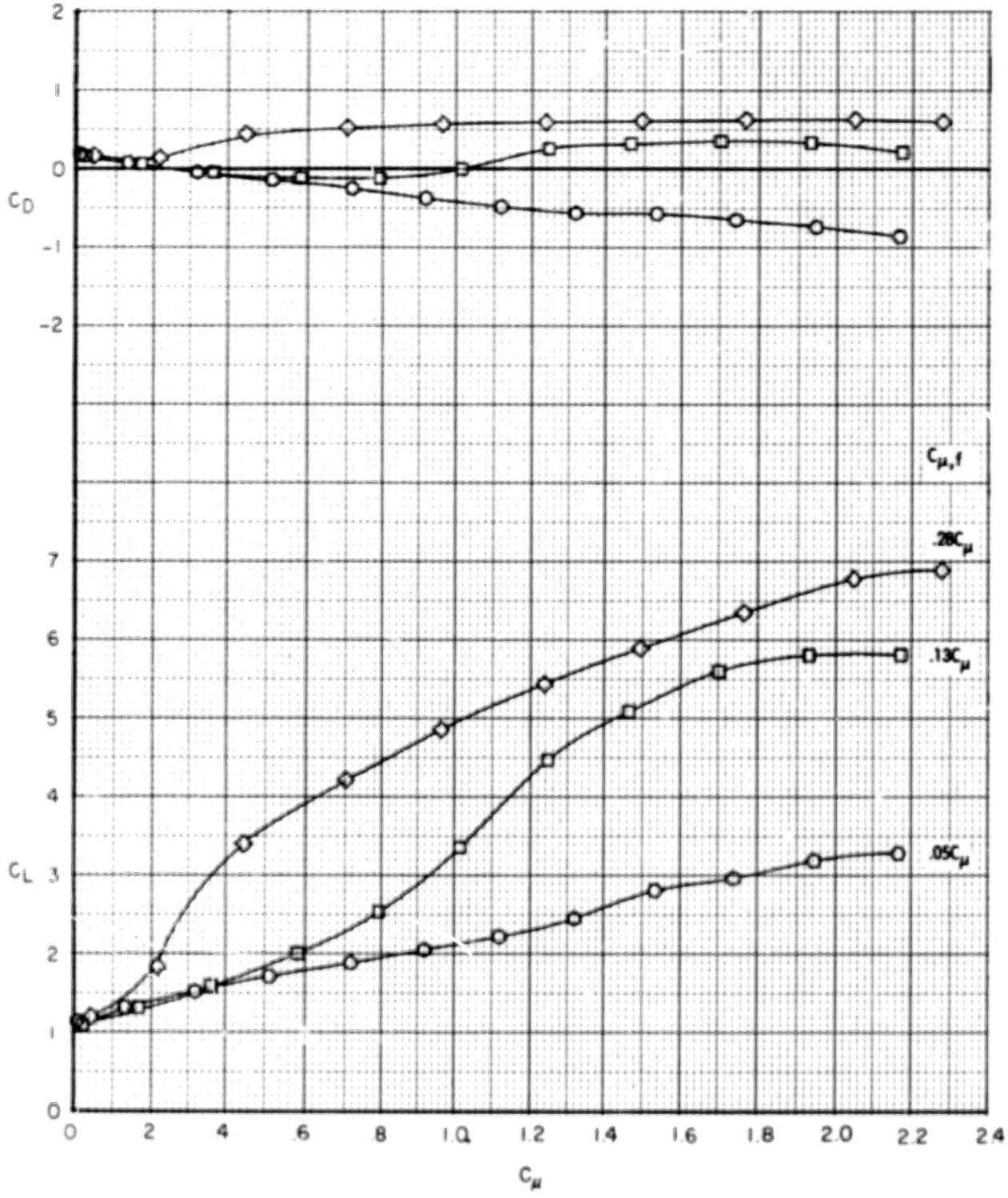

(a) δ_f = 60-0.

Figure 9.- Lift and drag coefficients at 0° angle of attack for model with combined leading-edge blowing and flap blowing.

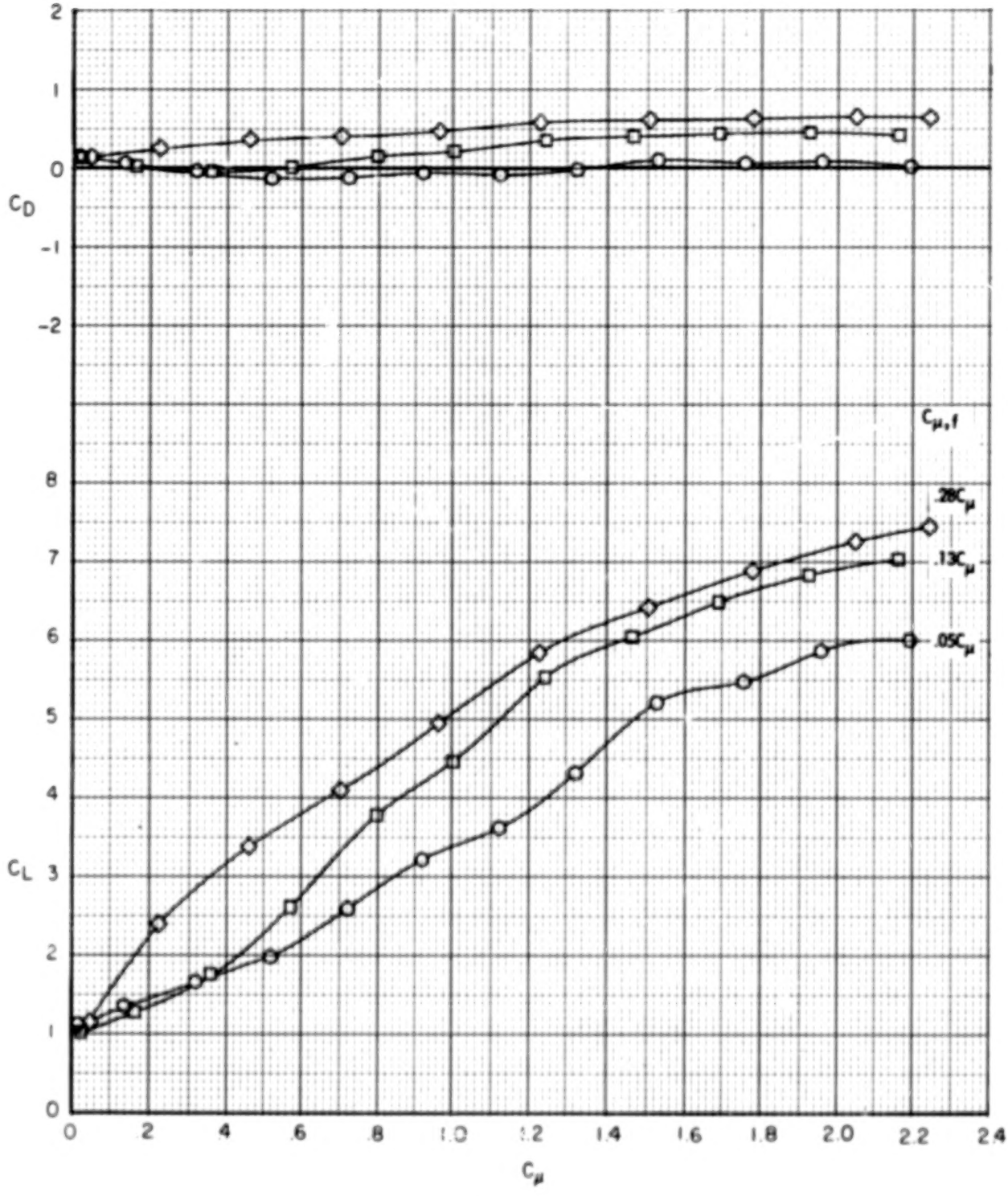

(b) δ_f = 45-15.

Figure 9.- Concluded.

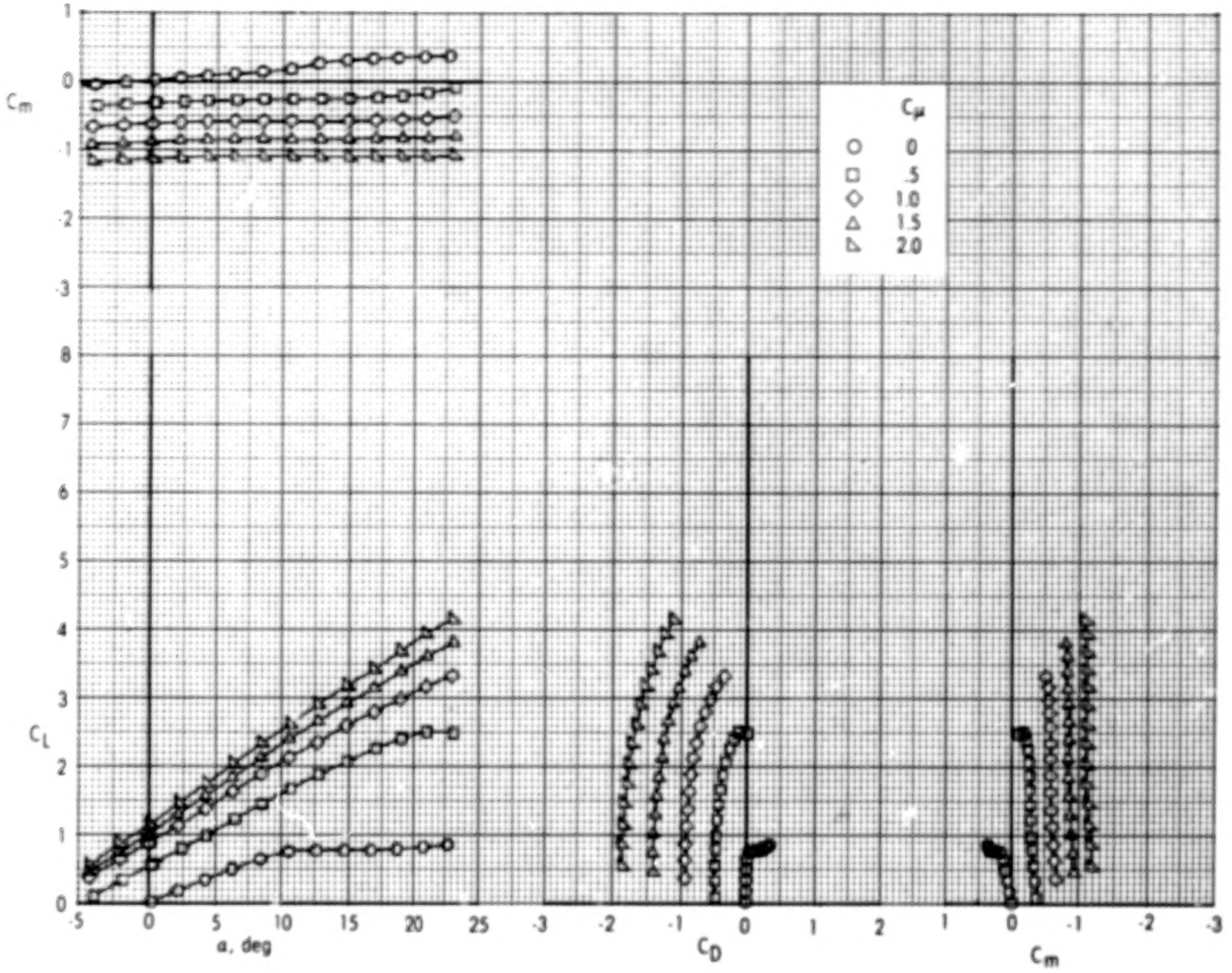

(a) δ_f = 0-0.

Figure 10.- Effect of thrust coefficient on longitudinal aerodynamic characteristics of model with leading-edge blowing and rear element undeflected.

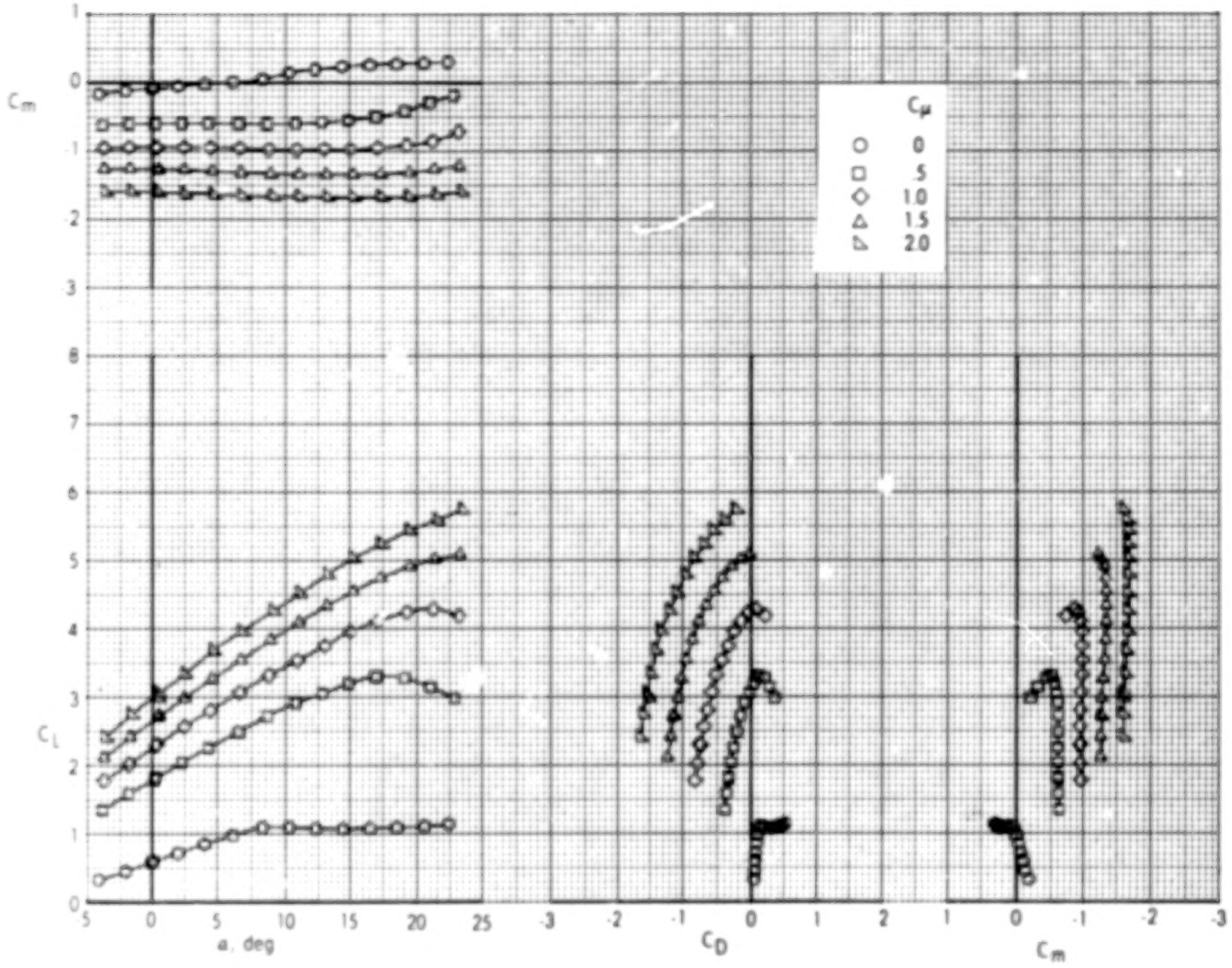

(b) δ_f = 15-0.

Figure 10.- Continued.

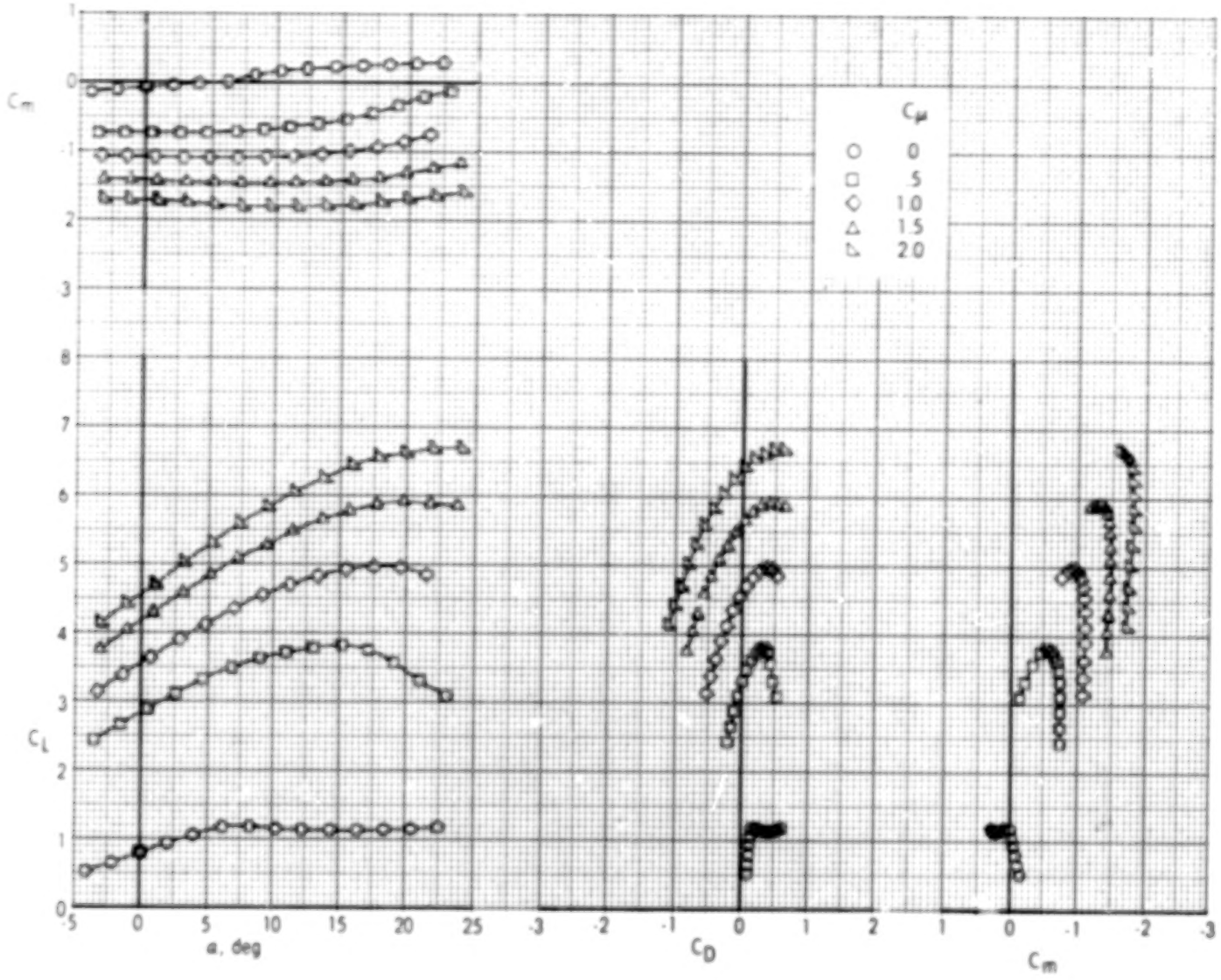

(c) δ_f = 30-0.

Figure 10.- Continued.

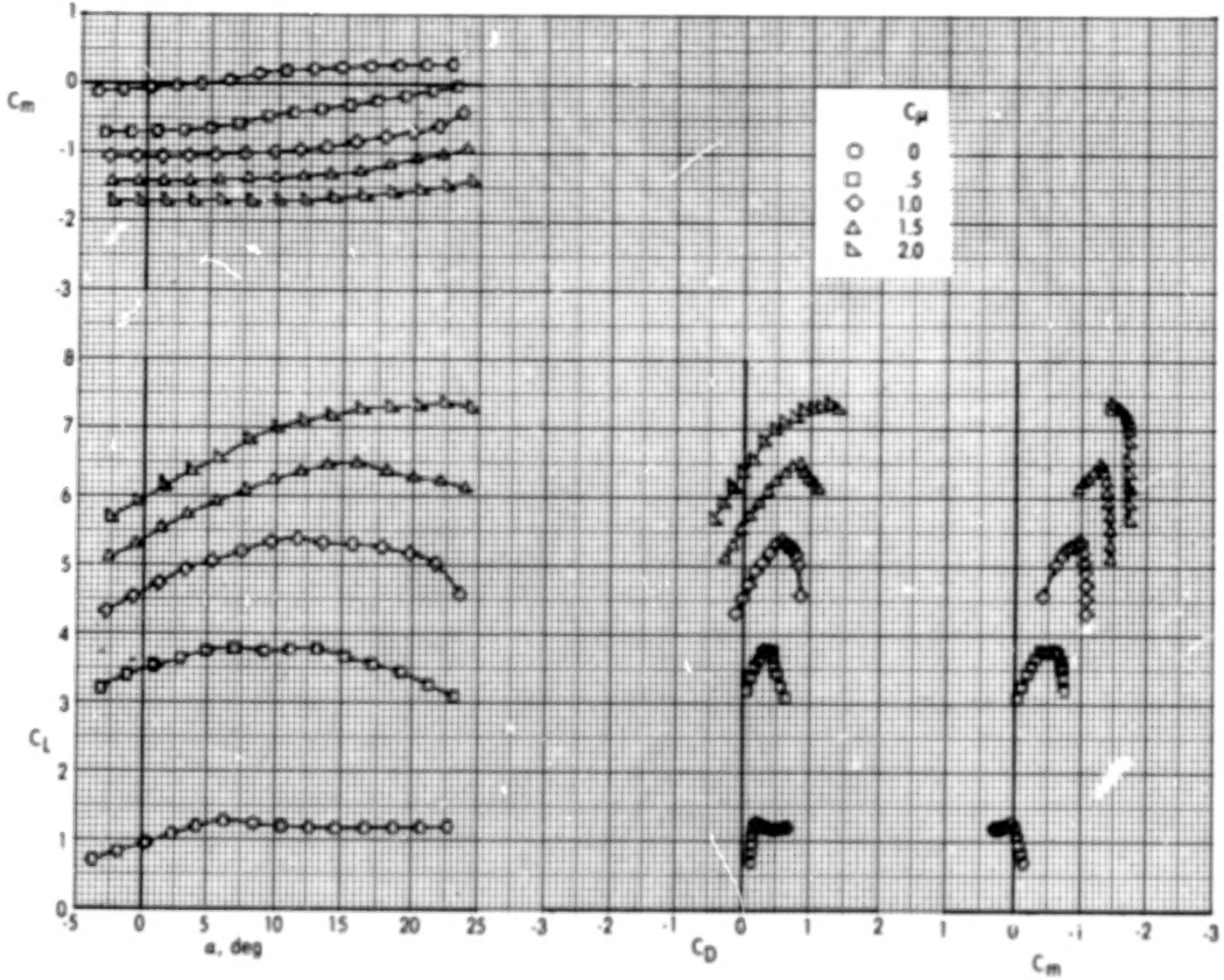

(d) δ_f = 45-0.

Figure 10.- Continued.

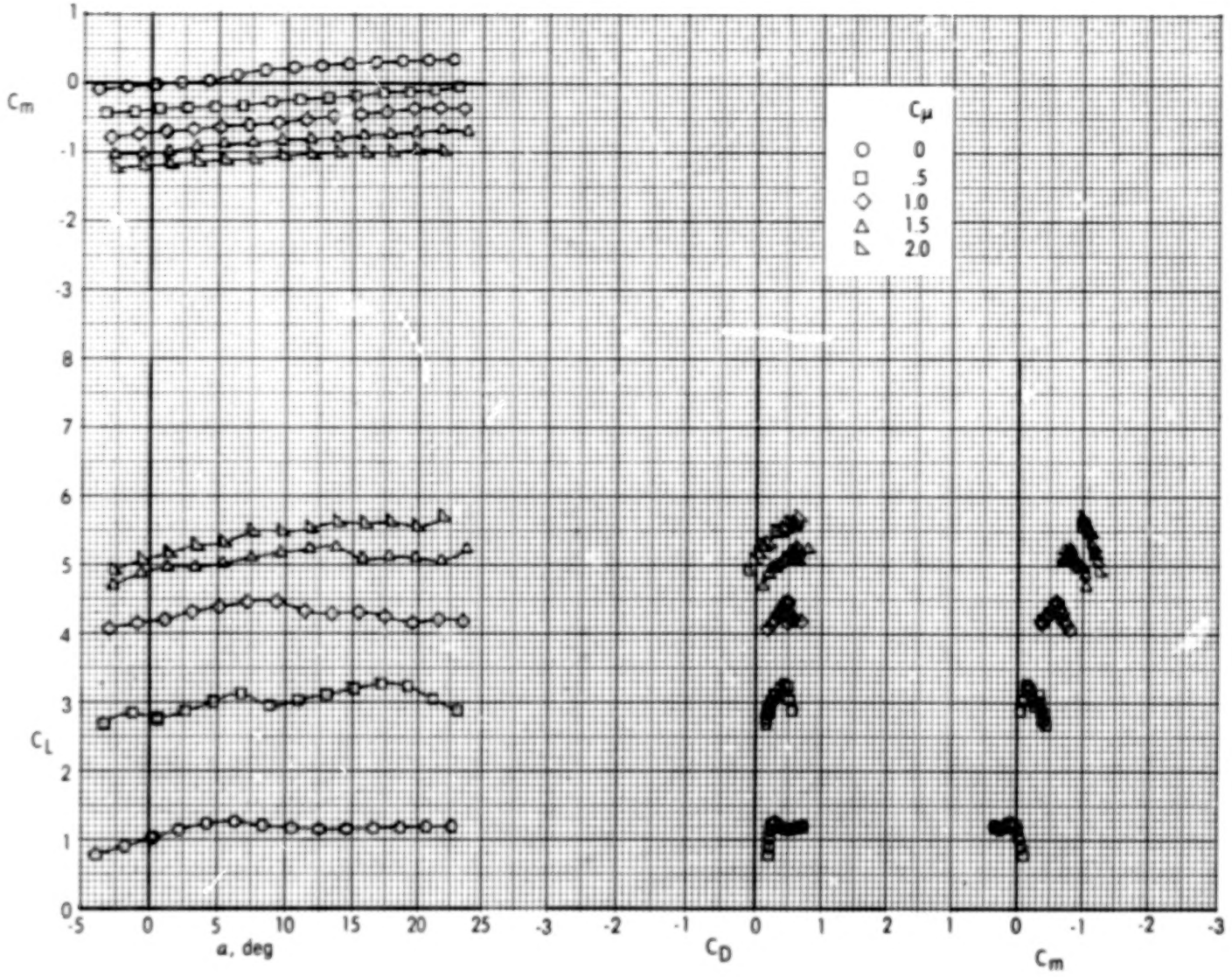

(e) δ_f = 60-0.

Figure 10.- Continued.

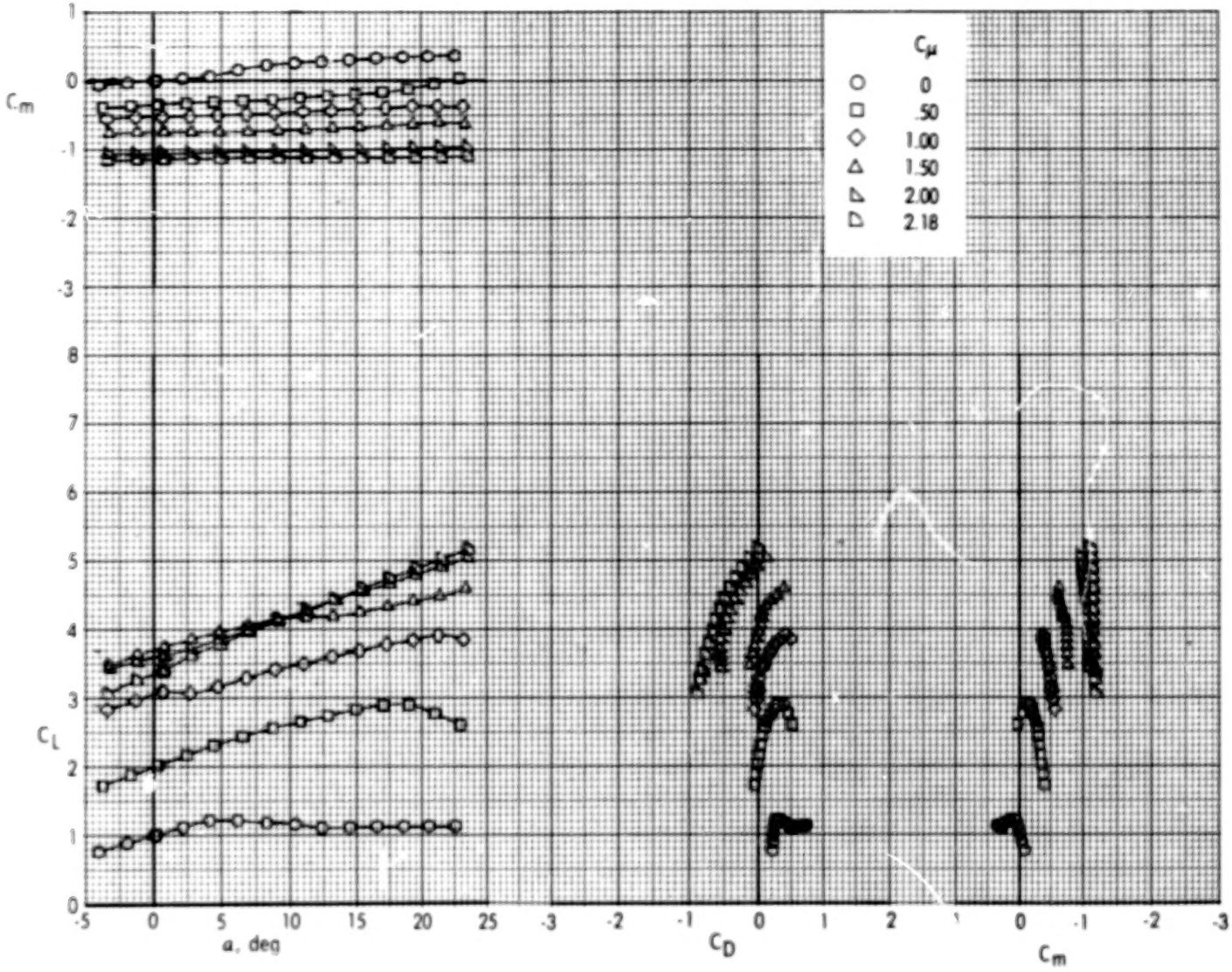

(f) δ_f = 70-0.

Figure 10.- Concluded.

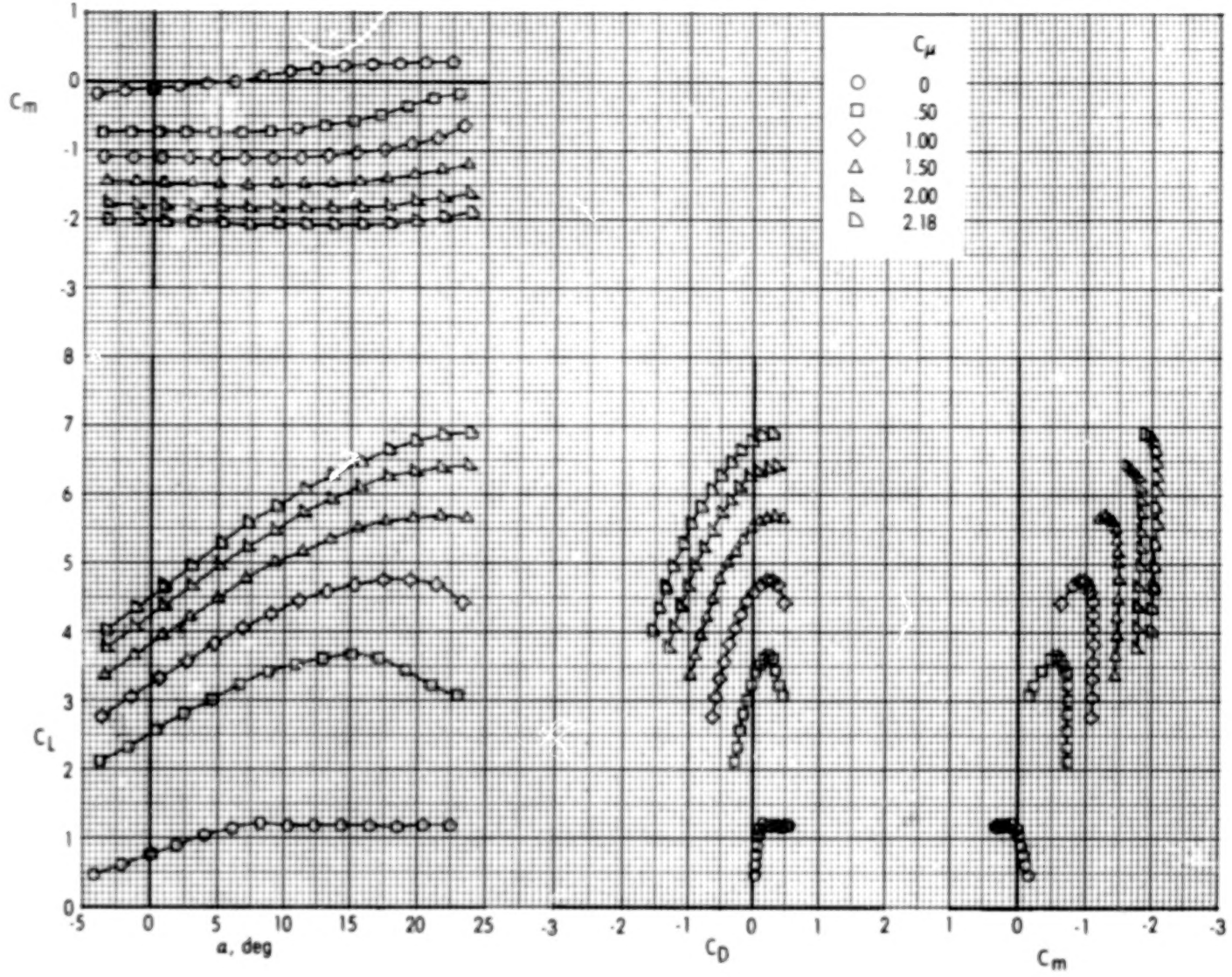

(a) δ_f = 15-15.

Figure 11.- Effect of thrust coefficient on longitudinal aerodynamic characteristics of model with leading-edge blowing and rear element deflected 15°.

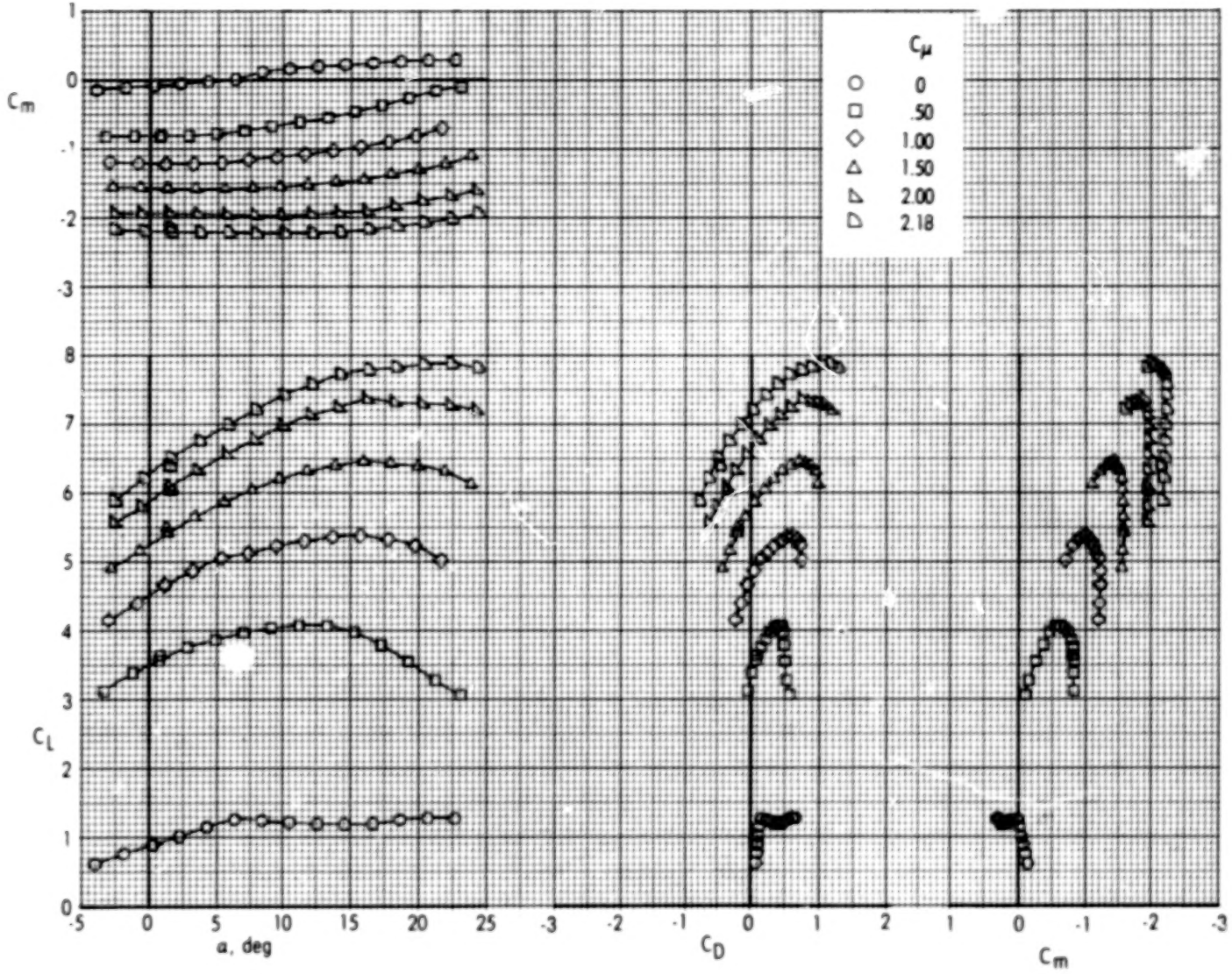

(b) δ_f = 30-15.

Figure 11.- Continued.

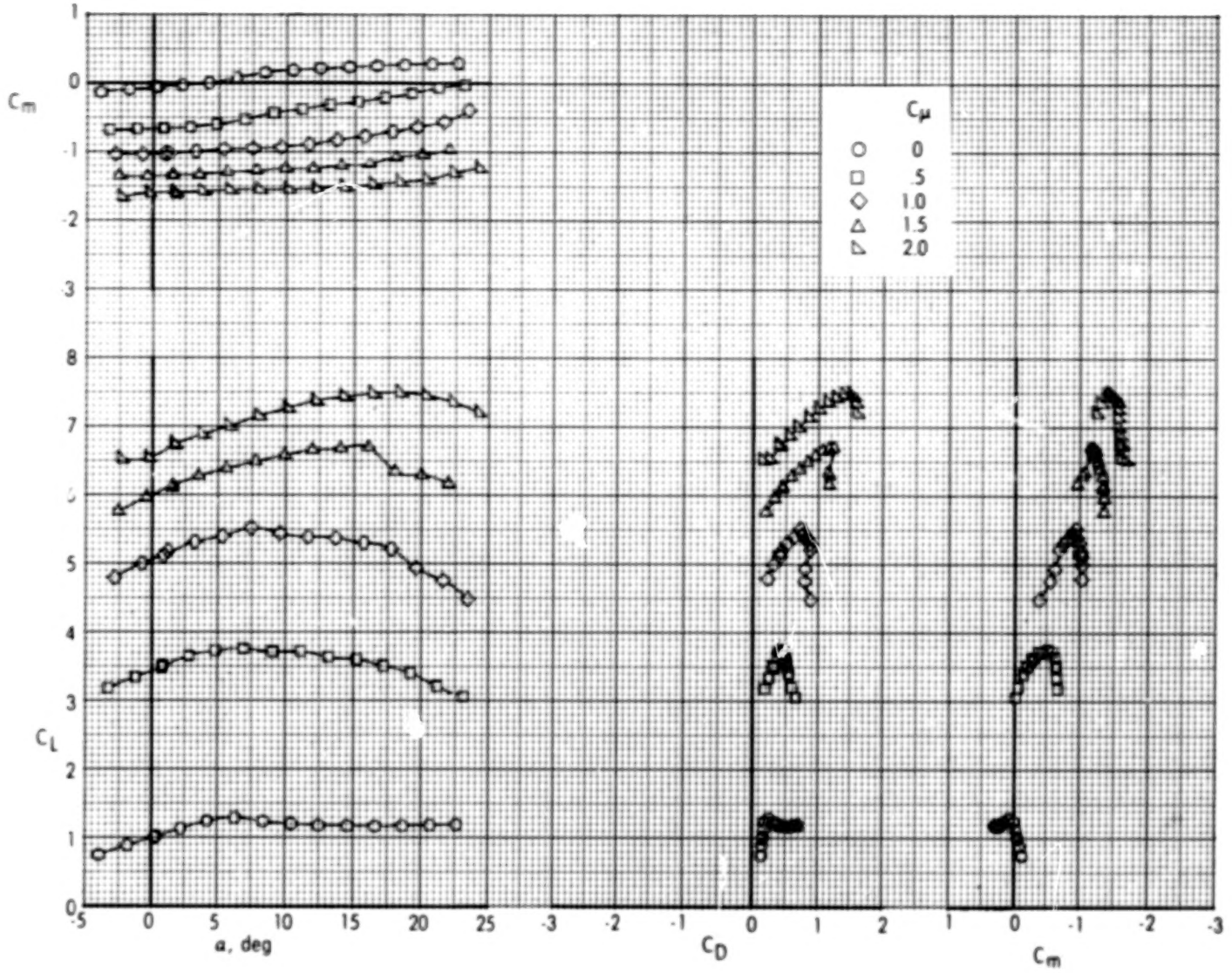

(c) δ_f = 45-15.

Figure 11.- Continued.

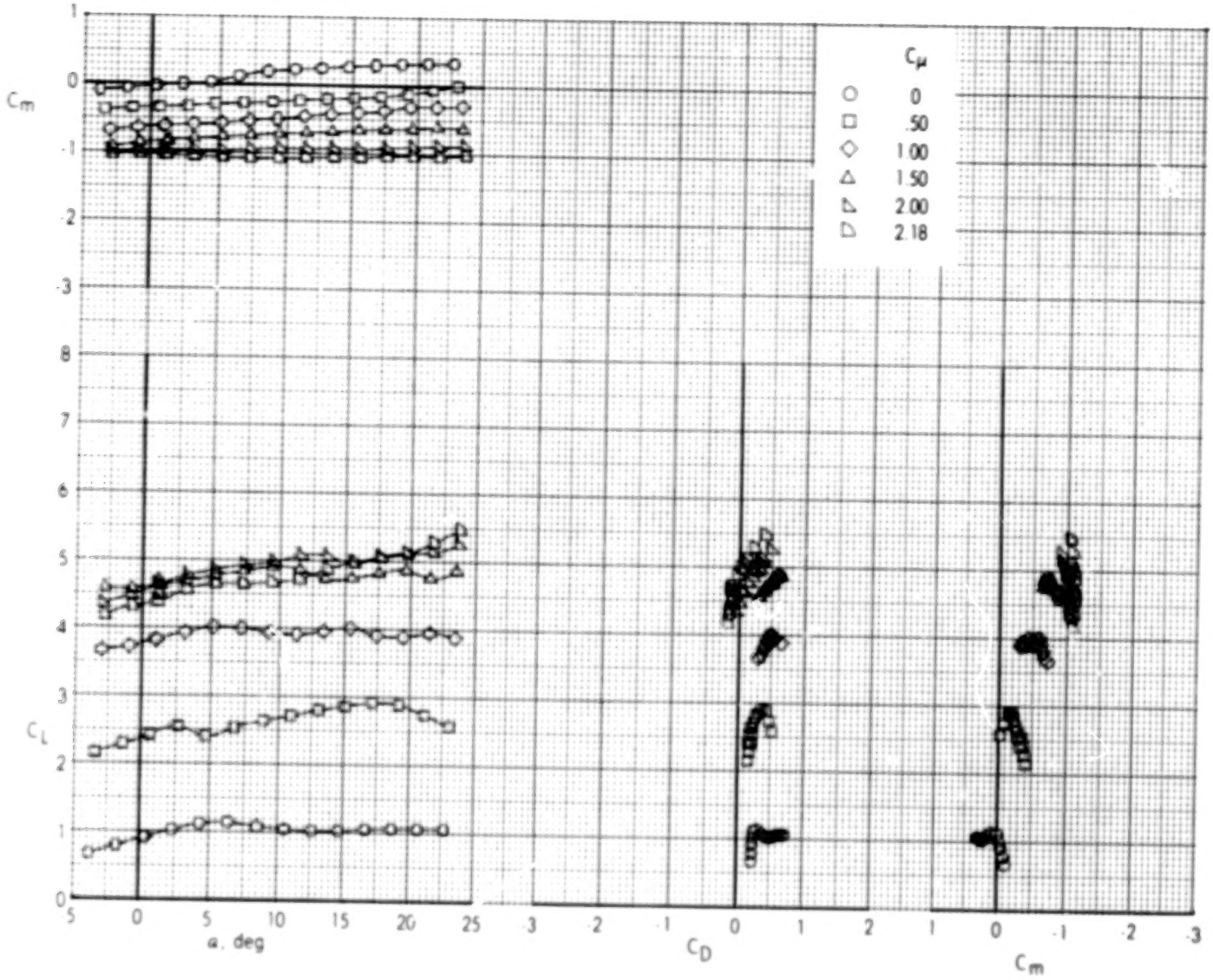

(d) δ_f = 60-15.

Figure 11.- Continued.

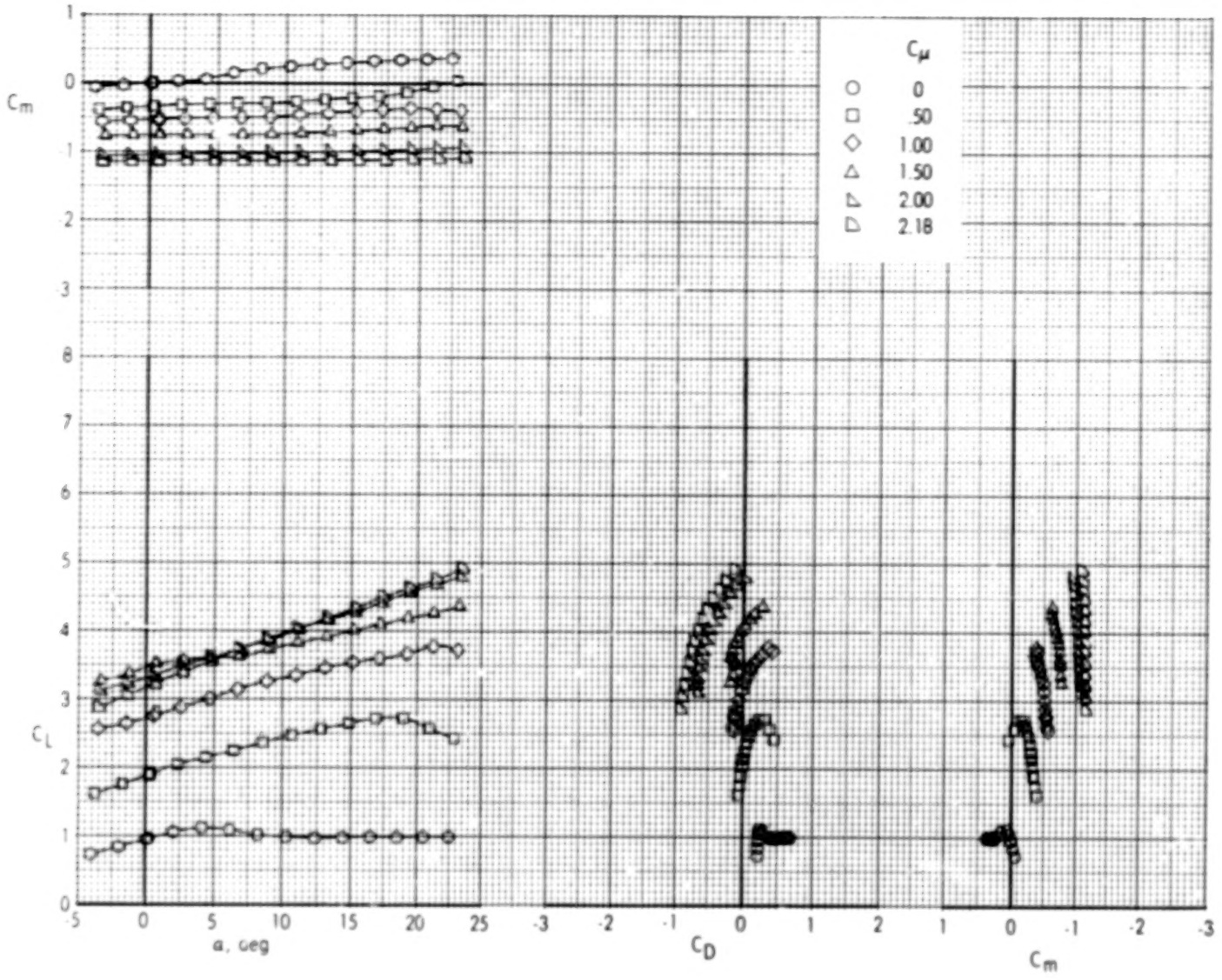

(e) δ_f = 70-15.

Figure 11.- Concluded.

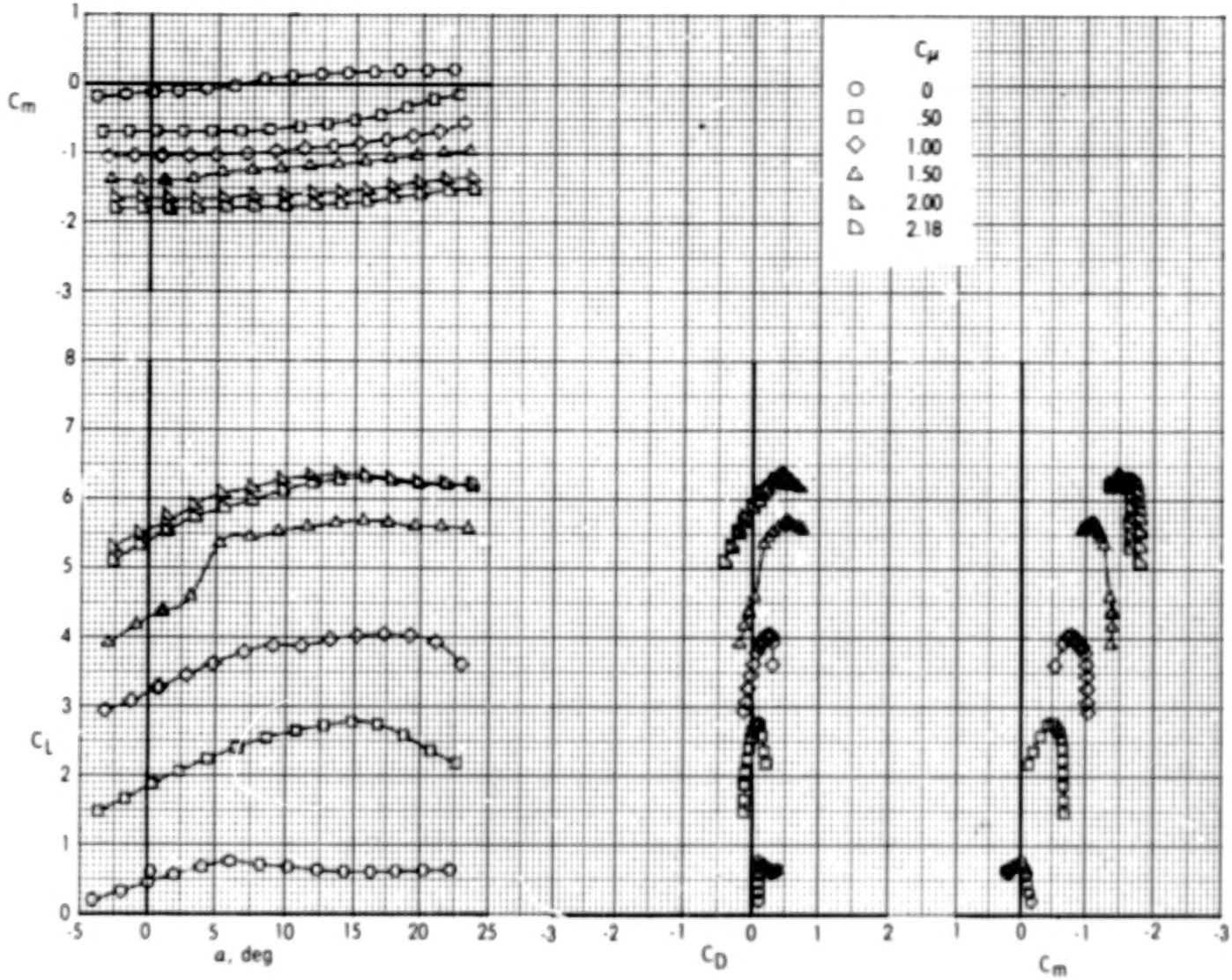

(a) δ_f = 30-30.

Figure 12.- Effect of thrust coefficient on longitudinal aerodynamic characteristics of model with leading-edge blowing and rear element deflected 30°.

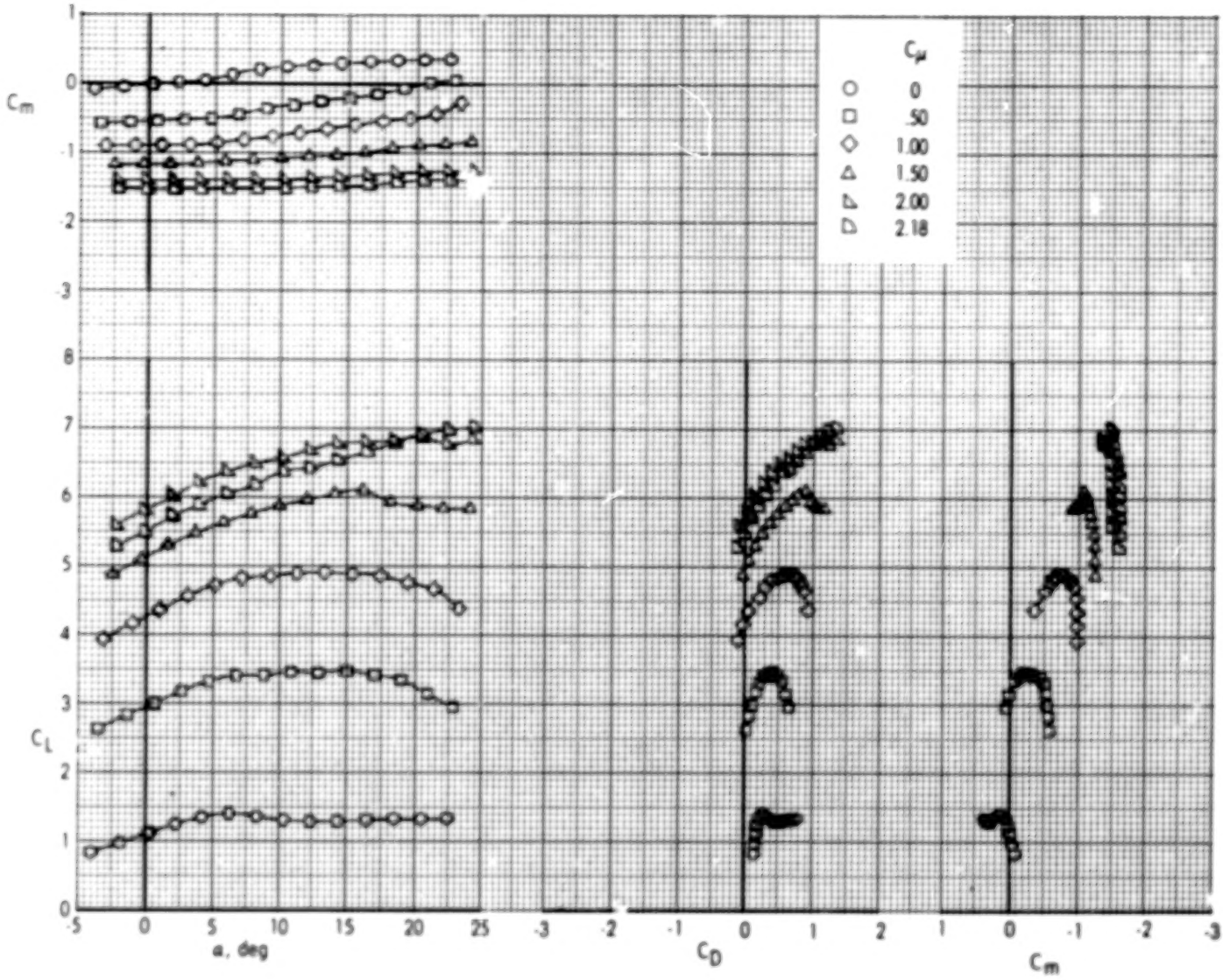

(b) δ_f = 45-30.

Figure 12.- Continued.

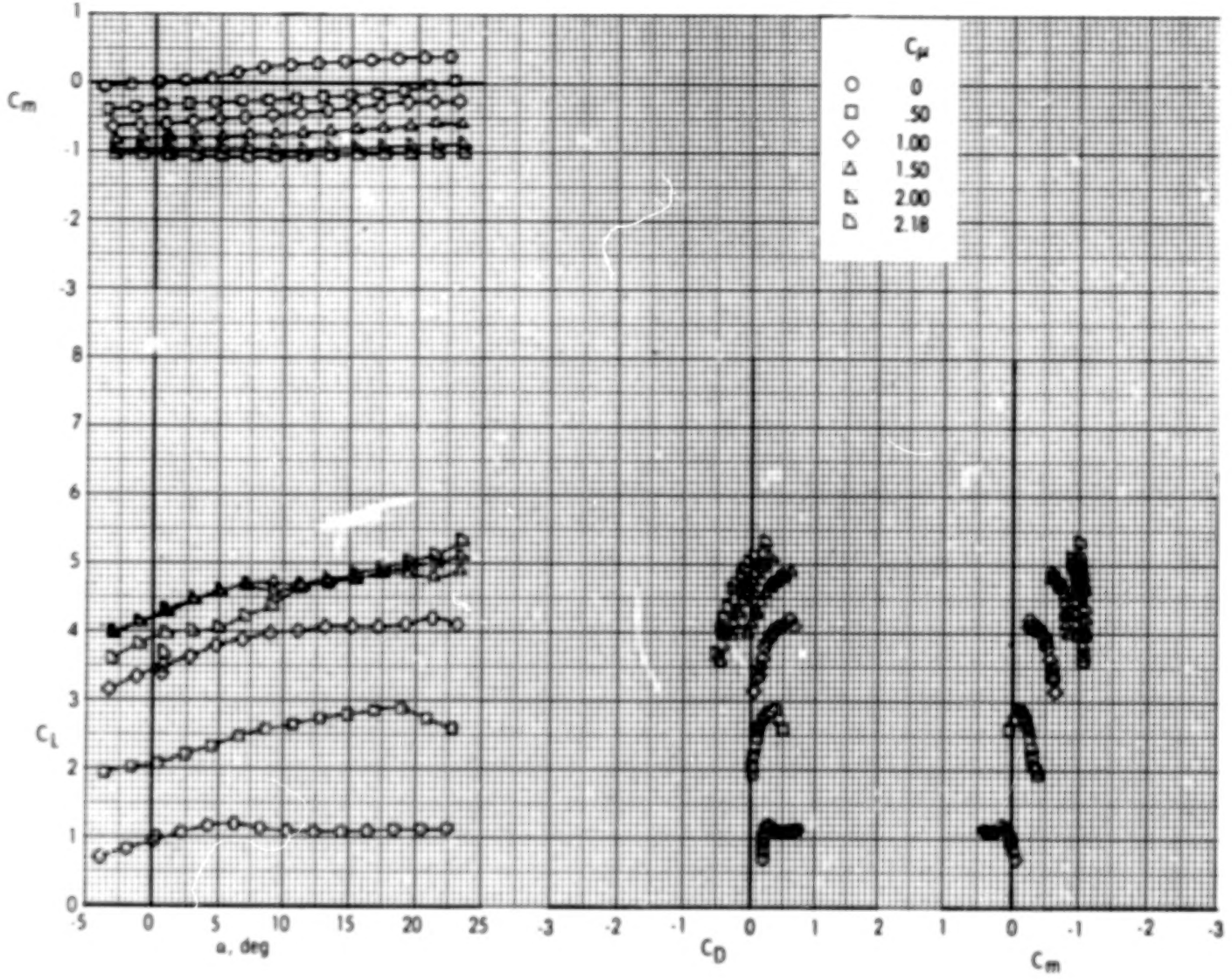

(c) δ_f = 60-30.

Figure 12.- Continued.

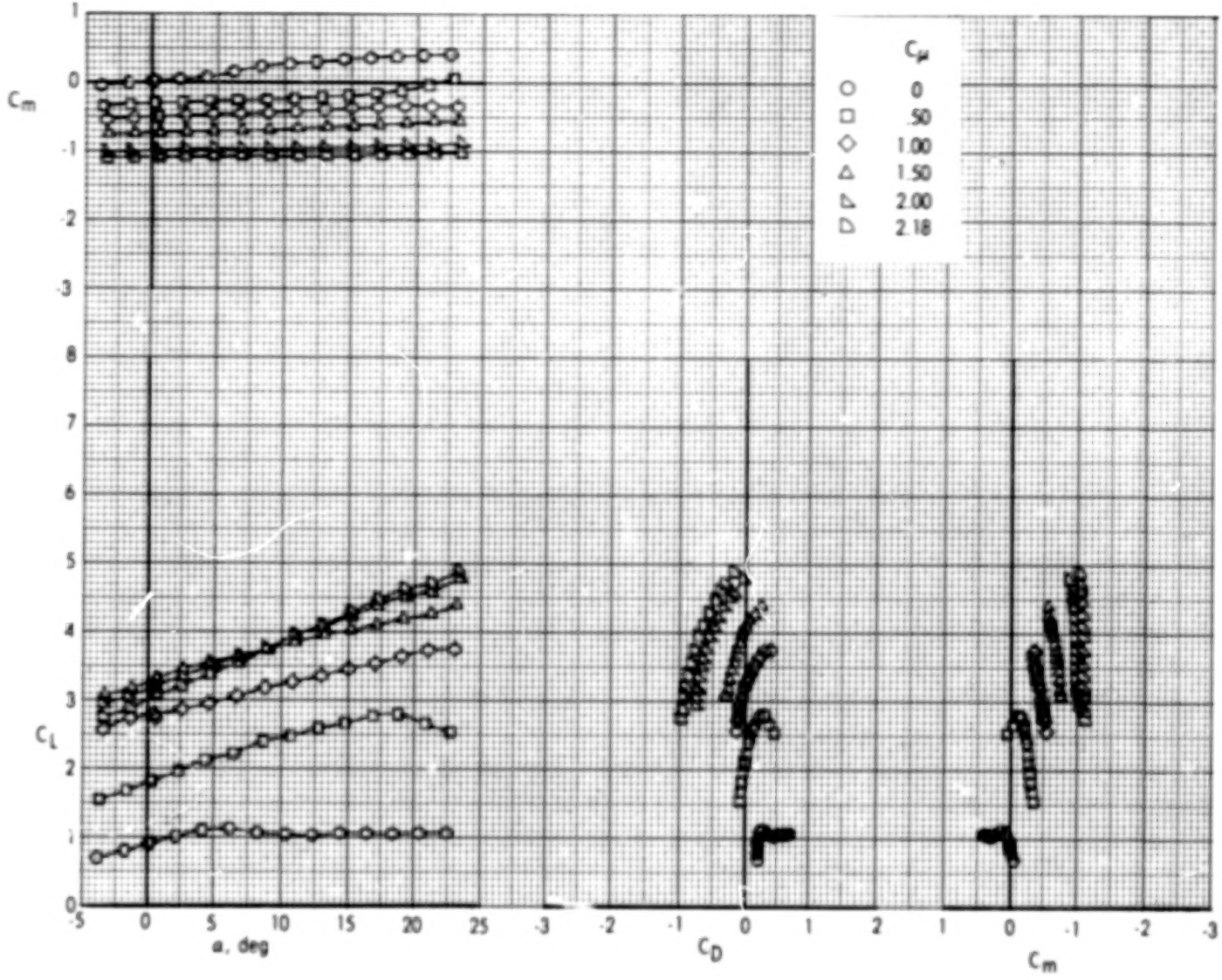

(d) δ_f = 70-30.

Figure 12.- Concluded.

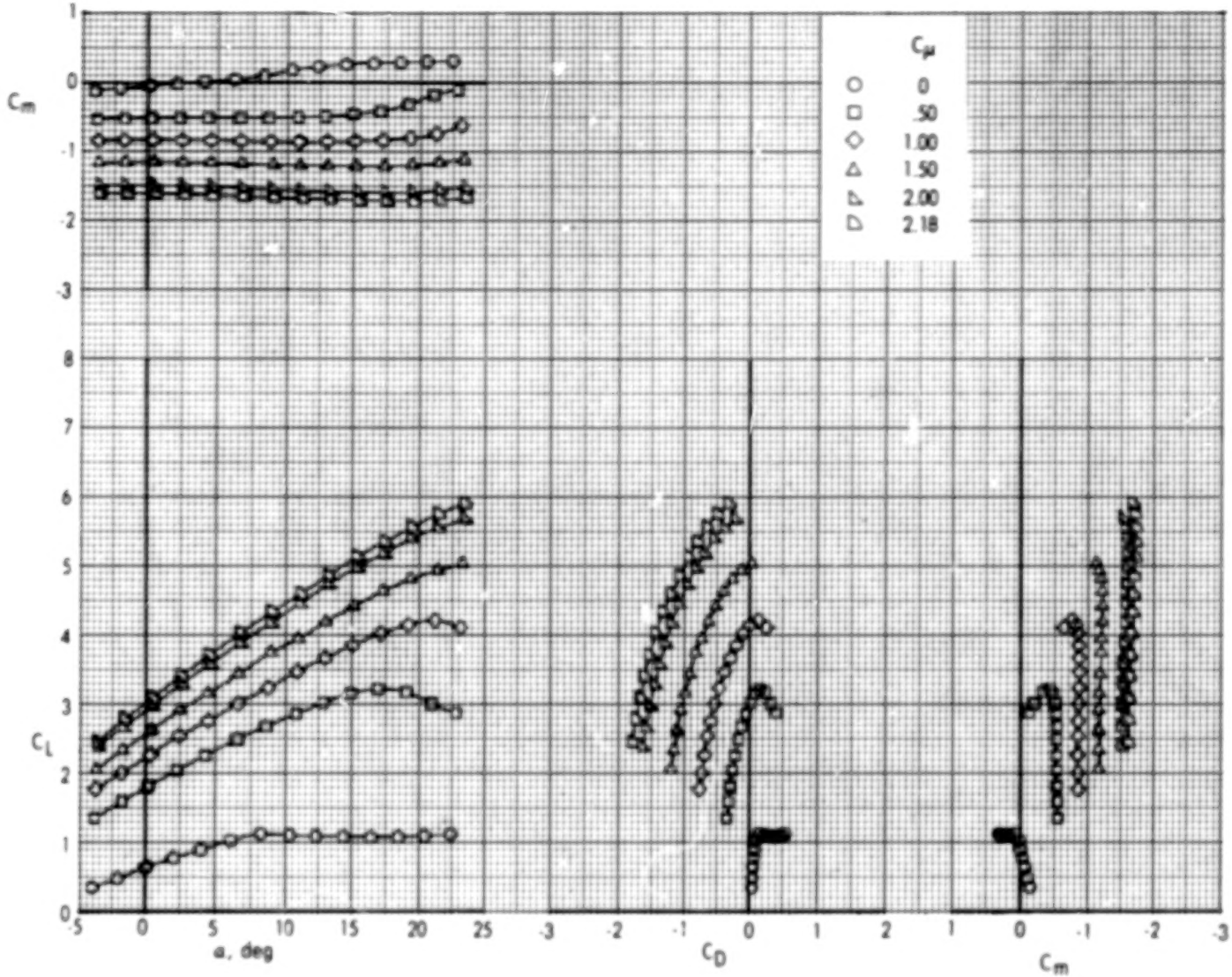

(a) δ_f = 30-(-20).

Figure 13.- Effect of thrust coefficient on longitudinal aerodynamic characteristics of model with leading-edge blowing and rear element deflected -20°.

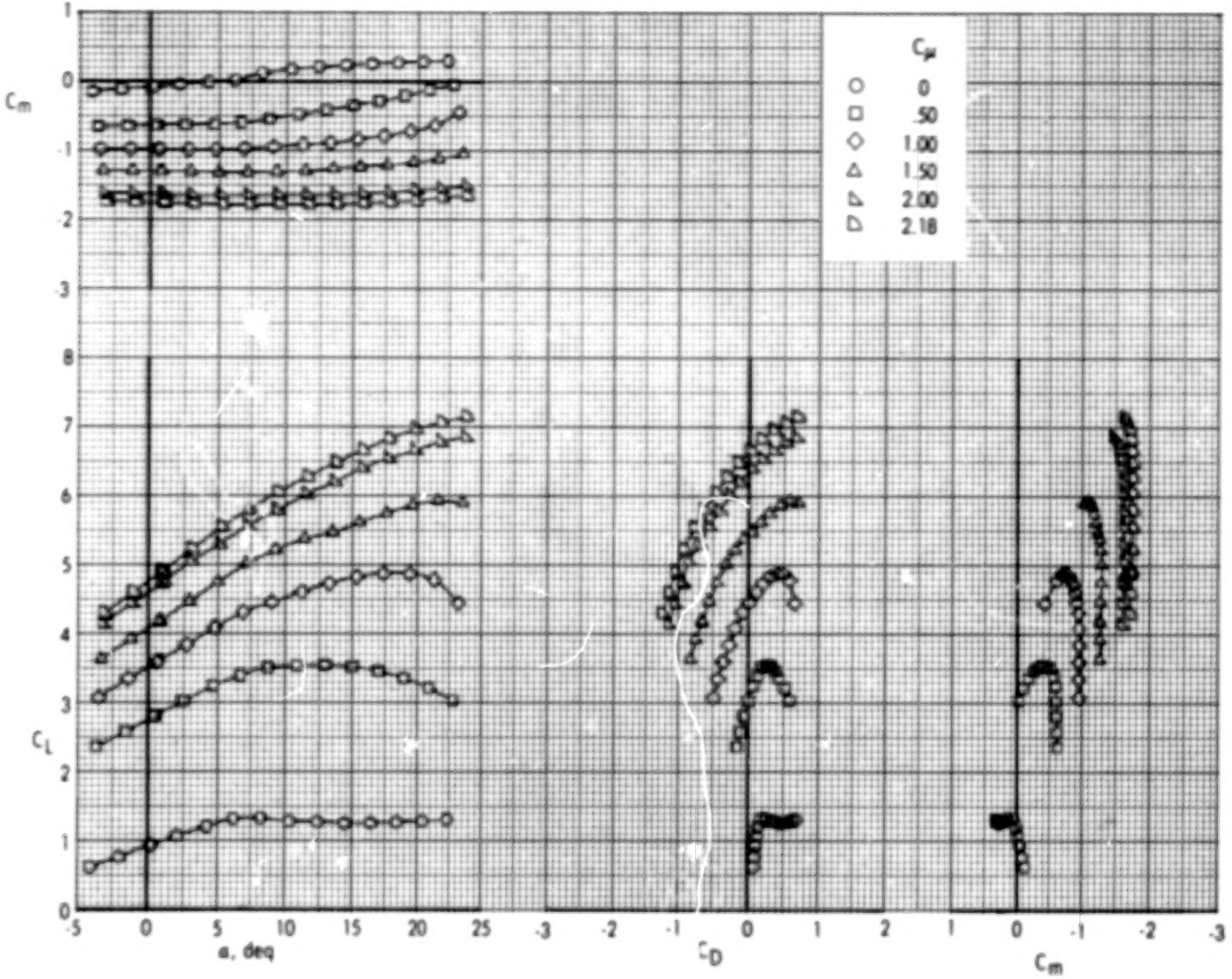

(b) δ_f = 45-(-20).

Figure 13.- Continued.

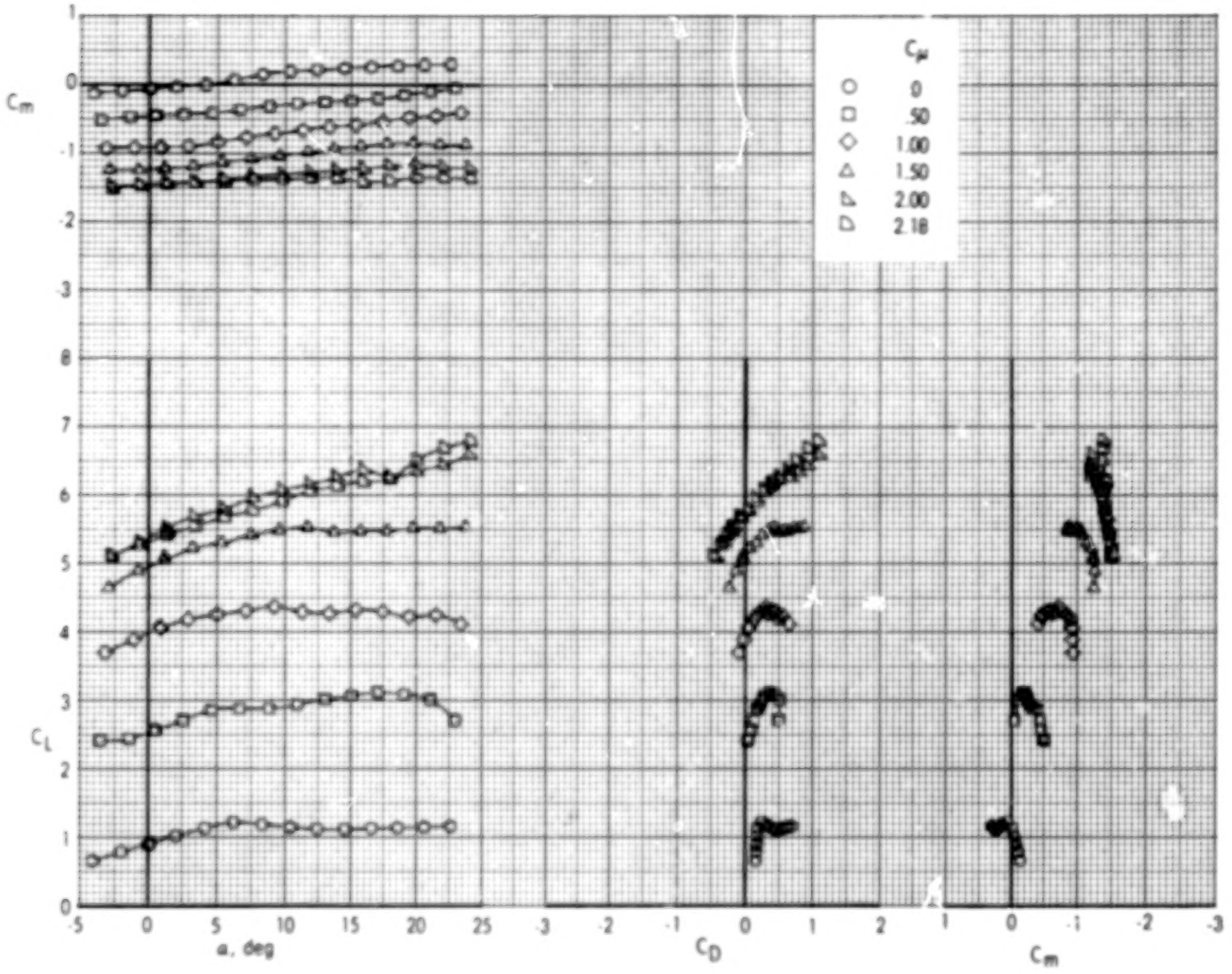

(c) δ_f = 60-(-20).

Figure 13.- Continued.

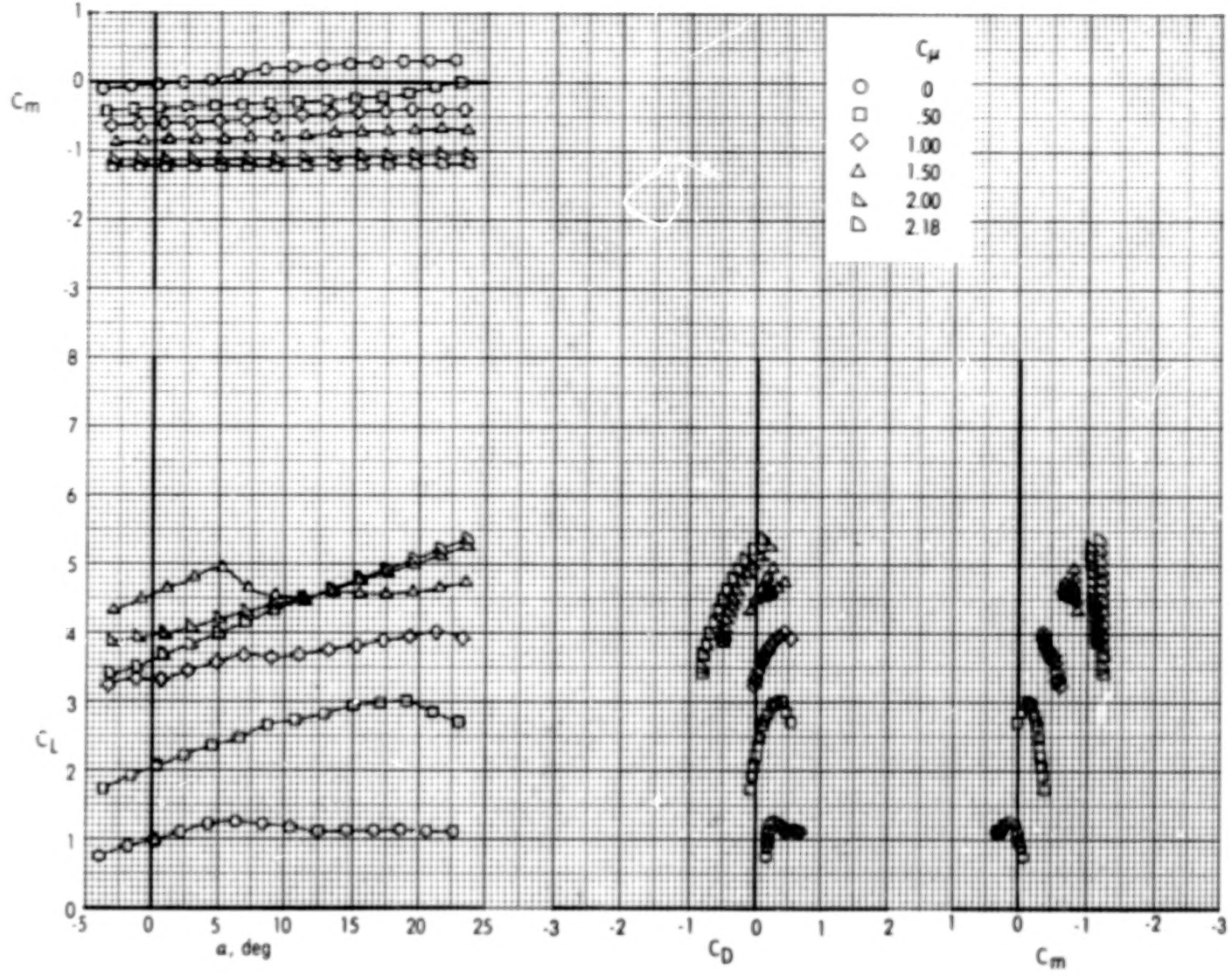

(d) δ_f = 70-(-20).

Figure 13.- Concluded.

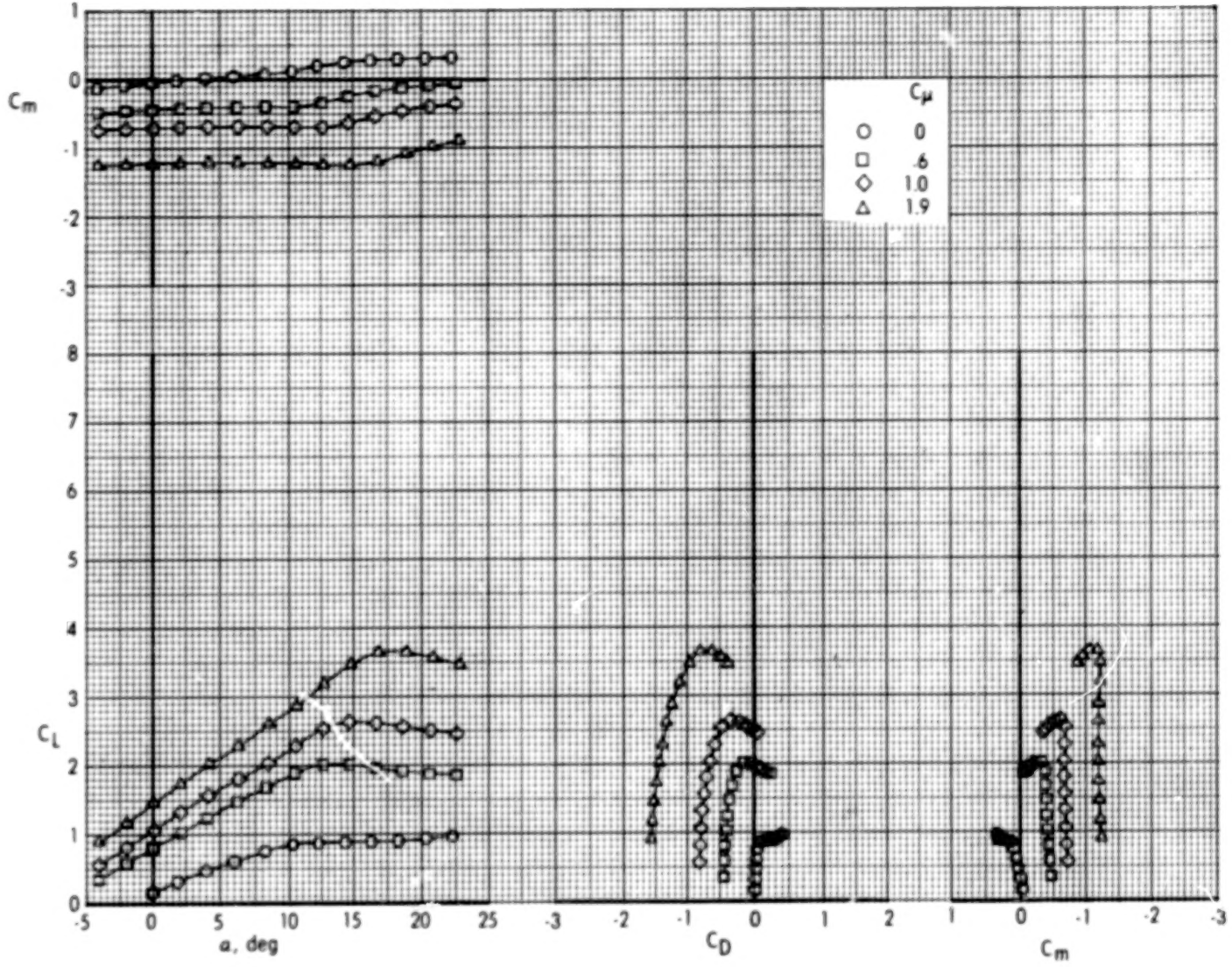

(a) δ_f = 0-0.

Figure 14.- Effect of thrust coefficient on longitudinal aerodynamic characteristics of model with flap blowing and rear element undeflected.

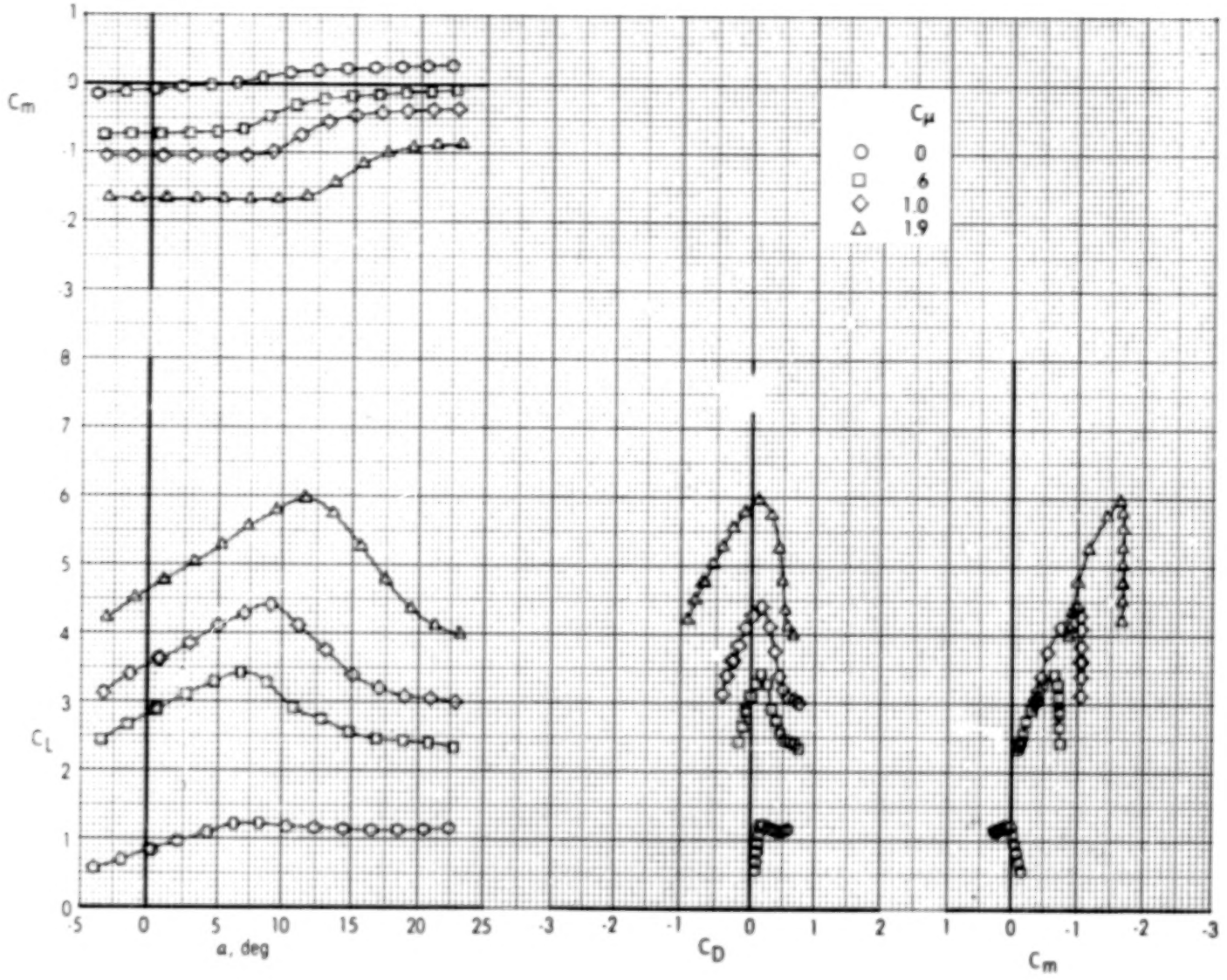

(b) δ_f = 30-0.

Figure 14.- Continued.

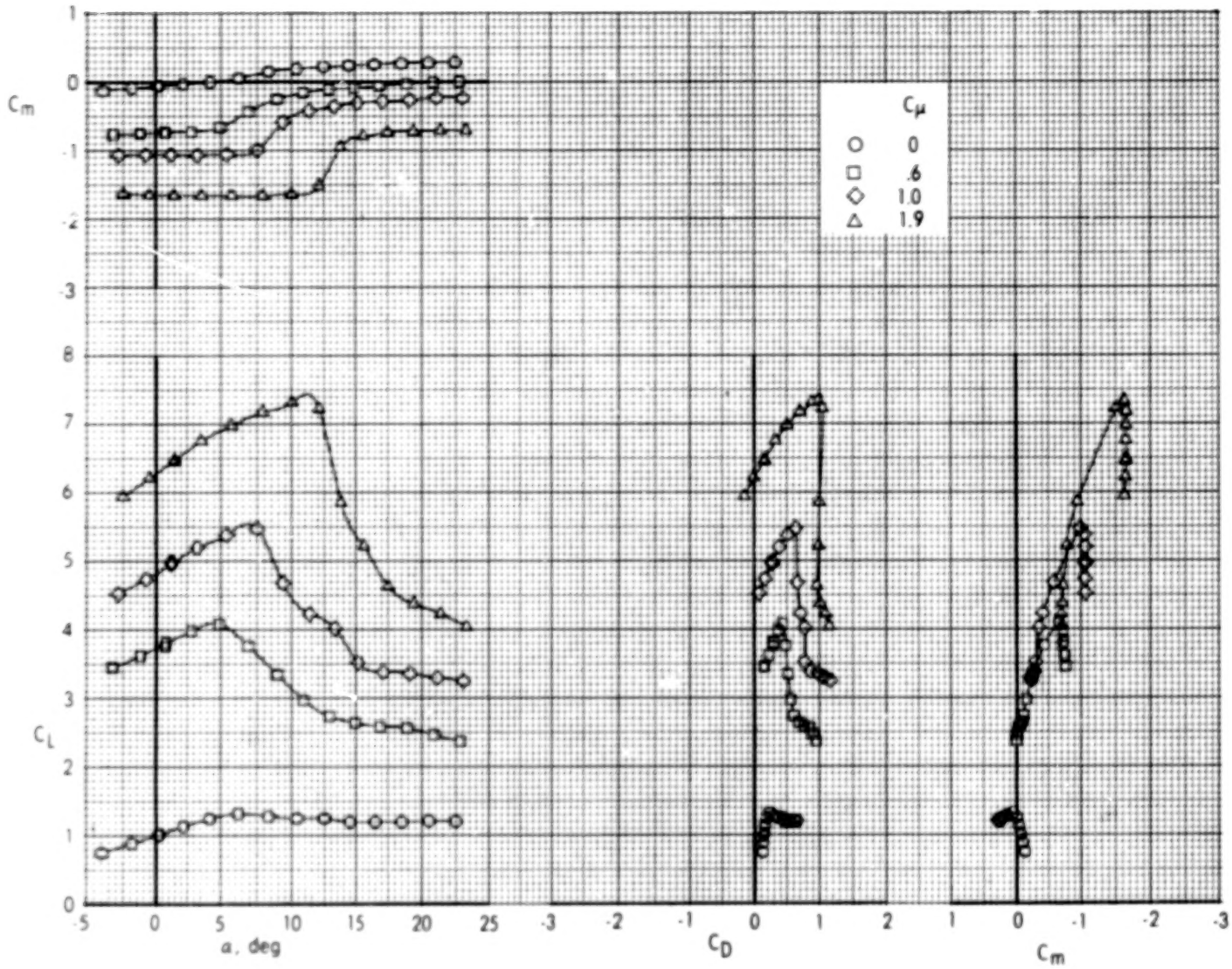

(c) δ_f = 45-0.

Figure 14.- Continued.

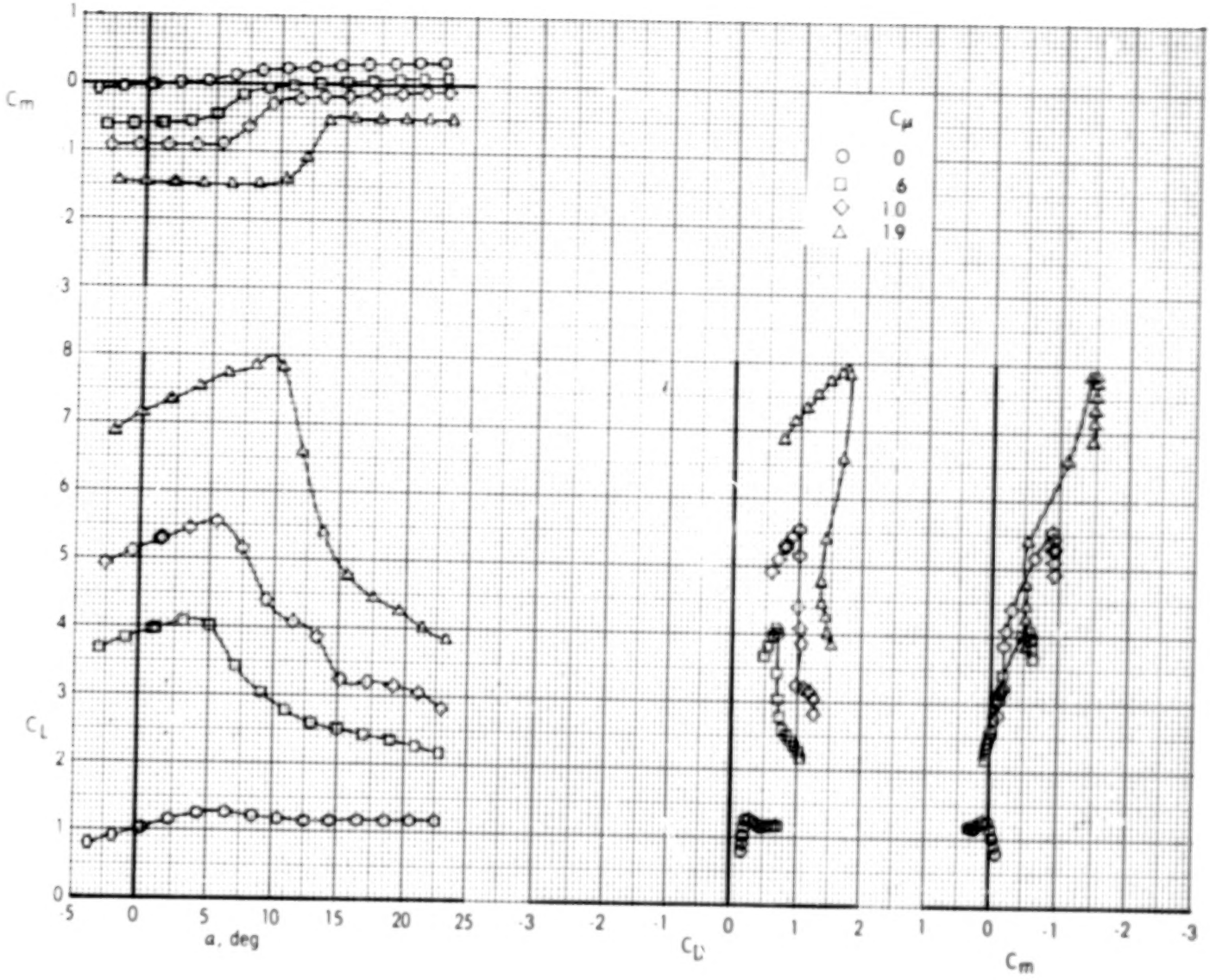

(d) δ_f = 60-0.

Figure 14.- Continued.

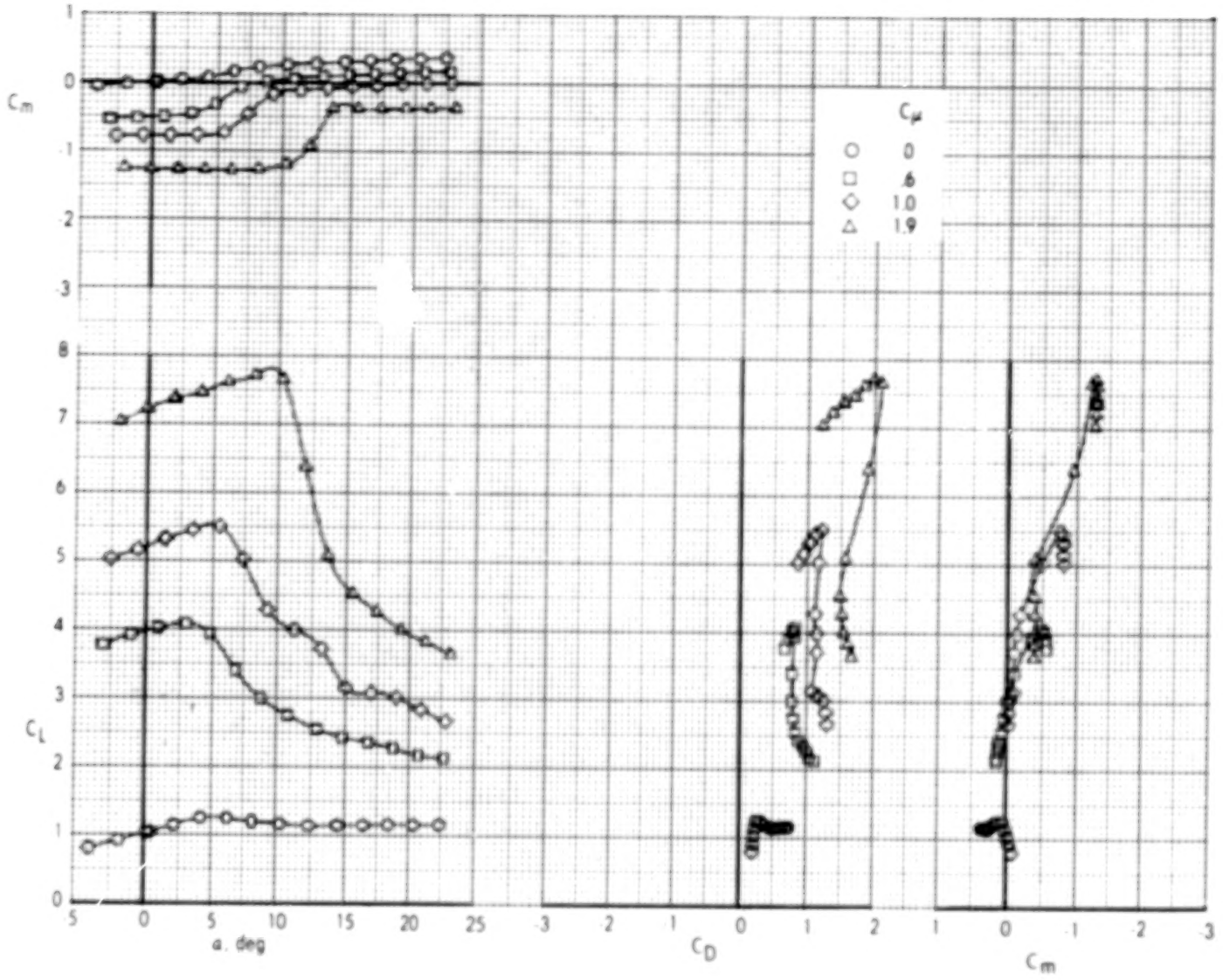

(e) δ_f = 70-0.

Figure 14.- Concluded.

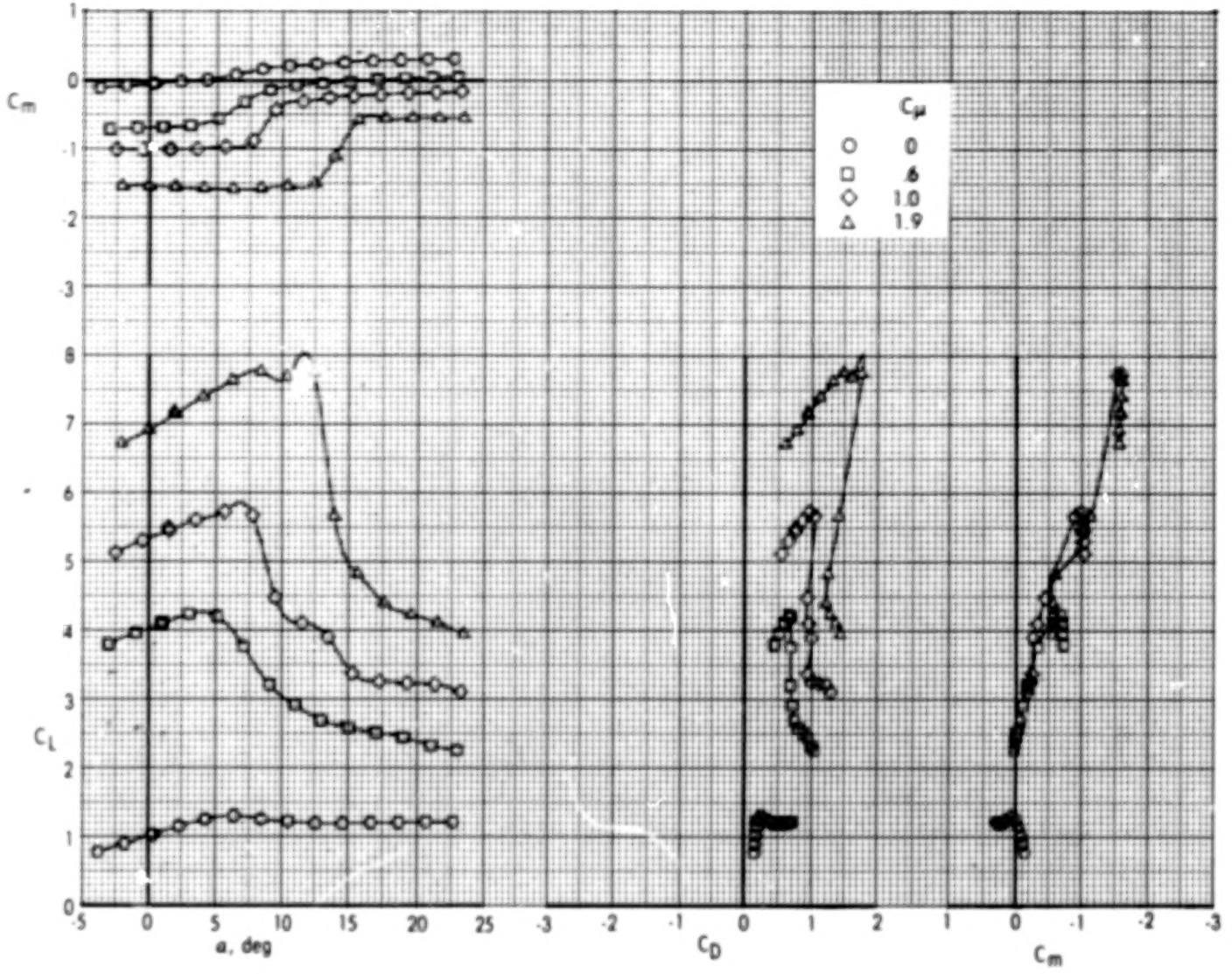

Figure 15.- Effect of thrust coefficient on longitudinal aerodynamic characteristics of model with flap blowing and δ_f = 45-15.

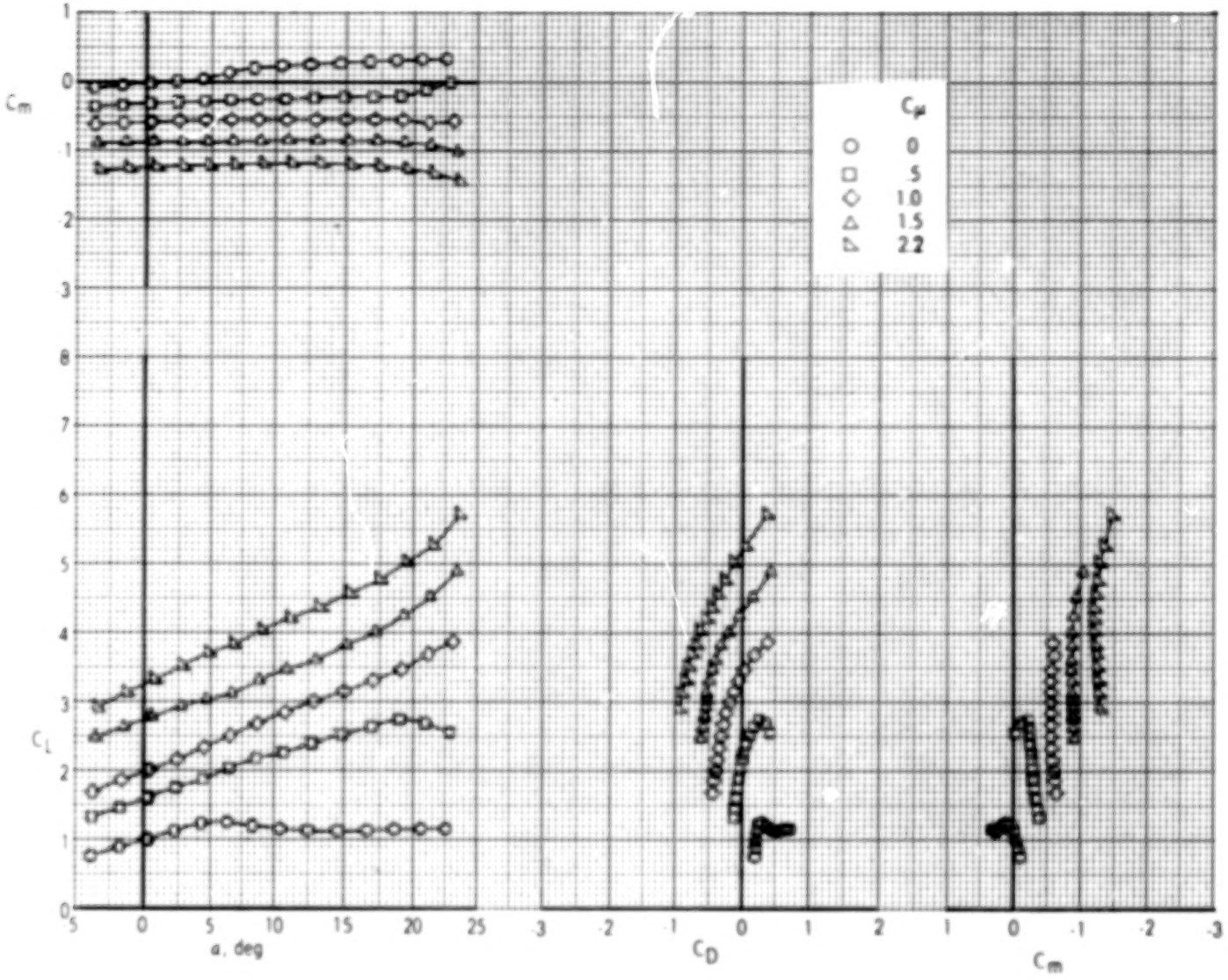

(a) Flap blowing 5 percent of total thrust.

Figure 16.- Effect of thrust coefficient on longitudinal aerodynamic characteristics of model with combined leading-edge and flap blowing and δ_f = 60-0.

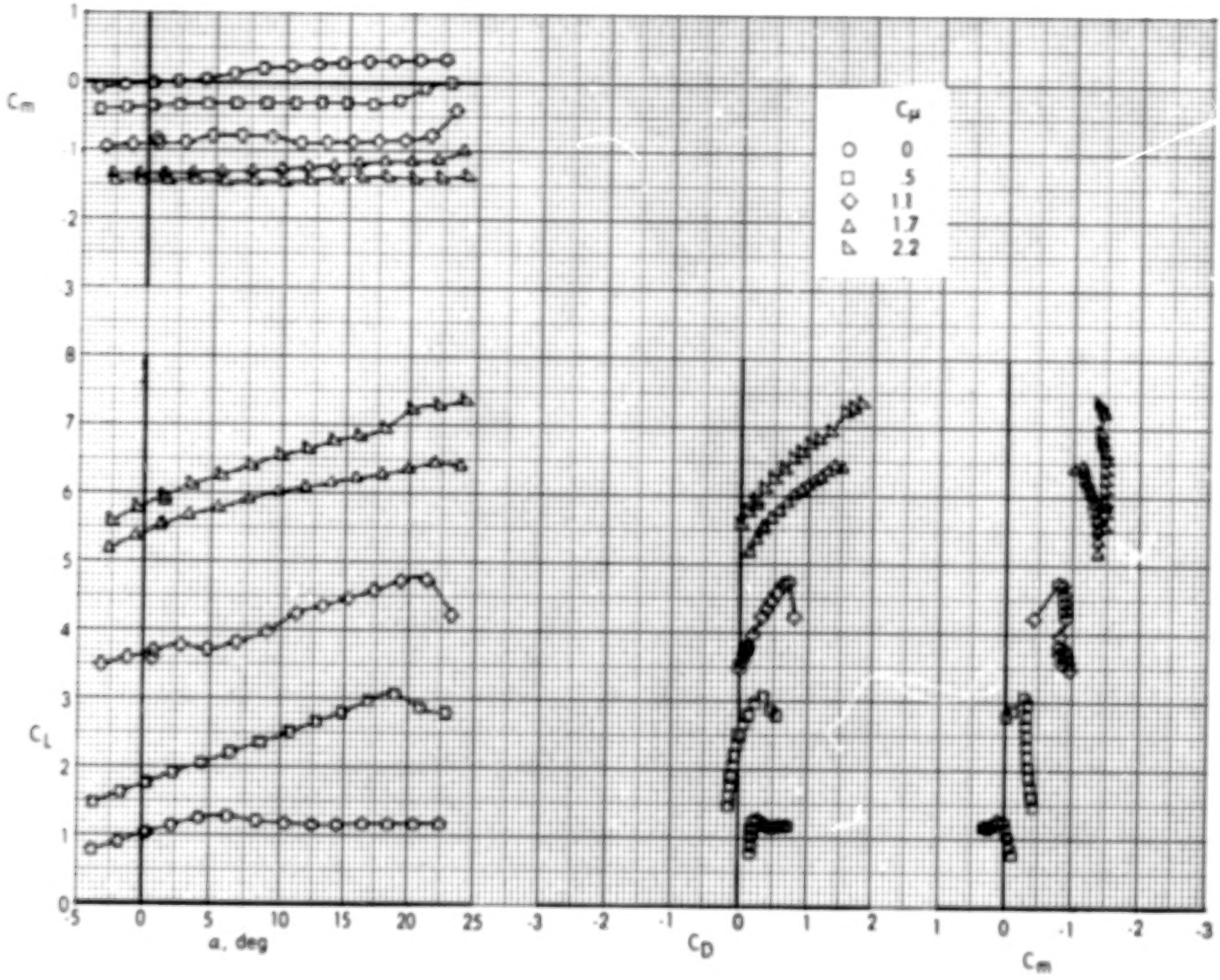

(b) Flap blowing 13 percent of total thrust.

Figure 16.- Continued.

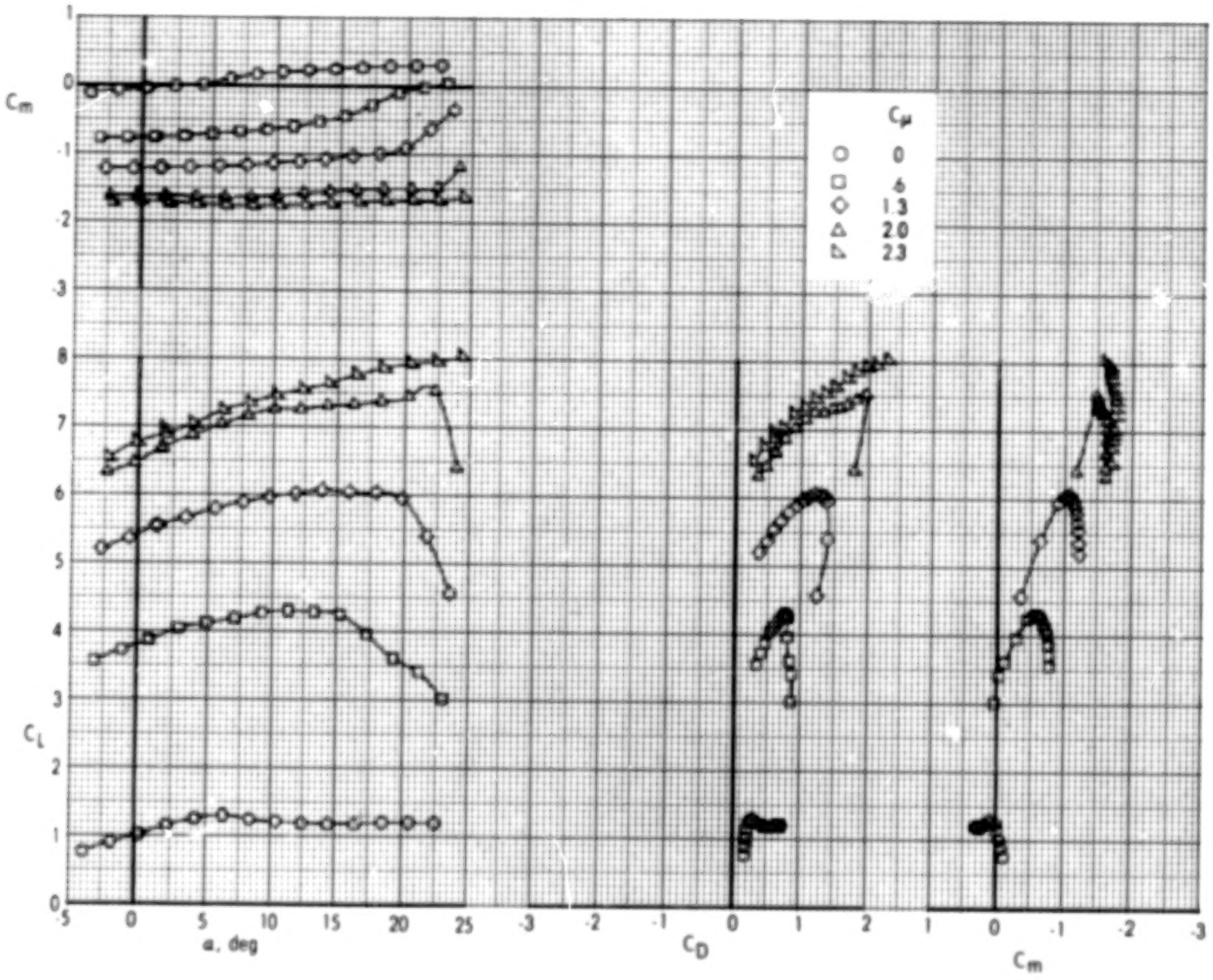

(c) Flap blowing 28 percent of total thrust.

Figure 16.- Concluded.

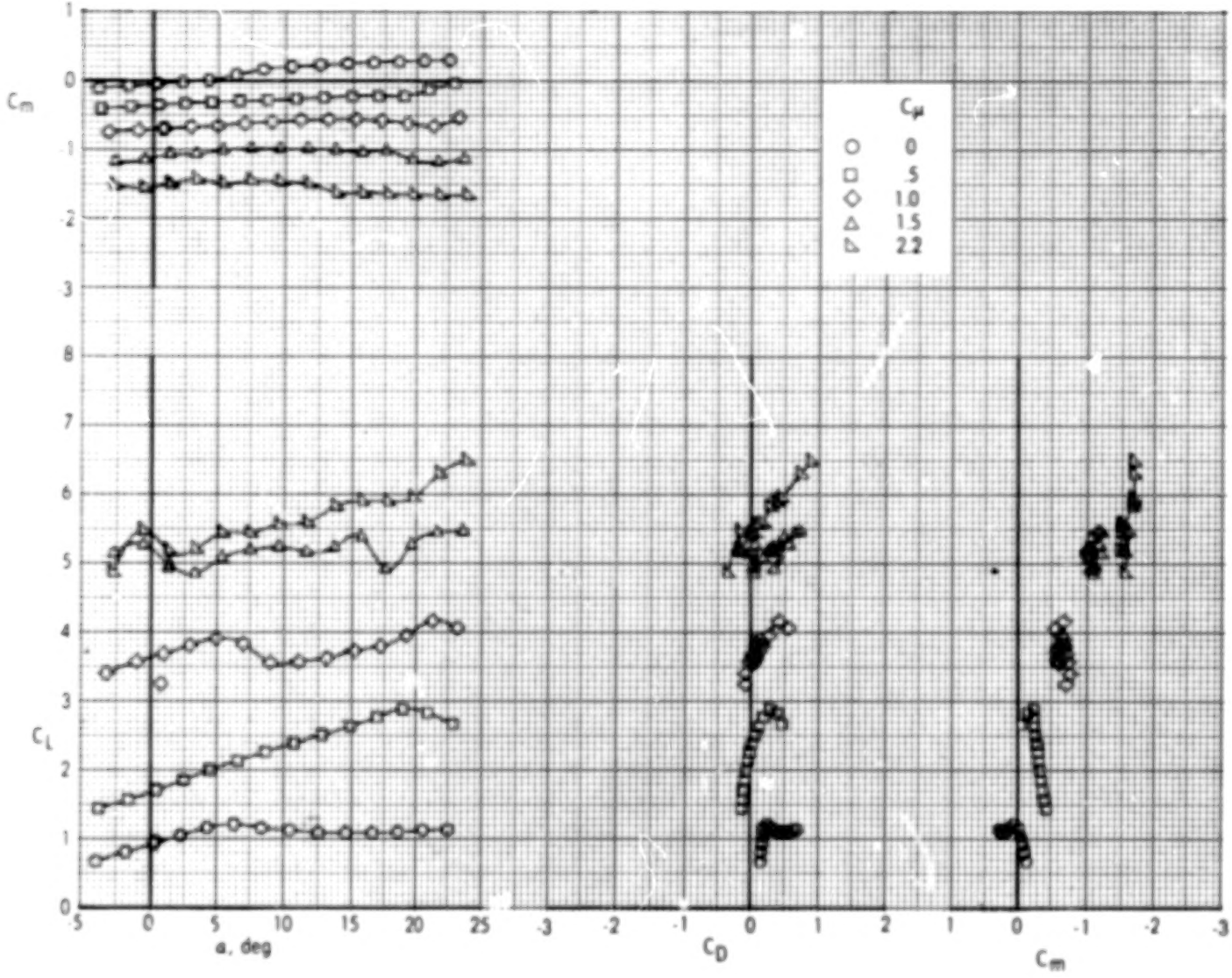

(a) Flap blowing 5 percent of total thrust.

Figure 17.- Effect of thrust coefficient on longitudinal aerodynamic characteristics of model with combined leading-edge and flap blowing and δ_f = 45-15.

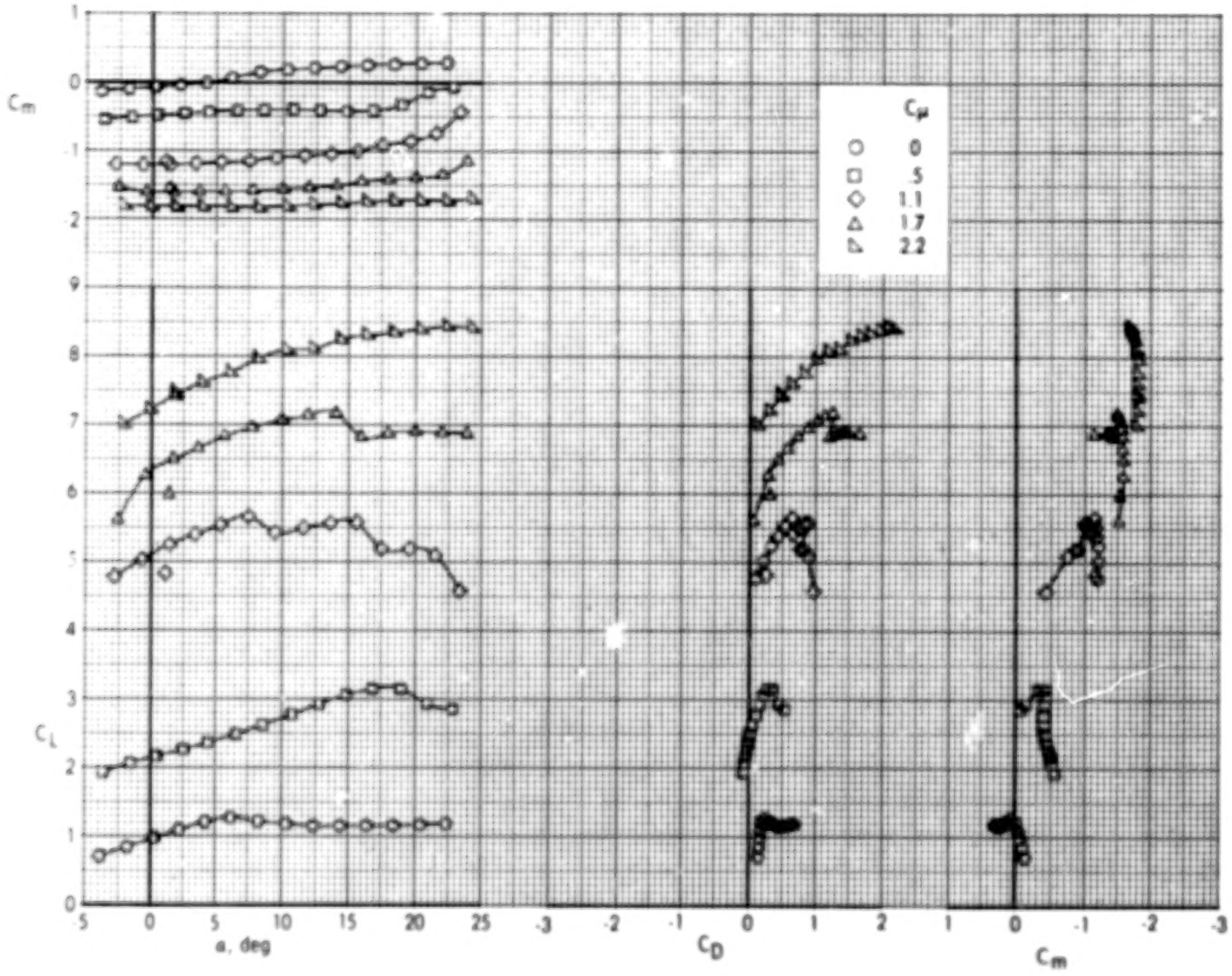

(b) Flap blowing 13 percent of total thrust.

Figure 17.- Continued.

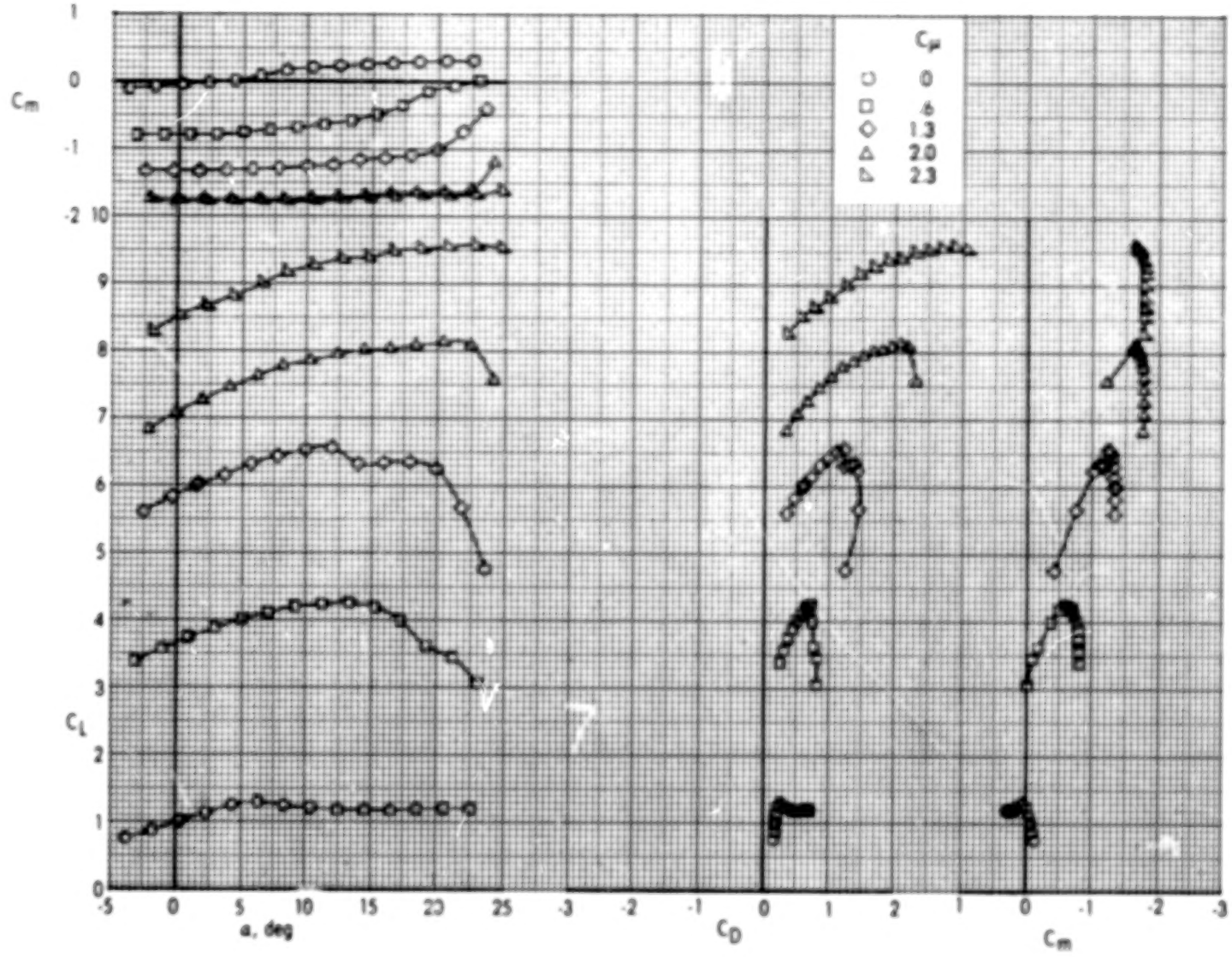

(c) Flap blowing 28 percent of total thrust.

Figure 17.-Concluded.

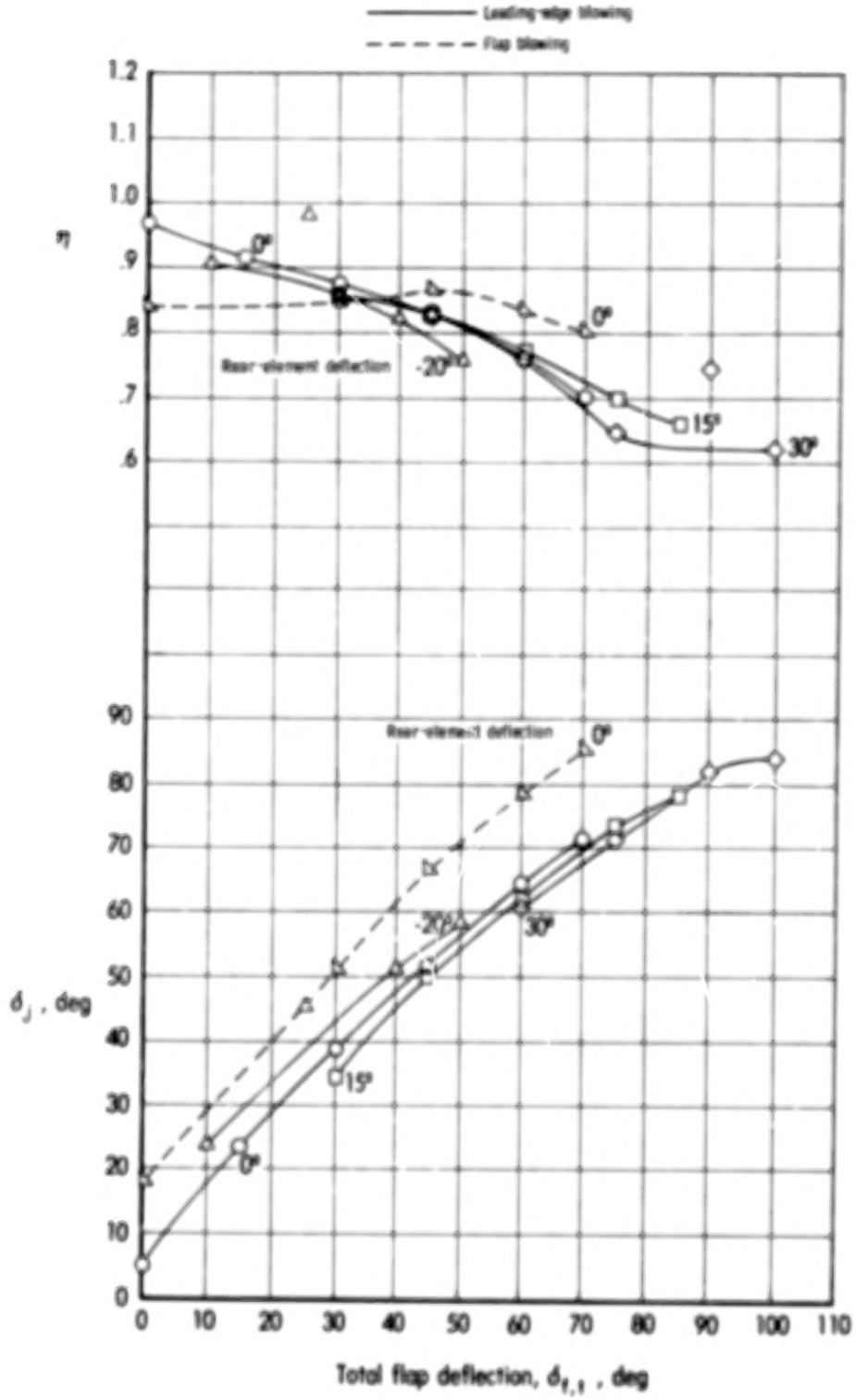

(a) Static turning angle and static thrust-recovery efficiency

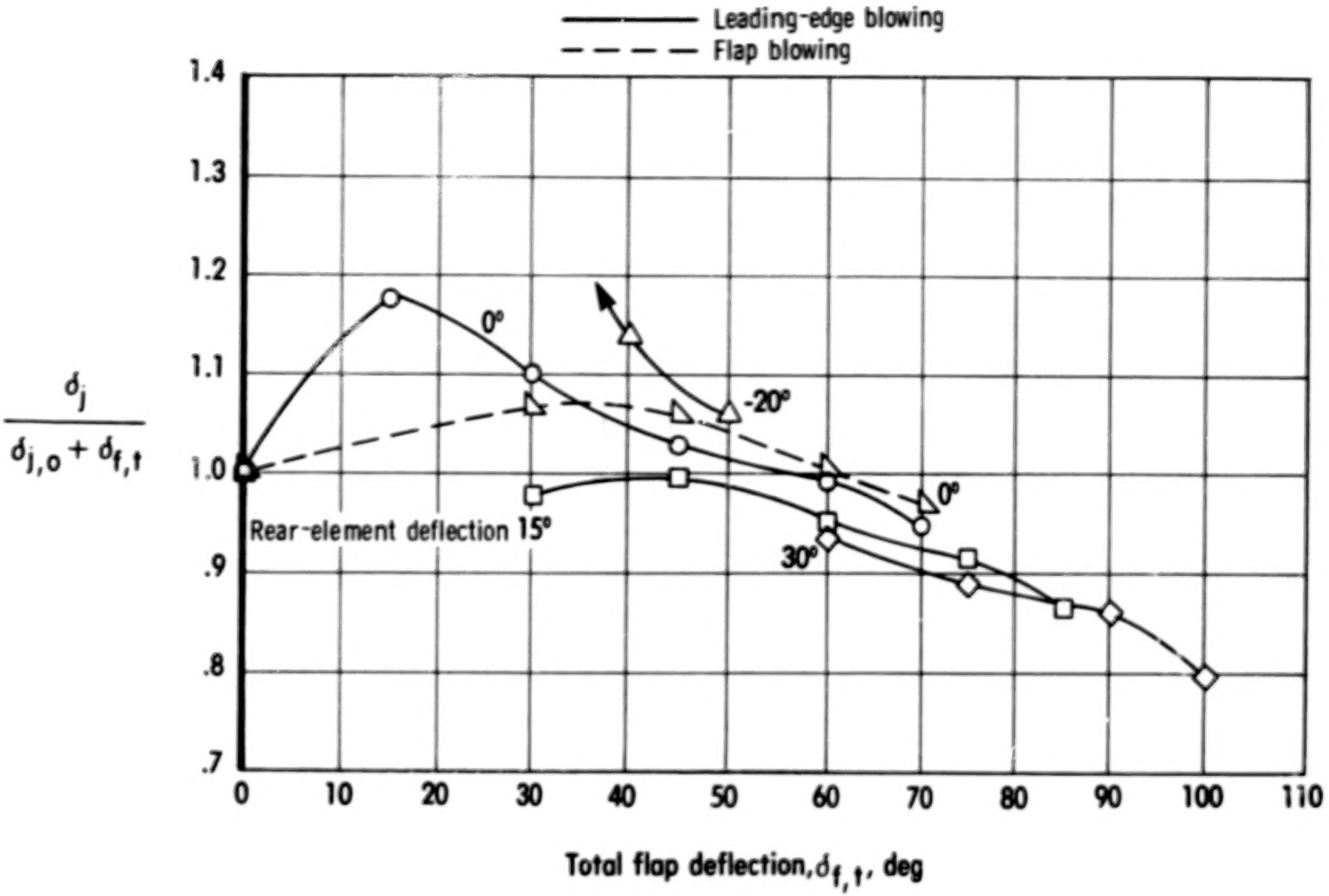

(b) Flap static turning efficiency.

Figure 18.- Concluded.

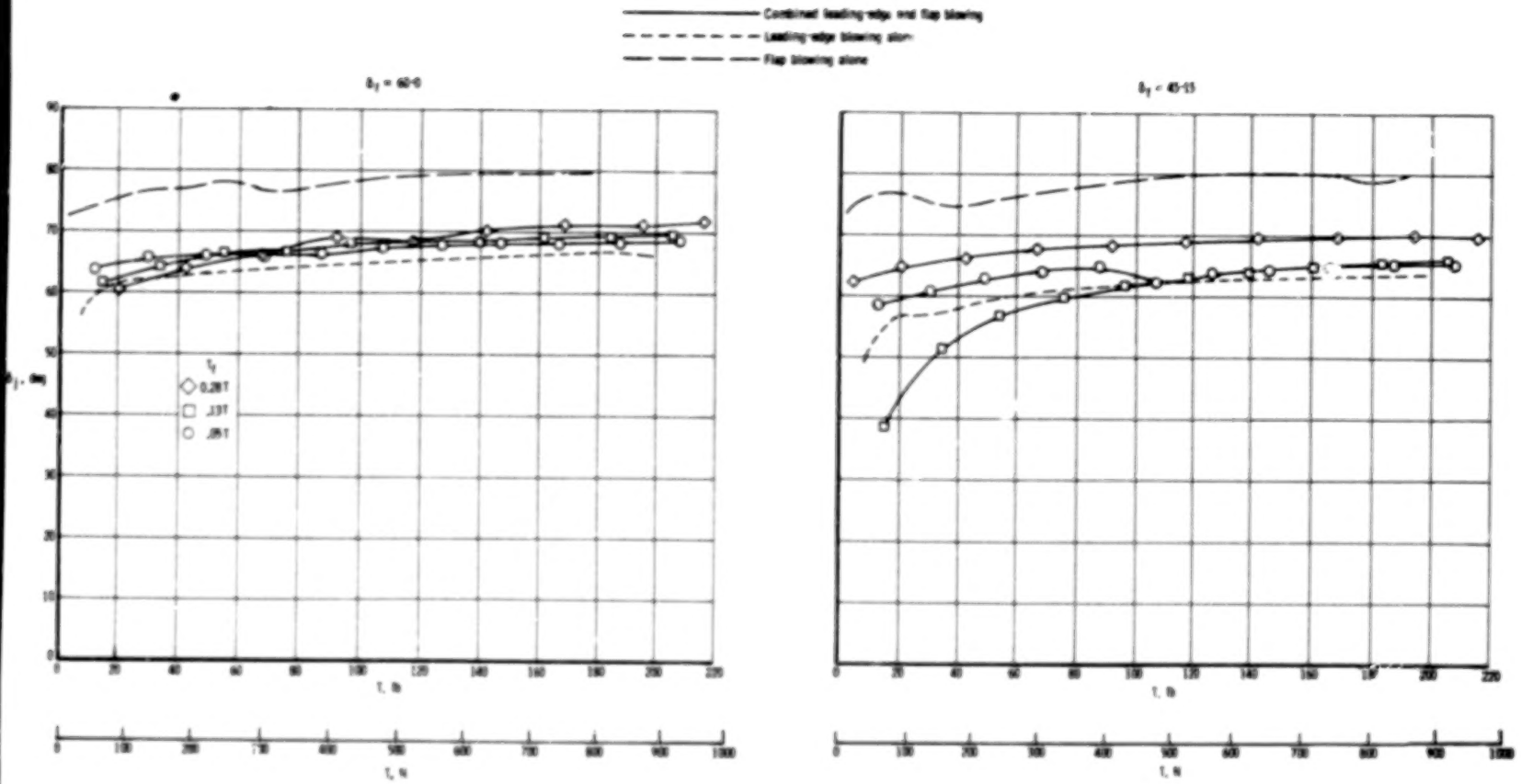

Figure 19.- Comparison of static turning angles obtained with leading-edge blowing, flap blowing, and combined leading-edge and flap blowing.

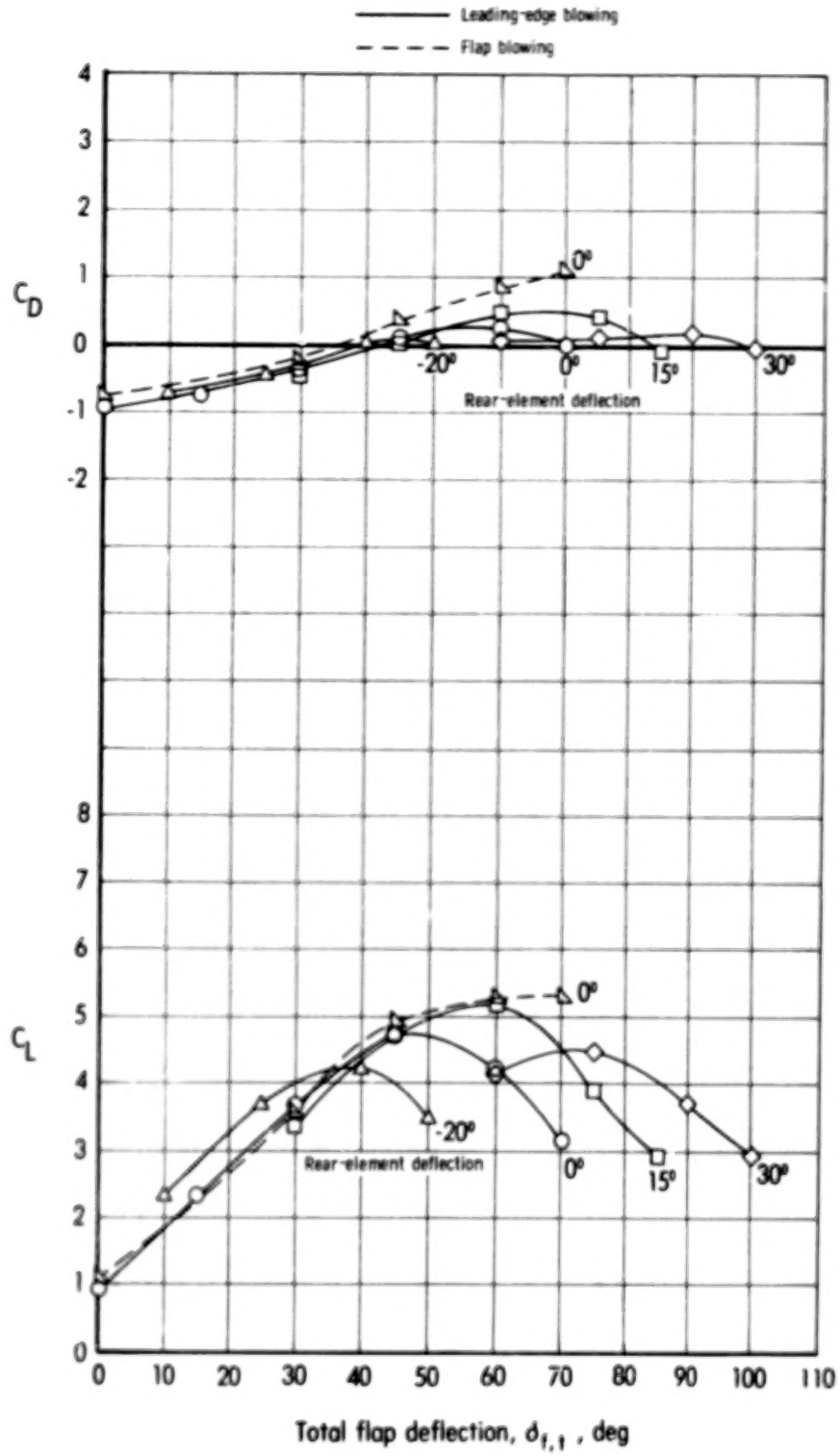

(a) Lift and drag coefficients.

Figure 20.- Summary of aerodynamic characteristics at $\alpha = 0^\circ$ for $C_\mu = 1.0$.

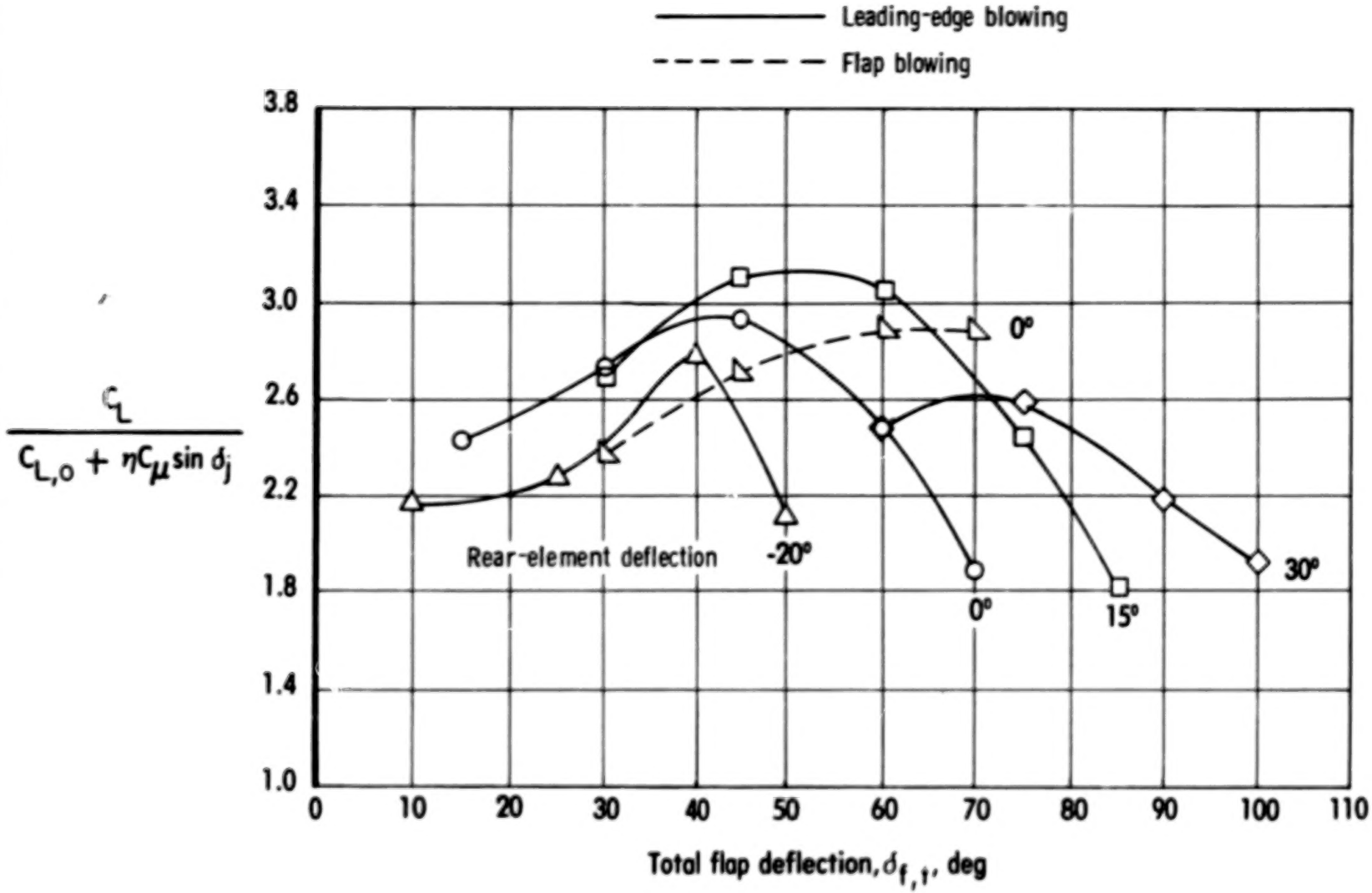

(b) Powered circulation-lift ratios.

Figure 20.- Concluded.

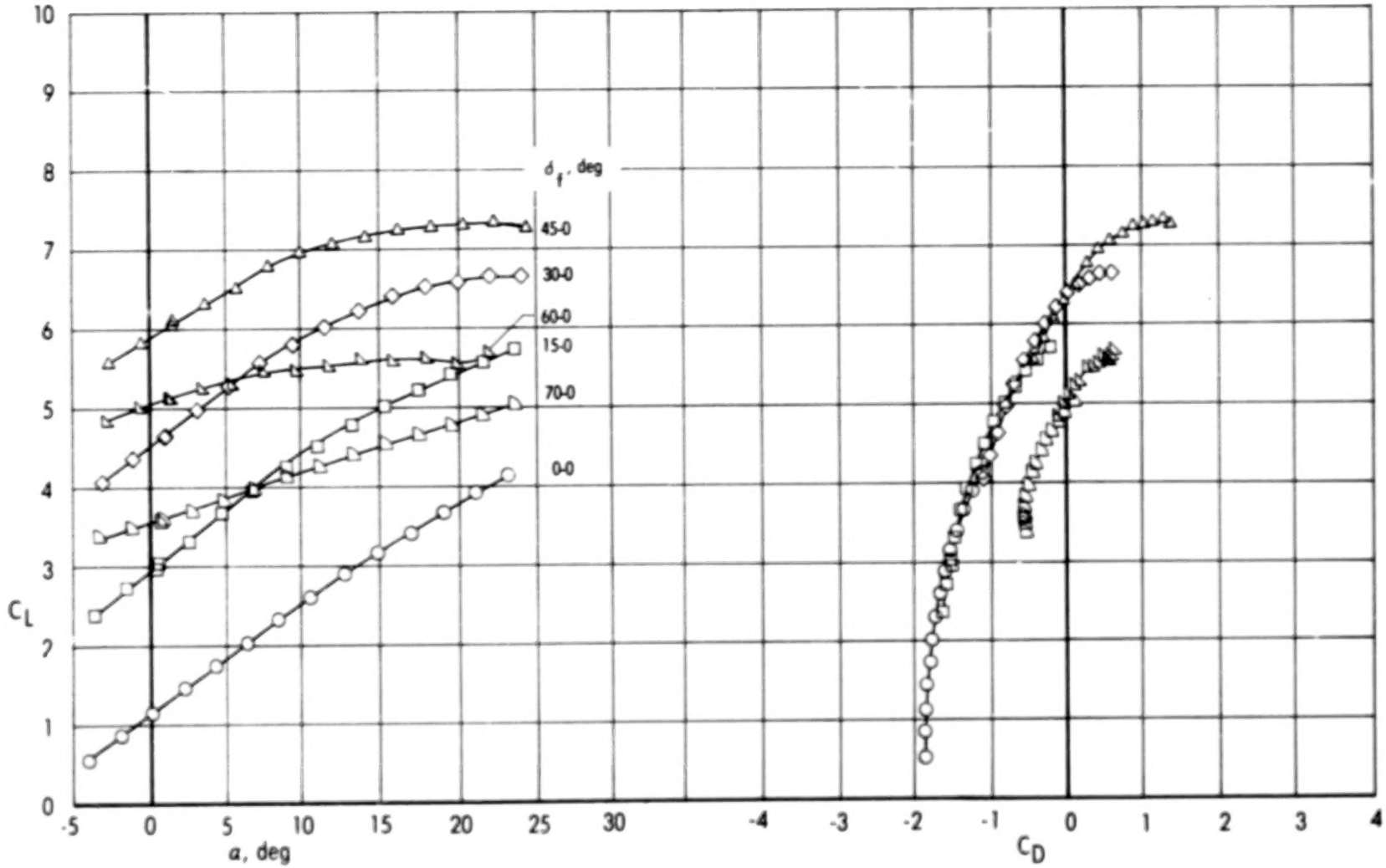

Figure 21.- Effect of flap deflection on lift and drag coefficients over angle-of-attack range for leading-edge blowing at $C_\mu \approx 2.0$, with rear element undeflected.

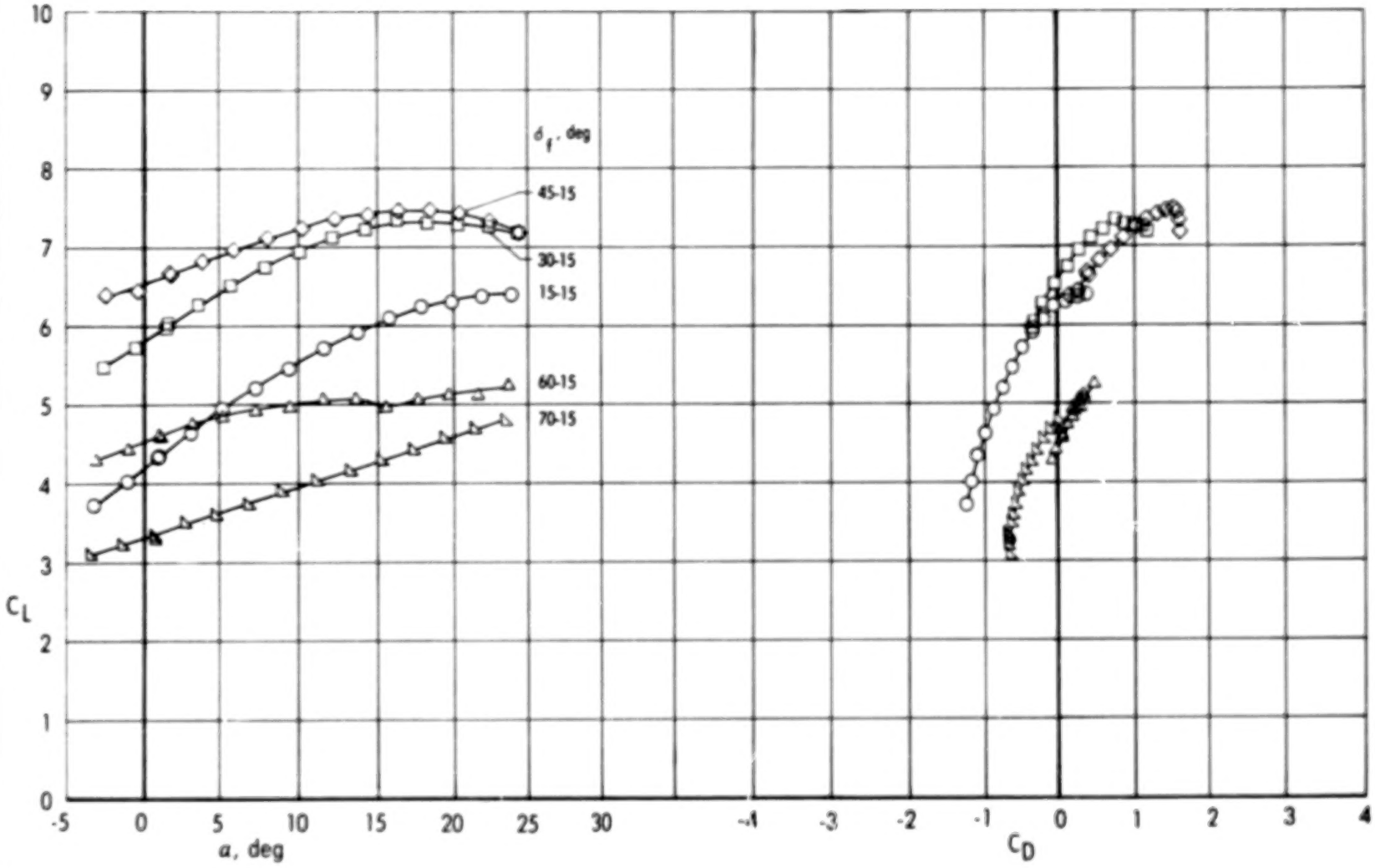

Figure 22.- Effect of flap deflection on lift and drag coefficients over angle-of-attack range for leading-edge blowing at $C_\mu \approx 2.0$, with rear element deflected 15°.

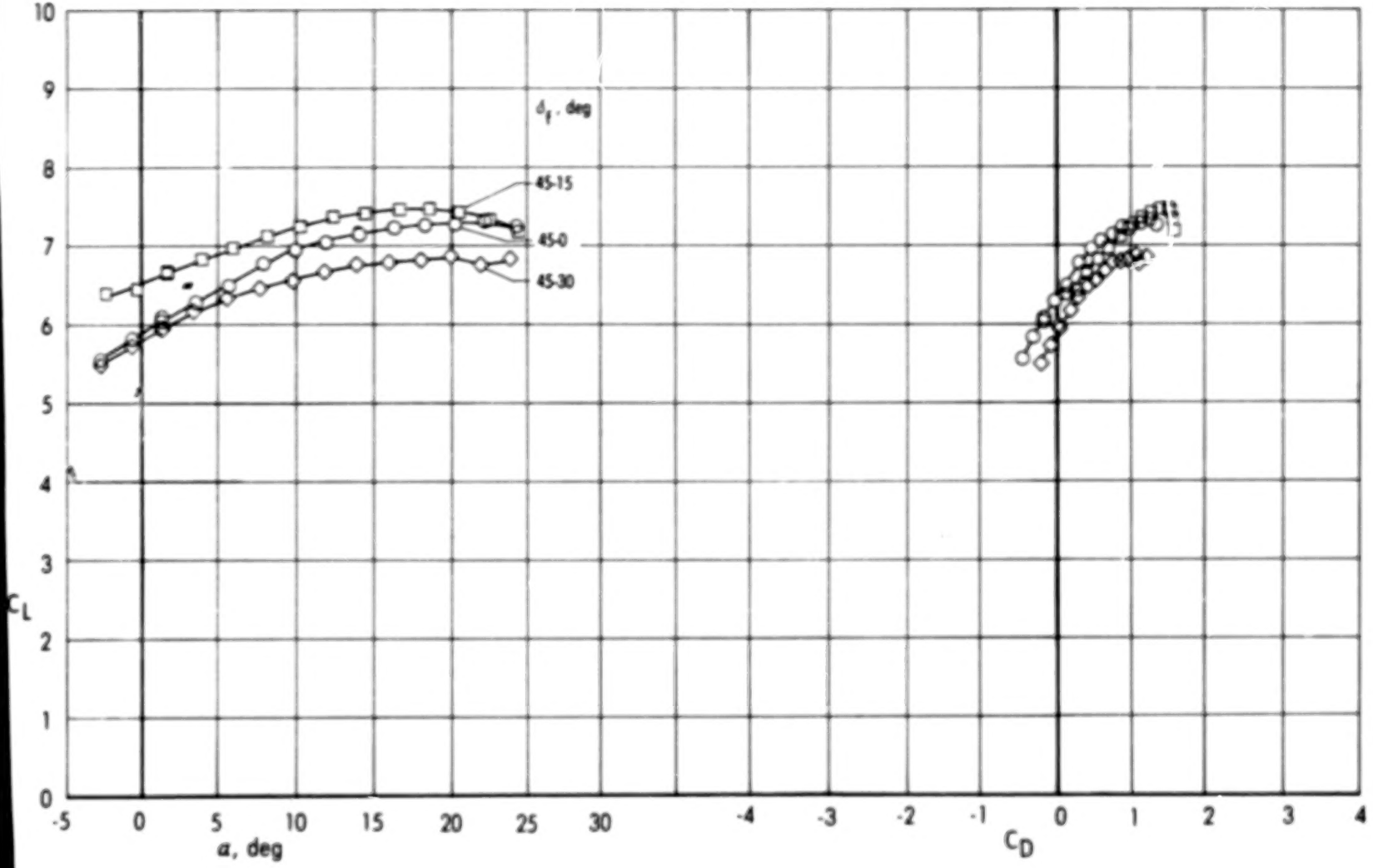

Figure 23.- Effect of rear-element deflection on lift and drag coefficients over angle-of-attack range for leading-edge blowing at $C_\mu \approx 2.0$, with forward element deflected 45°.

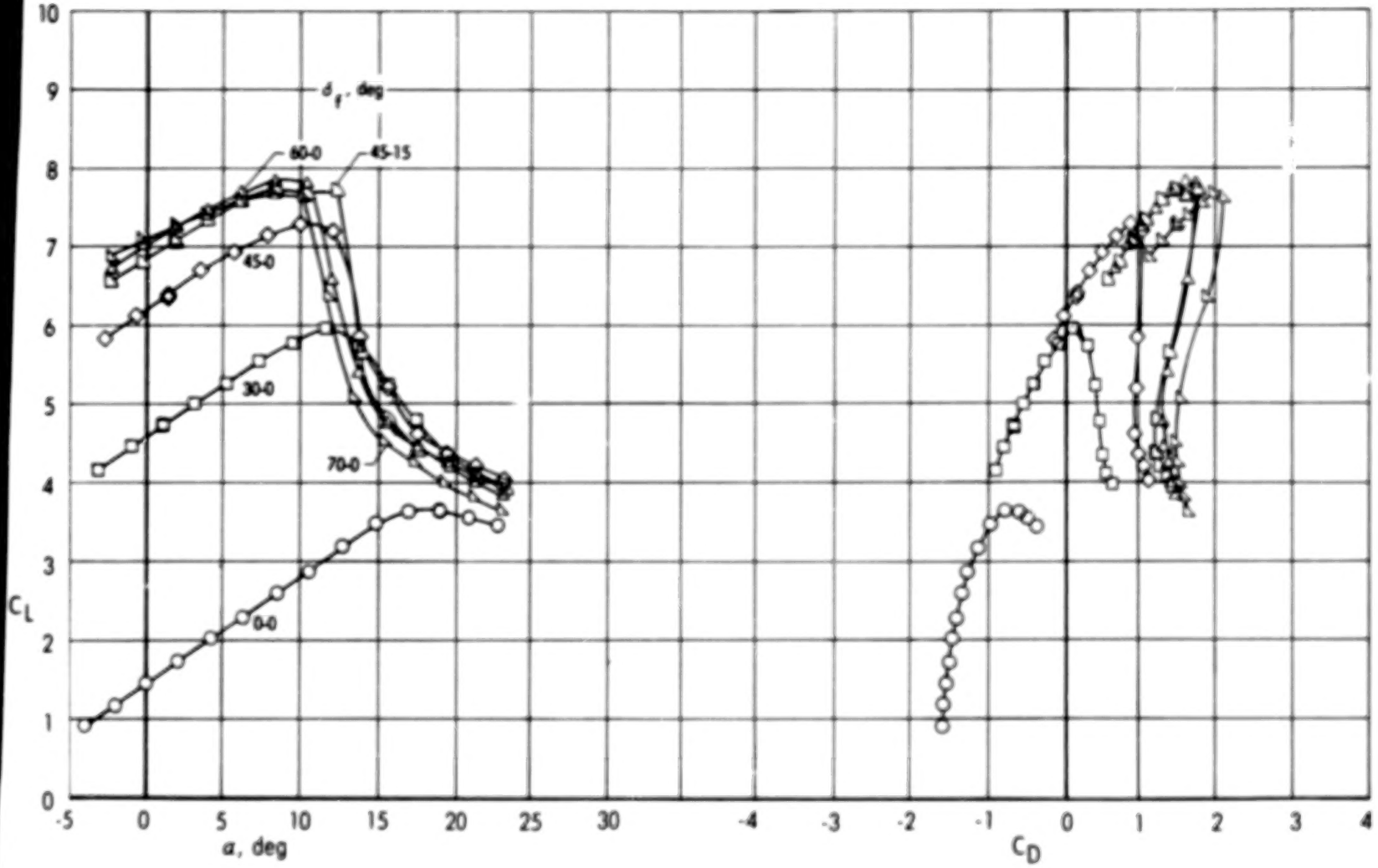

Figure 24.- Effect of flap deflection on lift and drag coefficients over angle-of-attack range for flap blowing at $C_\mu \approx 2.0$, with rear element undeflected.

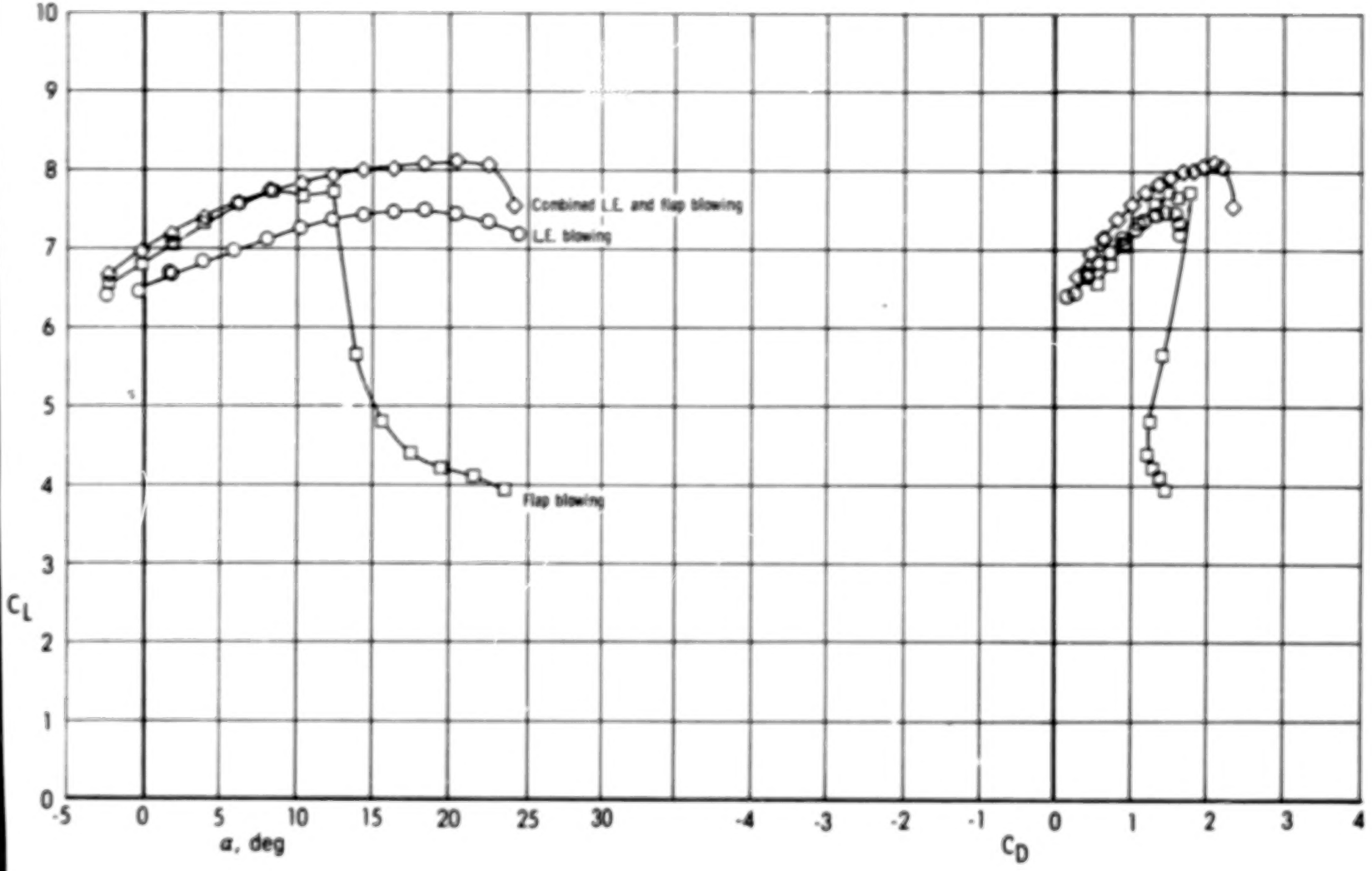

Figure 25.- Comparison of lift and drag coefficients over angle-of-attack range for leading-edge blowing, flap blowing, and combined leading-edge and flap blowing with flap blowing 28 percent of total thrust. Flap deflection, 45-15.

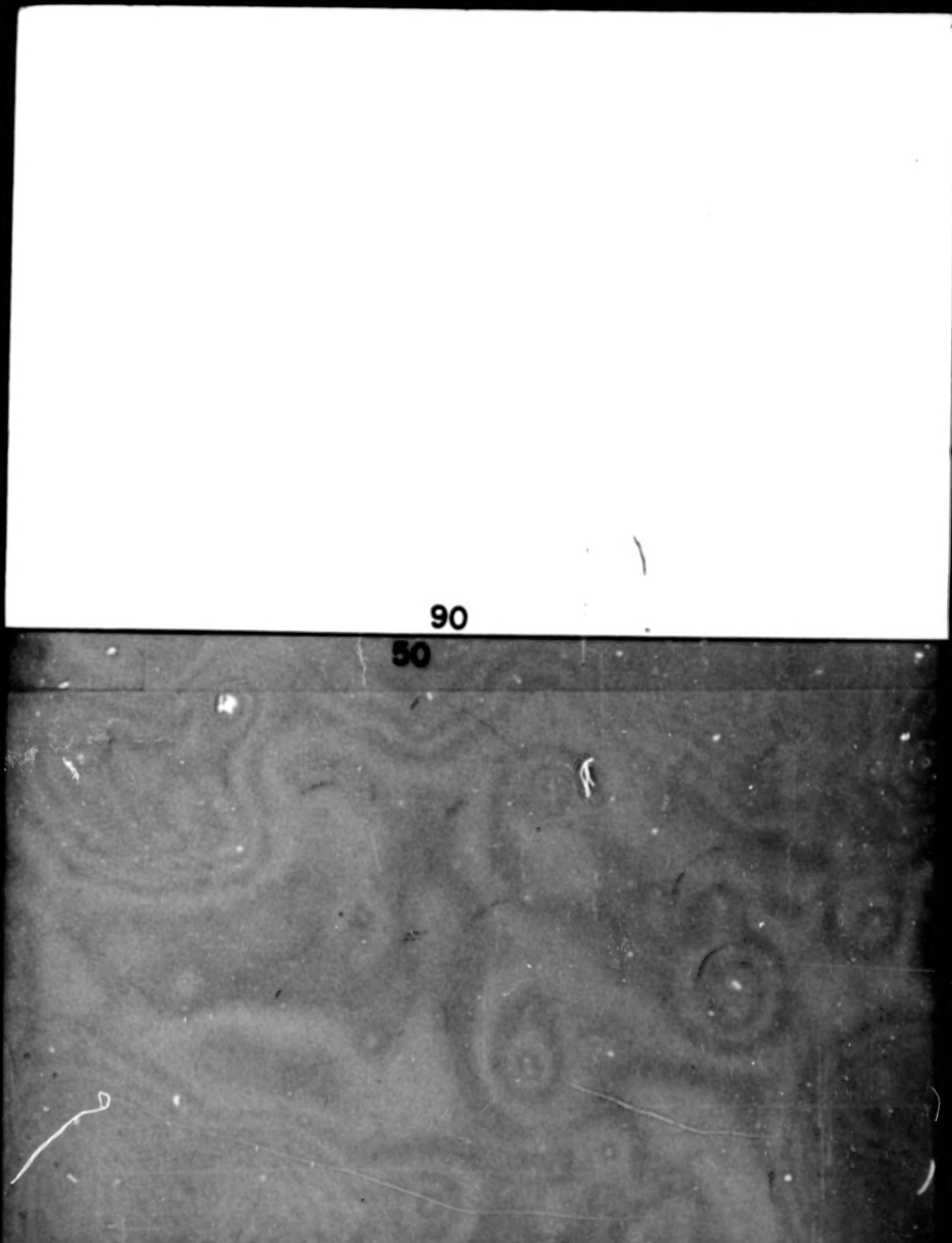
90
50

END

5.2278